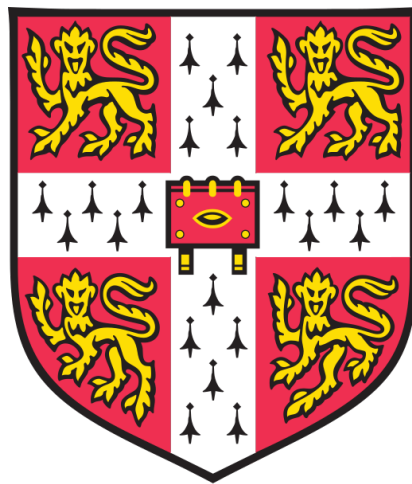


Understanding the activation mechanism of the Chk1 kinase



Yue Zhang

This dissertation is submitted for the degree of Doctor of Philosophy

Murray Edwards College

January 2019

Understanding the activation mechanism of the Chk1 kinase

Yue Zhang

Abstract

Faithful replication of DNA and correct segregation of duplicated chromosomes into two daughter cells are essential to ensure genome integrity and cell survival. Genome integrity is constantly threatened by endogenous and exogenous sources of DNA damage. Consequently, eukaryotic cells have evolved the DNA damage response (DDR), a signalling network that monitors and repairs DNA lesions promptly and efficiently. The ATR-Chk1 pathway is an essential component of the DDR, which is activated by single-strand DNA (ssDNA) generated as a result of DNA replication stress in S phase. Chk1 is a threonine/serine kinase that transduces the DNA damage signal and promotes cell cycle arrest to allow time for DNA repair. The Chk1 structure consists of conserved N-terminal kinase (Chk1KD) and C-terminal regulatory domains (Chk1RD). Available evidence has shown that the isolated Chk1KD is constitutively active, but how the enzymatic activity is regulated in the context of the full length (Chk1FL) kinase is unknown.

In this thesis, the relative enzyme efficiency of purified, recombinant Chk1KD and Chk1FL was quantitatively studied using kinase assays. It was found that the enzyme efficiency of Chk1FL was up to two orders of magnitude lower than that of Chk1KD. Biophysical and biochemical characterisation of Chk1FL provided evidence of a compact shape and an intramolecular association of the Chk1RD with the Chk1KD. A putative Chk1RD-binding site on the Chk1KD surface was identified and disrupted by mutagenesis, resulting in partial increase of Chk1FL kinase activity, thus supporting an inhibitory role of the Chk1RD in controlling kinase activity.

Activation of Chk1 requires its phosphorylation by the PI3K-like ATR kinase and its recruitment to the replisome via a direct interaction with the core replisome

component, Claspin. The Chk1-binding domain of Claspin contains a tandem repeat of three phosphothreonine/serine motifs, which need to be phosphorylated for interaction. However, the structural basis of Chk1 binding remains presently unclear. The Chk1-Claspin interaction was analysed by alanine scanning of Claspin's Chk1-binding motif and Chk1 binding to the mono-phosphorylated Chk1-binding domain of Claspin prepared using the amber codon suppression method. Furthermore, the affinity of Chk1KD and Chk1FL for a phosphorylated Claspin peptide spanning a single Chk1-binding motif or the three motifs was determined using fluorescence polarization and bio-layer interferometry. Chk1FL kinase activity was increased by the presence of a Claspin peptide corresponding to a single phosphorylated Chk1-binding motif.

The results of my thesis provide new insights into the mechanism of Chk1 function. They support a model of Chk1 auto-inhibition mediated by the intramolecular interaction of its kinase and regulatory domains, and of Chk1 enhanced activity promoted by interaction with its replisome partner Claspin.

Declaration

This dissertation is the result of my own work and includes nothing which is the outcome of work done in collaboration except as specified in the text.

It is not substantially the same as any that I have submitted, or, is being concurrently submitted for a degree or diploma or other qualification at the University of Cambridge or any other University or similar institution. I further state that no substantial part of my dissertation has already been submitted, or, is being concurrently submitted for any such degree, diploma or other qualification at the University of Cambridge or any other University or similar institution.

It does not exceed the prescribed word limit for the Degree Committee for the Faculty of Biology.

Yue Zhang

January 2019

Acknowledgement

First and foremost, I would like to express my gratitude to my supervisor, Prof. Luca Pellegrini, who offered me the opportunity to work on this PhD project. I would like to thank him for his support, guidance and patience throughout my PhD studies.

I would like to thank current and former members of Pellegrini lab: Dr. Joe Maman for his advice on biophysical experiment design and for being helpful on data interpretation; Dr. Mairi Kilkenny for experiment design in the first year of my PhD; Dr. Neil Rzechorzek for advice and discussions; Dr. Sandro Holzer for advice on experiment design and for always being patient on my questions; Dr. Luay Joudeh for advice and good discussions on biophysical experiment design and data interpretation; My fellow PhD student, Chris Morton, for his kind support and good discussions in the lab; Aji Jatikusumo for the good advice and discussions.

I would also like to thank other scientists from Department of Biochemistry: Dr. Kasia Katarzyna for her help on handling radioactive substrate and for being patient on my questions; Dr. Xuelu Wang for her help on biophysical data interpretation and for the good discussions on experiment design; Dr. Anna Reva for being supportive and helpful both inside and outside the lab.

Last but not the least, I would like to thank my parents for their consistent support and unconditional love throughout my life. I am extremely grateful to my mother who supported and accompanied me at the most difficult moments during the course of my PhD studies.

Abbreviations

| | |
|--------|--|
| AP | Acidic Patch |
| ATM | Ataxia-Telangiectasia Mutated kinase |
| ATR | ATM and Rad3-related kinase |
| ATRIP | ATR-Interacting Protein |
| ATX3 | Ataxin-3 |
| BER | Base Excision Repair |
| BLM | Bloom syndrome protein |
| BP | Basic Patch |
| BPDE | Benzo[a]pyrene |
| BRCA1 | Breast Cancer type 1 susceptibility protein |
| BTG3 | B-cell Translocation Gene 3 |
| CD | Circular Dichroism |
| CDK | Cyclin-Dependent Kinase |
| CFS | Common Fragile Sites |
| Chk1 | Checkpoint Kinase 1 |
| Chk1FL | Chk1 Full Length |
| Chk1KD | Chk1 Kinase Domain |
| Chk1RD | Chk1 Regulatory Domain |
| CKBD | Chk1 Binding Domain |
| CM | Conserved Motif |
| CMG | Cdc45, Mcm2–7, GINS |
| DDK | Dfb4-dependent kinase |
| DDR | DNA Damage Response |
| DSB | Double Strand Break |
| DTT | Dithiothreitol |
| EDTA | Ethylenediaminetetraacetic acid |
| EM | Electron Microscopy |
| ETAA1 | Ewing's Tumour-Associated Antigen 1 |
| FA | Fanconi Anaemia |
| FANCD2 | Fanconi anemia group D2 protein |
| FAT | FRAP-ATM-TRRAP |
| FP | Fluorescence Polarization |
| FPC | Fork-Pausing Complex |
| GINS | Go-Ichi-Ni-San |
| GST | Glutathione S-Transferase |
| HEAT | Huntingtin, Elongation factor 3, protein phosphatase 2A and TOR1 |
| His | Histidine |
| HR | Homologous Recombination |

| | |
|----------|---|
| HU | Hydroxyurea |
| IPTG | Isopropyl β -D-1-Thiogalactopyranoside |
| IR | Ionising Radiation |
| KA1 | Kinase Associated 1 domain |
| LS | Light Scattering |
| MAPK | Mitogen-Activated Protein Kinase |
| MM | Molar Mass |
| MOI | Multiplicity Of Infection |
| MRN | Mre11-Rad50-Nbs1 |
| NES | Nuclear Export Sequence |
| NHEJ | Non-Homologous End Joining |
| NLS | Nuclear Localization Signal |
| PARP | Poly(ADP-ribose)-polymerase |
| PBD | Polo-Box Domain |
| PCNA | Proliferating Cell Nuclear Antigen |
| PCR | Polymerase Chain Reaction |
| pfu | plaque forming units |
| PIKKs | Phosphatidylinositol-3-Kinase-like Kinases |
| PKA | cAMP-dependent Protein Kinase |
| RFC | Replication Factor C |
| RFID | Replication Fork Interacting Domain |
| RI | Refractive Index |
| ROS | Reactive Oxidative Species |
| RPA | Replication Protein A |
| SAXS | Small-Angle X-ray Scattering |
| SDS-PAGE | Sodium Dodecyl Sulphate-Polyacrylamide Gel Electrophoresis |
| SEC-MALS | Size Exclusion Chromatography- Multi-Angle Light Scattering |
| SMARCAL1 | SWI/SNF-related Matrix-associated Actin-dependent Regulator of Chromatin subfamily A-like protein 1 |
| SSB | Single Strand Break |
| ssDNA | single strand DNA |
| SUMO | Small Ubiquitin-like Modifier |
| TCEP | Tris(2-Carboxyethyl)Phosphine |
| TEV | Tobacco Etch Virus |
| TopBP1 | Topoisomerase II Binding Protein 1 |
| USP3 | Ubiquitin-Specific Protease 3 |
| UV | Ultraviolet |
| WRN | Werner syndrome protein |

| | |
|--|-----------|
| CHAPTER 1 INTRODUCTION | 1 |
| 1.1 Cell cycle regulation | 1 |
| 1.1.1 G1 phase | 1 |
| 1.1.2 S phase and G2/M transition | 4 |
| 1.1.3 M phase | 6 |
| 1.1.4 Cell cycle checkpoints | 7 |
| 1.2 DNA damage response | 8 |
| 1.2.1 Overview of DNA damage response | 8 |
| 1.2.2 Features of DDR sensor proteins | 10 |
| 1.2.3 Activation of the ATR-Chk1 pathway..... | 11 |
| 1.2.4 Causes of DNA replication stress | 15 |
| 1.2.5 Inhibition of late origin firing | 16 |
| 1.2.6 Protection of replication fork..... | 18 |
| 1.2.7 Recovery from checkpoint activation | 20 |
| 1.2.8 DDR and cancer therapy | 21 |
| 1.3 Enzymatic and structural characterization of Chk1 | 24 |
| 1.3.1 Brief overview of protein kinase superfamily | 24 |
| 1.3.2 PKA is a prototype of kinase studies | 25 |
| 1.3.3 Structural features and activation mechanism of Chk1 | 27 |
| 1.3.4 Chk1 functions outside checkpoint signalling..... | 29 |
| 1.4 Fork pausing complex and Claspin | 31 |
| 1.4.1 Claspin structure and its intermolecular interactions..... | 31 |
| 1.4.2 Claspin function in FPC | 34 |
| 1.4.3 Regulation of Claspin stability..... | 35 |
| 1.5 Perspective and aims | 36 |
| CHAPTER 2 BIOPHYSICAL STUDIES ON CHK1 | 38 |
| 2.1 Results | 38 |
| 2.1.1 Chk1 constructs and purification | 38 |
| 2.1.2 Post-translational modifications of recombinant Chk1..... | 41 |
| 2.1.3 Size-exclusion multi-angle laser scattering (SEC-MALS)..... | 43 |
| 2.1.4 Small Angle X-ray Scattering (SAXS) | 44 |
| 2.1.5 Attempts towards crystallization of Chk1FL..... | 46 |
| 2.1.6 The kinase and regulatory domains of Chk1 co-elute in size-exclusion chromatography | 49 |
| 2.2 Discussion | 53 |
| 2.3 Materials and methods | 54 |
| 2.3.1 Generation and expression of Chk1 constructs | 54 |
| 2.3.2 Purification of Chk1 constructs | 56 |
| 2.3.3 Generation and purification of EcChk1 constructs | 56 |
| 2.3.4 Generation of 8xHis-Chk1FL, Chk1 ^{D130A} and Chk1 ^{TEV} constructs | 57 |
| 2.3.5 Purification of Chk1 ^{D130A} and Chk1 ^{TEV} | 57 |
| 2.3.6 Purification and tag removal of 8xHis-Chk1FL | 58 |
| 2.3.7 SEC-MALS..... | 58 |
| 2.3.8 Dephosphorylation of Chk1FL..... | 58 |

| | |
|---|------------|
| 2.3.9 SEC-SAXS | 59 |
| 2.3.10 TEV treatment and co-elution of Chk1KD and Chk1RD | 59 |
| 2.3.11 Crystallization trials of Chk1FL | 59 |
| CHAPTER 3 ENZYMATIC STUDIES OF CHK1 ACTIVITY | 61 |
| 3.1 Results | 61 |
| 3.1.1 S216 is a major phosphorylation site of Chk1 on 14xHis-SUMO-Cdc25C ²⁰⁰⁻²⁵⁶ | 61 |
| 3.1.2 NADH-coupled assays of Chk1 activity..... | 62 |
| 3.1.3 Determination of ATP concentration for kinase assays..... | 65 |
| 3.1.4 Chk1 kinase assays at different Cdc25C peptide concentration..... | 67 |
| 3.1.5 Chk1 kinase assays at different ATP concentration | 71 |
| 3.1.6 Chk1 intramolecular interacting interface studies | 74 |
| 3.1.7 Attempts towards understanding binding affinity between ATP and Chk1 | 83 |
| 3.2 Discussion | 85 |
| 3.3 Materials and Methods | 87 |
| 3.3.1 Generation, expression and purification of 14xHis-SUMO-Cdc25C ²⁰⁰⁻²⁵⁶ | 87 |
| 3.3.2 Generation of 14xHis-SUMO-Cdc25C ^{200-256-S216A} | 87 |
| 3.3.3 Chk1 substrate specificity kinase assays | 88 |
| 3.3.4 NADH-coupled assays of Chk1 activity..... | 88 |
| 3.3.5 Generation of Chk1 ^{S317E/S345E} , Chk1 ^{Δturn} , Chk1 ^{E17T/E22T} and Chk1 ^{E32T/E33S} | 89 |
| 3.3.6 Determination of ATP concentration in kinase assays | 89 |
| 3.3.7 Validation of linear ³² P counts range on scintillation counter..... | 90 |
| 3.3.8 Time range determination at highest and lowest Cdc25C peptide concentration . | 90 |
| 3.3.9 Chk1 kinase assay at different concentration of Cdc25C peptide..... | 92 |
| 3.3.10 Time range determination at highest and lowest ATP concentration..... | 92 |
| 3.3.11 Chk1 kinase assay at different concentration of ATP | 92 |
| 4 THE INTERACTION OF CHK1 WITH CLASPIN | 93 |
| 4.1 Results | 93 |
| 4.1.1 Expression and purification of Claspin constructs | 93 |
| 4.1.2 Phosphoserine incorporation in Claspin CKBD using amber codon suppression.... | 96 |
| 4.1.3 Interaction studies between Claspin and Chk1..... | 104 |
| 4.1.4 Quantitative analysis of Chk1-Claspin binding using biolayer-interferometry..... | 108 |
| 4.1.5 Scanning of kinase responsible to Claspin phosphorylation on CKBD | 116 |
| 4.1.6 Alanine scanning of the Claspin Chk1-binding motif | 118 |
| 4.1.7 Binding affinity determination between Claspin motif and Chk1..... | 121 |
| 4.1.8 Effect of Claspin binding on Chk1 activity | 122 |
| 4.1.9 Attempts towards co-crystallization of Chk1KD and phospho-Claspin peptide.... | 123 |
| 4.2 Discussion | 124 |
| 4.3 Materials and Methods | 126 |
| 4.3.1 Generation and expression of Claspin constructs in Rosetta 2 (DE3) | 126 |
| 4.3.2 Purification of Claspin constructs expressed in Rosetta 2 (DE3)..... | 127 |
| 4.3.3 Generation of Claspin ^{3T/SE} construct..... | 127 |
| 4.3.4 Generation of pMBAT4 vector | 127 |
| 4.3.5 Generation of MBP-Claspin ⁸⁸⁴⁻⁹⁹² -8xHis constructs..... | 128 |
| 4.3.6 Generation and expression of MBP-Claspin ⁸⁸⁴⁻⁹⁹² -8xHis amber codon suppression | |

| | |
|---|------------|
| constructs | 128 |
| 4.3.7 Generation of MBP-Claspin ⁸⁸⁴⁻⁹⁹² -8xHis-Avi constructs..... | 129 |
| 4.3.8 Generation of MBP-pS945Claspin ⁸⁸⁴⁻⁹⁹² -8xHis-Avi alanine scanning constructs ... | 129 |
| 4.3.9 Generation of Strep-SUMO-Claspin ⁸⁸⁴⁻⁹⁹² -8xHis constructs | 129 |
| 4.3.10 Purification of Claspin constructs expressed in amber codon suppression system | 130 |
| 4.3.11 Pull-down assays between Claspin and Chk1 constructs | 131 |
| 4.3.12 Generation, expression and purification of CK1 γ 1 ⁴³⁻³⁵² | 131 |
| 4.3.13 Kinase activity and substrate specificity test of CK1 γ 1 ⁴³⁻³⁵² and Cdc7 ^{Δ1-36} /Dbf4 . | 132 |
| 4.3.14 Western blotting | 132 |
| 4.3.15 Bio-layer interferometry studies on Claspin and Chk1 constructs using ForteBio Octet | 133 |
| 4.3.16 Circular dichroism analysis for pS945Claspin ⁸⁸⁴⁻⁹⁹² -8xHis-Avi constructs..... | 134 |
| 4.3.17 Fluorescence polarization assay for Claspin peptide and Chk1 constructs..... | 134 |
| 4.3.18 Kinase assays of Chk1 constructs in the presence of pClaspin peptide | 135 |
| 4.3.19 Crystallization trials of Chk1 and Claspin peptide | 135 |
| CHAPTER 5 DISCUSSION AND FUTURE DIRECTIONS..... | 137 |
| REFERENCE | 140 |
| APPENDIX A | 151 |

CHAPTER 1 INTRODUCTION

1.1 Cell cycle regulation

1.1.1 G1 phase

Mitotic cell division is critical to life propagation in eukaryotes. It consists of two main events: faithful replication of DNA and correct segregation of the replicated chromosomes into two daughter cells. A cell cycle comprises the stages of DNA synthesis (S phase) and mitosis (M phase), separated by intervening gap phases (G1 and G2). Cell cycle progression is tightly regulated by activation and deactivation of the cyclin-dependent family of protein kinases (CDKs). CDKs are highly conserved from yeast to humans and can be subdivided into cell-cycle-related subfamilies (represented by CDK1, CDK4 and CDK5 in humans) and transcriptional subfamilies (represented by CDK7, CDK8, CDK9, CDK11 and CDK20 in humans) (Malumbres, 2014). Activation of CDKs requires binding to a cyclin to form a holoenzyme and phosphorylation on its activation loop by CDK-activating kinase (CAK). Different combinations of CDKs with cyclins lead to different functions in cell cycle regulation (Figure 1.1). The concentration of CDKs during a whole cell cycle is mostly constant while cyclins concentration oscillates in different stages. CDKs activity can be inhibited by degradation of cyclins through ubiquitination-regulated proteolysis, binding to CDKs inhibitors (CKIs) or inhibitory phosphorylation (Hochegger et al., 2008). Inhibitory phosphorylation on two adjacent threonine and tyrosine residues on CDKs subunit are conducted by Wee1 and Myt1 and removal of this inhibitory phosphorylation is regulated by cell division cycle 25 (Cdc25), a dual specificity phosphatase (DSP) (Malumbres and Barbacid, 2005). When both activating and deactivating modifications appear on same CDKs molecule, the kinase remains in the inactive state (Malumbres and Barbacid, 2005). Cells can remain quiescent (G0) when there is not enough cell division stimulation and then re-enter into G1 under the regulation of cyclin C/Cdk3 complex (Ren and Rollins, 2004).

A restriction point (R point) in G1 in mammalian cells, which is called start in yeast, marks the commitment to a cell cycle. Progression to cell division after the R point is irreversible even when growth factors are removed. Growth factors stimulate expression of cyclin D which activate CDK4 by forming cyclin D/CDK4 complex. The complex inhibits transcriptional inhibitor retinoblastoma protein (Rb) via phosphorylation and frees E2F transcription factor, which in turn promotes expression of cyclins E and CDK2. Cdc25A removes inhibitory phosphorylation on CDK2 and promotes its activation at G1/S transition. In addition to Cdc25A, human Cdc25 has another two isoforms Cdc25B and Cdc25C, which mainly regulate G2/M transition in each cell cycle (Sur and Agrawal, 2016).

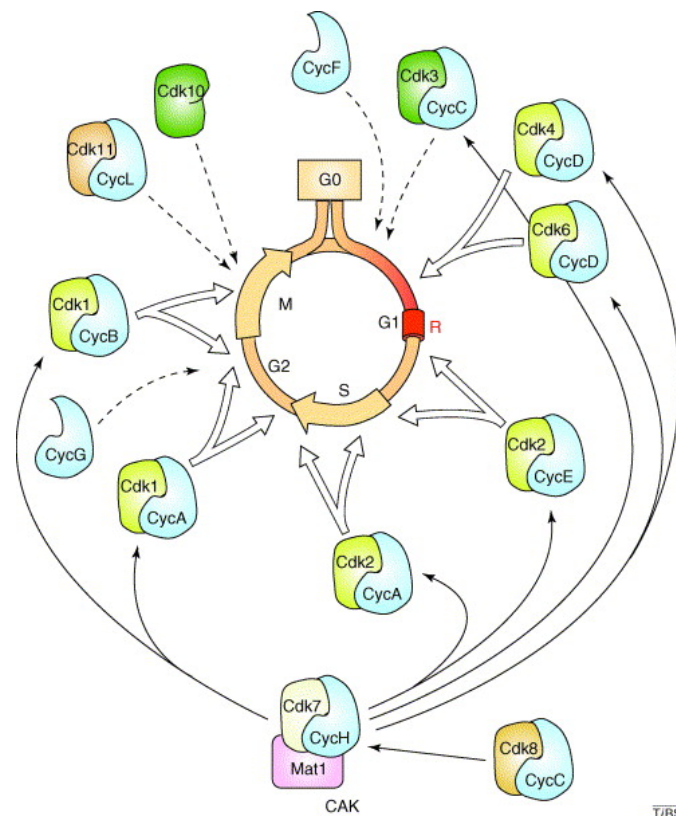


Figure 1.1 Cyclin-Cdk complexes in each cell cycle phase (Malumbres and Barbacid, 2005)

Cell cycle progression is regulated by CDKs activity. The catalytic subunit of CDKs acquires cell-cycle-specific activity by forming a complex with different cyclins.

Active cyclin E/Cdk2 complex leads to complete inactivation of Rb and E3 ubiquitin

ligase anaphase promoting complex/cyclosome (APC/C), thus promoting S phase entry (Cappell et al., 2016; Harbour et al., 1999). APC/C activity is regulated by two co-activators, Cdc20 and Cdh1, which function mainly in early M and late M to G1/S transition respectively (Peters, 2002). Apart from APC/C, Skp1–Cullin-1–F-box (SCF) is another ubiquitin-protein ligase which regulates cell cycle through cyclin ubiquitination. SCF regulates G1 cyclin ubiquitination and proteolysis by the 26S proteasome to avoid DNA re-replication in S phase (Vodermaier, 2004). However, the R point model is challenged by studies using single-cell analysis which reveals that among actively cycling cells, only a subset of cells which undergoes replication stress or obstacles in MAPK signalling in the previous cell cycle goes through R point. Other cycling cells contain a high level of CDK2 activity and hyperphosphorylated Rb and thus are committed to the next cell cycle (Moser et al., 2018).

Another important event in G1 phase is replication origin licensing, which prepares DNA for replication in S phase. Origin recognition complex (ORC), a hexameric complex composed of Orc1-6, recognises DNA replication origin. Yeast has a consensus AT-rich autonomous replication sequences (ARS) while the origin initiation sequence is more diverse in metazoan. Current evidence indicates that metazoan replication origin forms a special secondary structure which is recognised by ORC (Parker et al., 2017). Co-operating with another two licensing factors, Cdc6 (Cdc18 in fission yeast) and Cdt1, ORC regulates sequential loading of two minichromosome maintenance complexes (MCM, a hexameric complex composed of Mcm2-7) onto replication origin to form a pre-replicative complex (pre-RC). The licensing factors are released in sequence: Cdc6 dissociates first, which is followed by Mcm2-7 ring closure and simultaneous release of Cdt1 and ORC (Ticau et al., 2017). Prevention of re-initiation of DNA replication in one cell cycle is essential to maintain genome integrity and the re-licensing is inhibited after G1 phase when the CDK activity begins to increase. In *S. cerevisiae*, Clb/Cdc28 prohibits re-initiation through phosphorylating and inhibiting ORC, triggering the ubiquitin-regulated destruction of Cdc6 and nuclear exclusion of MCM (Nguyen et al., 2001). In *S. pombe*, re-licensing

in S phase is inhibited by the down-regulation of licensing factors Cdt1 and Cdc18 as a consequence of increased Cdc2 activity (Gopalakrishnan et al., 2001). Metazoan re-licensing is prevented by Cyclin A/Cdk2-regulated Cdc6 destruction after G1 phase and prohibition of Cdt1 loading on chromatin by Cdk1 in mitosis (Ballabeni et al., 2004; Coverley et al., 2000).

1.1.2 S phase and G2/M transition

DNA is replicated in S phase and faithful genome duplication is essential to cell survival and proliferation. Licensed origin remains unfired until S phase. Not all licensed origins are activated and many origins remain dormant during DNA replication. The flexibility of origin firing is believed to be essential to ensure the completion of DNA replication in each cell cycle and to protect genome stability. Two kinases, S-phase CDK and Dbf4-dependent kinase (DDK), regulate DNA replication at origin (Bell and Dutta, 2002). Like CDKs, the catalytic subunit of DDK, Cdc7, remains constant in the cell cycle while the regulatory subunit Dbf4 oscillates and accumulates at S and G2 phase (Ferreira et al., 2000). The rise of the Dbf4 level triggers DDK activity in S phase and promotes origin firing.

In yeast, the Mcm2-7 complex is a target of DDK and phosphorylation on MCM subunits promotes its association with Cdc45 through chaperone Sld3 and Sld7. Sld2 and Sld3 are substrates of CDK and phosphorylation on these effector proteins lead to interaction with BRCT domain on Dpb11, which in turn recruits GINS to the origin and forms an active replicative helicase complex Cdc45-MCM-GINS (CMG) (Labib, 2010). The factors involved in metazoan helicase activation are largely conserved from the yeast factors, while some non-catalytic chaperones are different. RecQ4 is a Sld2 homolog candidate in metazoan and Sld3 is a homolog of a domain on human Treslin. Sld7 corresponds to MDM2 binding protein (MTBP) and Dpb11 is speculated to be a yeast ortholog of human TopBP1 (Garcia et al., 2005; Matsuno et al., 2006; Sanchez-Pulido et al., 2010). Mcm10 is a factor required for replication origin firing.

C-terminus of Mcm10 interacts with MCM in S phase and the interaction promotes helicase double hexamer splitting and activation (Quan et al., 2015). The double hexamer of MCM is necessary and sufficient for origin firing. After origin firing, the two helicases are separated and move in opposite direction to conduct a bidirectional DNA replication (Duzdevich et al., 2015).

In each DNA replication cycle, helicase needs to unwind every base and overcome replication barriers formed by bound proteins and DNA structure. DNA polymerase is responsible for synthesis of nascent DNA strands with high fidelity and maintains the coupling status with helicase (Gambus et al., 2009; Kim et al., 1996). Eukaryotic DNA replication is mainly conducted by three DNA polymerases: polymerase α , ϵ and δ . Polymerase α contains a primase and a polymerase subunit and functions in priming Okazaki fragment. Polymerase ϵ and δ are supposed to conduct DNA replication on leading and lagging strands respectively. GINS complex directly binds to MCM, polymerase α and ϵ , thus plays a structural role in linking helicase and polymerases (Sengupta et al., 2013). A fork pausing complex (FPC) functions in maintaining replication fork integrity and prevents fork collapse through coupling helicase and polymerase. Human FPC consists of four components: Timeless (Tim1), Timeless-interacting protein (Tipin), And1 and Claspin. And1 and Tipin directly interact with lagging-strand polymerase α and the other two components, Tim1 and Claspin, interact with leading-strand polymerase ϵ (Errico and Costanzo, 2012). Proliferating cell nuclear antigen (PCNA) forms a homo-trimeric ring-shaped complex which encircles DNA and bridges polymerase ϵ and δ to enhance their progressivity (Kang et al., 2017).

Termination of DNA replication occurs when two replication forks converge. CMG complexes disassemble from DNA after ligation of nicks at opposing forks and DNA dissolution (Dewar et al., 2015). Polyubiquitylation on Mcm7 by p97 triggers the unloading of replisome from DNA at termination (Moreno et al., 2014).

Progression of the cell cycle from G2 to M phase is driven by cyclin B/CDK1. Y15 on CDK1 is an inhibitory phosphorylation site and Wee1 and Cdc25C directly regulate Cdk1 activity by phosphorylating and dephosphorylating this site respectively. The activity of these two regulators are mediated by polo-like kinase 1 (Plk1) and checkpoint kinase 1 (Chk1). Plk1 is a key regulator of mitosis progression. The activity of Plk1 is suppressed by an intramolecular interaction between its kinase domain and a C-terminal Polo-box domain (PBD) which buries a nuclear localization signal (NLS) and keeps Plk1 in the cytoplasm. During G2 phase, Aurora A activates Plk1 through phosphorylation under the regulation of cyclin A/Cdk1. Activated Plk1 undergoes a conformational change and exposes NLS which leads to its nuclear transportation (Pintard and Archambault, 2018). Active Plk1 promotes Cdc25C nuclear translocation through phosphorylating on its S198 (Toyoshima-Morimoto et al., 2002). In combination with Cdk1 and casein kinase 2 (CK2), Plk1 generates phosphodegrons on Wee1 and targets it for SCF-mediated proteolysis (Watanabe et al., 2005). Chk1, however, functions in an opposing way to regulate cyclin B/Cdk1 activation when the G2 checkpoint is activated by unrepaired DNA damage. Chk1 phosphorylates Wee1 and promotes its interaction with 14-3-3 which results in Wee1 activation and phosphorylation on Cdk1 Y15 (Lee et al., 2001). Chk1 phosphorylates Cdc25C on S216 and results in its nuclear export. Cdc25C undergoes cytoplasmic sequestration via interaction with 14-3-3 protein, preventing its ability to dephosphorylate and activate cyclin B/Cdk1 (Sanchez et al., 1997). Chk1 translocates to the cytoplasm in a Crm1-dependent manner after being phosphorylated at S286 and S301 by Cdk1 at G2/M transition which further increases Cdk1 activity and drives the transition (Enomoto et al., 2009).

1.1.3 M phase

Cells divide and sister chromatids separate into two newly formed daughter cells in M phase. It is sub-divided to four phases: prophase, metaphase, anaphase and telophase. APC/C plays a pivotal role in M phase progression by regulating the exit of

metaphase and mitosis. APC/C activity is depressed by Emi1, an inhibitor of APC/C co-activator Cdc20, during S and G2 phase. In early M phase, Emi1 undergoes phosphorylation by Cdk1 on its degron which leads to its destruction by SCF-mediated proteolysis (Margottin-Goguet et al., 2003). Cyclin B/Cdk1 also phosphorylates APC/C and enhances its interaction with a coactivator Cdc20. Activated APC/C^{Cdc20} targets cyclin B, resulting in its proteasomal destruction and thus deactivation of Cdk1. Reduced Cdk1 activity leads to decreased APC/C phosphorylation and inactivation of APC/C^{Cdc20}. The completion of cyclin B destruction is mediated by APC/C with another coactivator Cdh1, which efficiently binds to dephosphorylated APC/C. APC/C^{Cdh1} promotes M phase exit by the ubiquitination-regulated destruction of Plk1 and Aurora kinases, leading to complete elimination of mitotic cyclins (Manchado et al., 2010).

1.1.4 Cell cycle checkpoints

To ensure the accurate replication and segregation of genomic information to daughter cells, eukaryotes have evolved a surveillance mechanism termed "cell cycle checkpoint" (Abraham, 2001). Checkpoint controls the timing of cell cycle progression and ensures the completion of one cell cycle phase before entry to the next phase. Checkpoint is activated in response to DNA damage, replication stress and spindle damage. Activated checkpoint delays cell cycle progression which allows time for DNA repair (Callegari and Kelly, 2007).

1.2 DNA damage response

1.2.1 Overview of DNA damage response

DNA damage response (DDR) is a complex and interconnected network of molecular signals that allow the cells to respond promptly and efficiently to the presence of DNA damage. Signal transduction is relayed across protein networks, from damage sensors that detect the lesion to transducers that transmit and amplify the signal and eventually to effectors that repair the damage. DDR functions in stabilization of replication fork, stimulation of cell cycle arrest to allow recovery time for DNA repair, inhibition of late origin firing and recovery of the cell cycle when replication stress is removed. In the DDR, the signal is mainly transduced by phosphorylation events from kinase cascade, but other post-translational modifications such as ubiquitination and sumoylation are also involved in the signal transduction. When the DNA damage is severe and irreparable, the DDR drives the cell to senescence or cell death, depending on cell context, type and extent of stimulus (Surova and Zhivotovsky, 2013).

Three serine/threonine kinases belonging to the phosphatidylinositol-3-kinase-like kinase family (PIKKs) are the main upstream DNA damage sensors: ataxia-telangiectasia mutated (ATM), ATM- and Rad3-related (ATR), and DNA-dependent protein kinase (DNA-PKs). ATM is activated mainly by double strand DNA breaks (DSBs), while ATR responds to a wide spectrum of DNA damage or replication stress, including DNA breaks, base adducts, crosslinks, dNTP depletion, polymerase inhibition and topoisomerase inhibition (Flynn and Zou, 2011). DNA-PKs responds to DSB and regulates non-homologous end joining (NHEJ).

Activation of the two major sensor proteins ATM and ATR requires the association to its co-factor, Mre11-Rad50-Nbs1 (MRN) complex and ATRIP respectively. The sensor kinases then undergo activation through autophosphorylation. The DDR signal is spread to chromatin flanking DSB sites by phosphorylation of histone variant

H2AX which then becomes a platform for proteins involved in DNA repair and chromatin remodelling (Marechal and Zou, 2013). Central transducers in the two pathways, Chk2 and Chk1 are activated through phosphorylation and transduce DNA damage signal to effector proteins. Mass spectrometry has been intensively used in the identification of ATM/ATR substrates in response to DNA damage. Over 900 regulated phosphorylation sites on more than 700 proteins containing the consensus ATM/ATR phosphorylation motif S/TQ were enriched after ionising radiation (IR) and 570 phosphorylation sites were identified in UV-damaged cells (Matsuoka et al., 2007; Stokes et al., 2007). Genome ontology analysis on these substrate proteins reveals that DDR encompasses DNA replication, DNA repair, cell cycle and other signalling pathways interfering with DNA damage pathway (Matsuoka et al., 2007). DNA-PK catalytic subunit is recruited to DSB ends and forms a holoenzyme with a heterodimer of Ku70/80. DNA-PK promotes the alignment and ligation of the DNA ends in NHEJ (Graham et al., 2016).

The DDR pathways are not completely independent and function in an overlapping but non-redundant way. ATR acts as a downstream target of ATM in response to DSB when RPA-ssDNA is generated from resection of DNA ends (Jazayeri et al., 2005). On the other hand, ATR-Chk1 pathway activated in response to HU and UV mediates ATM activation through phosphorylation on S1981, which further leads to ATM-Chk2 pathway activation. These two DDR pathways function in an overlapping manner and contribute to G2/M arrest (Stiff et al., 2006). In response to UV-induced replication stress, all the three DDR pathways are involved in the DDR signalling. ATR-Chk1 pathway is activated immediately while ATM and DNA-PK are activated with a delay to complete DDR signalling and the cooperation of these pathways maintain the genome stability (Yajima et al., 2009). Studies on DDR inhibition reveal that cells treated with Chk1 inhibitor are more vulnerable than cells treated with ATR inhibitor. It provides evidence on a backup DDR pathway hypothesis which circumvents ATR during Chk1 activation, indicating an interconnecting function between the pathways (Buisson et al., 2015).

1.2.2 Features of DDR sensor proteins

The three DNA damage sensors kinases are large proteins and share similar domain organisations and features. A helical solenoid HEAT-repeat domain (Huntingtin, elongation factor 3 (EF3), protein phosphatase 2A (PP2A) and TOR1) at varying length locates at N-terminus which regulates protein-protein interaction. This domain is proposed to interact with a conserved C-terminal motif on NBS1, ATRIP and Ku80, which promotes stable DNA damage site recruitment of ATM, ATR and DNA-PK, respectively (Falck et al., 2005). A catalytic domain is located at C-terminus which is flanked by a FRAP-ATM-TRRAP (FAT) domain and a FAT C-terminal (FATC) motif (Blackford and Jackson, 2017). Structural determination on DNA-PKcs in complex with the C-terminal 194 amino acid of Ku80 was resolved at a resolution of 4.3 Å. The complex fold into three structural units including a head region formed by FAT and FATC domains, a circular cradle region formed by the carboxyl side of HEAT repeats and an N-terminal subunit of the N-terminus of HEAT. The active site on the bilobal kinase domain is buried and activation requires conformational change of the kinase (Sibanda et al., 2017). More detailed description on kinase catalytic domain is discussed in 1.3.1. Another common feature of the three sensor proteins is the capability of autophosphorylation while the function of this modification varies among the kinases. ATM autophosphorylates S1981 on FAT domain and whether this modification activates ATM remains controversial (Bakkenist and Kastan, 2003; Blackford and Jackson, 2017). ATR autophosphorylates T1989 on FAT domain which leads to ATR activation (Liu et al., 2011). DNA-PK autophosphorylates S2056 and T2609, which are not essential to kinase activation but are important to DNA repair (Jette and Lees-Miller, 2015). These kinases have a consensus substrate sequence of a serine or threonine followed by a glutamate (S/TQ). They are found to share some substrates and have overlapping functions in DDR (Bannister et al., 1993; Kim et al., 1999).

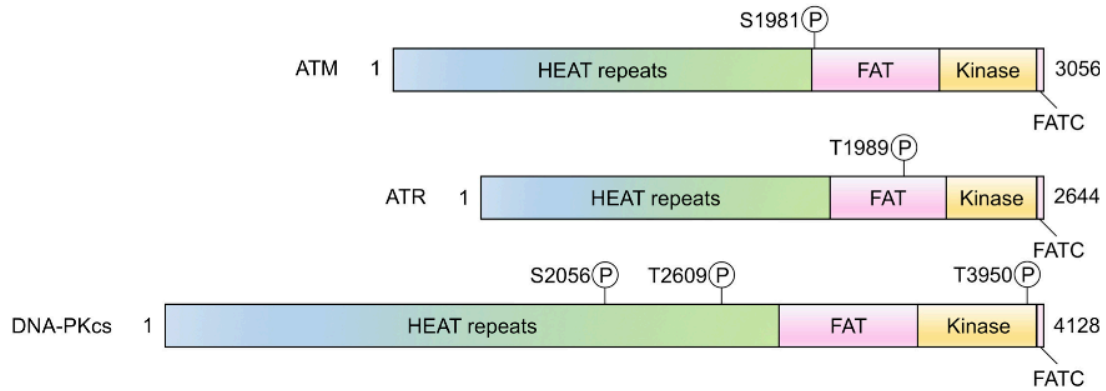
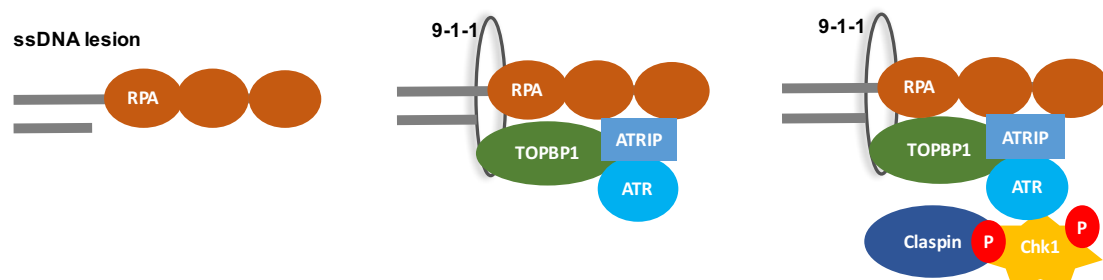


Figure 1.2 Domain organization of ATM, ATR and DNA-PKcs (Blackford and Jackson, 2017)

ATM, ATR and DNA-PKcs contains an N-terminal HEAT repeats and a C-terminal kinase domain flanked by a FAT and a FATC domain. Autophosphorylation sites are marked with residue number.

1.2.3 Activation of the ATR-Chk1 pathway

ATR is essential to cell survival and disruption of ATR in mice leads to early embryonic lethality (Brown and Baltimore, 2000). ATR is activated by an intermediate structure formed by ssDNA-RPA complex. This structure forms when the replicative polymerase stalls at the site of DNA lesion while helicase continues to unwind DNA. The uncoupling of polymerase and helicase generates ssDNA, which becomes coated with RPA to form a ssDNA-RPA complex that in turn recruits a heterodimer of ATR and its subunit, the ATR interacting protein (ATRIP) (Figure 1.3). The interaction of an acidic α -helix of ATRIP within an N-terminal basic cleft of RPA is required for the association of ATR-ATRIP complex to ssDNA-RPA (Ball et al., 2007). Resection of DNA strand at DNA damage site or replication fork is promoted by DDK, which initiates checkpoint signalling (Sasi et al., 2017).



(Caption on next page)

Figure 1.3 A brief schematic demonstration of ATR-Chk1 pathway activation

ssDNA is covered by RPA and the structure formed by the two components is crucial to ATR recruitment and activation. ATR further activates its substrate Chk1, which leads to signal transduction cascade through phosphorylating a wide spectrum of effector proteins. The activation of Chk1 requires a mediator, Claspin, which interacts with Chk1 and contributes to its full activation. Other factors are omitted in this figure for clarity.

The recruitment of ATR-ATRIP to RPA-bound ssDNA involves a precise sequence of molecular contacts. It is facilitated by Sirtuin 2 (SIRT2) deacetylation of K32 on ATRIP, which introduces a conformational change and strengthens the association of ATRIP with ssDNA-RPA (Zhang et al., 2016). The Rad17-RFC complex then binds to the junction of ssDNA-RPA and dsDNA and recruits the trimeric complex Rad9-Rad1-Hus1 (9-1-1) onto DNA damage site. S387 on the C-terminal tail of Rad9 is phosphorylated, which is required to interact with DNA topoisomerase II binding protein 1 (TopBP1) (Delacroix et al., 2007). TopBP1 is thus positioned next to the ATR-ATRIP complex and interacts and activates ATR through its activation domain (Zhou et al., 2013). Apart from TopBP1, Ewing's tumour-associated antigen 1 (ETAA1) is also identified as an ATR activator. ETAA1 directly interacts with RPA through two RPA-binding motifs. Recruitment of 9-1-1-TopBP1 and ATR-ATRIP complex requires the same intermediate but the process is mostly independent. It is intriguing that cells require two receptors to activate ATR pathway. An explanation for this phenomenon is to avoid false activation of ATR by ssDNA-RPA structure generated from the normal replication process on the lagging strand. Another possibility is that sustained recruitment of ATR-ATRIP and 9-1-1 complex to DNA damage site increases their local concentration which leads to sustained interaction between ATR-ATRIP and TopBP1 and thus ATR activation (Cimprich and Cortez, 2008).

In conditions of moderate replication stress, such as slowed replication speed induced by common fragile sites, ATR is recruited to chromatin and activated, while other crucial DDR factors including ATM, Chk1 and p53 remain inactive. The partial

activation of DDR allows protection of replication forks without delaying cell cycle progression. It indicates that the activation of the ATR pathway is dependent on the level of replication stress (Koundrioukoff et al., 2013).

Sensor protein ATR phosphorylates substrates on the site of DNA damage and the spread of DDR to the cell is mainly performed by its effector proteins. ATR activates Chk1 by sequentially phosphorylating Chk1 residues S317 and S345, an evolutionarily conserved activation step that is conserved from yeast to metazoan. Phosphorylation on S317 is a prerequisite of efficient phosphorylation on S345, which yields maximal checkpoint activation in response to DNA damage (Wang et al., 2012b). Nuclear retention of Chk1 with phosphorylated S345 is maintained by interaction with 14-3-3 β and ζ isoforms, which masks the NES on Chk1, thus leading to its nuclear retention (Jiang et al., 2003). In unperturbed conditions, phosphorylation of S317 is not essential to cell viability while phosphorylation of S345 is required to cell survival and localisation at centrosomes during prophase (Wilsker et al., 2008). Activated Chk1 is released from chromatin and undergoes autophosphorylation on S296 to acquire full activation (Okita et al., 2012).

Release of Chk1 from chromatin and spread in the nucleoplasm is supposed to be important to the transduction of DNA damage signal to effectors (Smits et al., 2006). Chromatin association of Chk1 is promoted by K63-linked ubiquitination on K132 under the regulation of B-cell translocation gene 3 (BTG3). Depletion of BTG3 leads to impaired chromatin localization and activation of Chk1 after UV irradiation in U2OS cells (Cheng et al., 2013). Chromatin association is important to Chk1 activation by ATR on S345 in response to replication stress, nevertheless the attachment of the ubiquitination chain inhibits Chk1 activity as K132 locates on the catalytic loop and functions in ATP binding. Deubiquitination at K132 on Chk1 by ubiquitin-specific protease 3 (USP3) leads to Chk1's chromatin dissociation and full activation (Cheng and Shieh, 2018).

The activation of Chk1 requires its interaction with an adaptor protein, Claspin. When Claspin is depleted, cells undergo reduced cell cycle arrest in response to DNA replication stress (Kumagai and Dunphy, 2000). Claspin undergoes phosphorylation on its Chk1 kinase binding domain (CKBD) which creates a Chk1-binding site. Several kinases, including Chk1, DDK and Casein kinase 1 γ 1 (CK1 γ 1) have been reported to be responsible for Claspin phosphorylation on CKBD, though the identity of the kinase remains to be confirmed and more observations are required to elucidate the exact mechanism of Claspin phosphorylation (Chini et al., 2006; Kim et al., 2007; Meng et al., 2011).

Chromatin association of Claspin is regulated by another FPC component, And1. Phosphorylation on T826 by ATR after replication stress promotes And1 localization at ssDNA and interaction with Claspin. Claspin is thus enriched on ssDNA which plays a vital role in mediating Chk1 activation at DNA damage site (Hao et al., 2015). Chromatin association of Claspin is also enhanced by BRCA1, which forms a heterodimer with Bard1 to acquire E3 ligase activity. It is found to selectively trigger Chk1 activation in response to topoisomerase inhibition through ubiquitinating Claspin and sustains its binding to DNA (Sato et al., 2012).

The Cdc25 phosphatase isoforms are important effectors in ATR-Chk1 checkpoint pathway. In addition to Cdc25C regulation discussed in section 1.1.2, Cdc25A undergoes regulation by checkpoint mechanism. Cdc25A forms a complex with 14-3-3 γ in response to DNA damage and it is speculated that the dimeric 14-3-3 γ bridges Chk1 and Cdc25A by forming a ternary complex which promotes Cdc25A phosphorylation on S76 by Chk1 (Kasahara et al., 2010). 14-3-3 is a family of acidic dimeric proteins involved in a wide range of cellular processing including signal transduction, cell cycle control and apoptosis. Seven isoforms have been identified in mammals, of which the β and ζ isoforms bind to S345-phosphorylated Chk1, while 14-3-3 γ specifically interacts with S296-phosphorylated Chk1 (Kasahara et al., 2010). Chk1-mediated phosphorylation of Cdc25A at S76 promotes further phosphorylation

within Cdc25A phosphodegron site by undefined kinases and leads to proteasomal degradation of Cdc25A by the ubiquitin ligase SCF^{βTrCP} (Jin et al., 2003). The activity of CDK2 is suppressed as a consequence of Cdc25A destruction, which leads to cell cycle arrest. In addition to the Cdc25A pathway, p53 regulates CDK2 suppression in an ATR/ATM and Chk1/Chk2 dependent manner. Active p53 triggers the expression of a CDK2 inhibitor, p21, which suppresses CDK2 activity and prevents entry into M phase (Moiseeva and Bakkenist, 2018).

1.2.4 Causes of DNA replication stress

Replication stress is a major cause of DDR activation. It refers to conditions that impede DNA synthesis or replication fork progression, resulting in generation of aberrant fork structure and function, and leading to DNA breakage and unscheduled recombination events (Jossen and Bermejo, 2013). It is being considered a hallmark of cancer as it occurs in most cancer cells and it is a cause of other cellular behaviour that promote cancer, such as apoptosis escape and genome instability (Macheret and Halazonetis, 2015). Replication stress can be generated from a wide spectrum of causes including endogenous and exogenous insults (Figure 1.4).

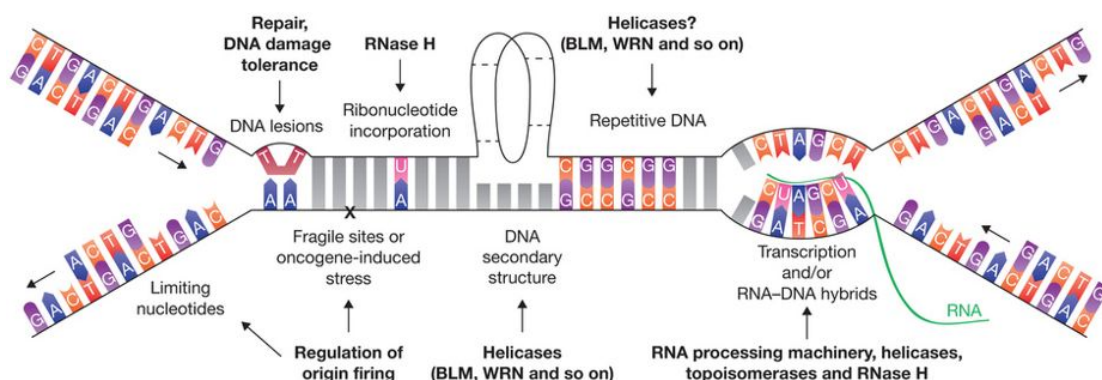


Figure 1.4 Causes of replication stress (Zeman and Cimprich, 2014)

Replications stress are caused by a variety of reasons including DNA lesions, CFS, transcription-replication conflicts, etc. DDR is activated in response to replication stress to maintain genome integrity.

Reactive oxidative species (ROS) produced by cellular metabolic reactions are a primary endogenous source of DNA damage which causes oxidised bases, ssDNA breaks and dsDNA breaks (Bont and Larebeke, 2004). Exogenous genotoxic factors can be further classified as having a physical and chemical nature. Physical factors include ultraviolet light (UV), which induces pyrimidine dimers and photoproducts. Ionising radiation (IR) promotes base oxidization, ssDNA and dsDNA breaks. DNA-damaging agents are used in chemotherapy, such as alkylating agents and crosslinking agents, which generate a range of DNA lesions including alkylated bases and intra- or inter-strand crosslinks. Topoisomerase inhibitors induce ssDNA and dsDNA breaks and covalent protein-DNA intermediates, while chemicals generated from cigarette smoking cause DNA adducts and oxidative damage (Ciccia and Elledge, 2010).

Replication stress can also be generated by misincorporated ribonucleotides, DNA secondary structure formed by trinucleotide repeats or GC-rich G-quadruplexes, collisions between the machineries of replication and transcription, shortage of replication factors, common fragile sites (CFS) and overexpressed oncogene (Zeman and Cimprich, 2014). These causes result in genome instability, and consequently DNA damage response (DDR) is activated to ensure faithful DNA replication in each cell cycle.

1.2.5 Inhibition of late origin firing

A consequence of checkpoint activation is inhibition of late origin firing, which prevents the formation of more stalled replication forks and ensures DNA integrity in response to replication stress. In bacteria, DNA replication initiates from a single origin on a circular chromosome. In contrast, eukaryotic cells have larger genomes which require that DNA replication is initiated from multiple origins. In eukaryotes, cells license many origins but only 10 % of these licensed origins are fired during DNA replication in unperturbed S phase (McIntosh and Blow, 2012). The unfired

origins remain dormant and only initiate when necessary. In human cells, over 5,000 replicons are activated for DNA replication in S phase (Chagin et al., 2016). Origin usage varies depending on its firing efficiency, the proportion of cells firing a specific origin in a population, and timing, which refers to the time an origin fires in S phase. An important feature of DNA replication is that different origins are programmed to fire at different times in S phase, and are therefore categorised as “early-” and “late-” firing origins. Early origins are frequently located in transcriptionally active chromatin domain whereas late origins are associated with transcriptionally inactive heterochromatic regions of the genome (Fragkos et al., 2015). Furthermore, the pattern of origin firing varies among cell types (Aze and Maiorano, 2018).

The S-phase checkpoint regulates DNA replication through origin firing control. Conversely, inhibition of the ATR/ATM pathway in unperturbed cells leads to unrestrained origin firing, which produces genome instability (Shechter et al., 2004). When checkpoint signalling is activated by replication fork arrest, local dormant origins in proximity to the stalled fork become activated while late origin firing is restrained globally (Yekezare et al., 2013). Thus, activated dormant origins in the vicinity of the arrested fork can complete the replication of the region where replication stalled, while inhibition of distal origins avoids generation of more stalled replication fork (Yekezare et al., 2013).

In budding yeast, active Rad53 downregulates both DDK and CDK pathways to block origin firing in different mechanisms during checkpoint activation. Direct Rad53 phosphorylation of Dbf4 prevents MCM activation by DDK whilst Rad53 targets a CDK substrate, Sld3, to prevent its interaction with Cdc45 and Dpb11 and to inhibit origin firing. This mechanism allows CDK to stay active which has a crucial function of preventing re-licensing of origins in budding yeast during S phase (Zegerman and Diffley, 2011). In metazoan, a global fork slowing and reversal under the regulation of ATR is initiated in response to replication stress. This global effect safeguards the chromosomal integrity by allowing time for repair or lesion bypass (Mutreja et al.,

2018). DNA replication components are also involved in origin firing regulation. Promotion of DNA replication requires an interaction between TopBP1 and Treslin. This interaction is promoted by cyclin E/CDK2 phosphorylation on Treslin while cells with abolished phosphorylation are deficient in DNA replication (Kumagai et al., 2011). CDK2 activity is suppressed in response to checkpoint activation which leads to disruption of origin firing. A Cdc25C/CDK2-independent origin inhibition pathway was revealed in response to replication stress generated by UVC and the reactive metabolite of benzo[a]pyrene (BPDE). Chk1 regulates DDK suppression through phosphorylating the Dbf4 subunit which inhibits replicon initiation. These results reveal the existence of several checkpoint mechanism in response to different stimuli (Heffernan et al., 2007).

1.2.6 Protection of replication fork

Another consequence of DDR regulation is replication fork protection. Replication fork stability can be protected through inhibition of late origin firing which maintains an RPA pool required to protect ssDNA generated from uncoupling of helicase and polymerase. RPA covers and prevents ssDNA from nucleolytic damage and hairpin structure formation. RPA regulates DNA repair activities and exhaustion of the cellular stocks of RPA leads to global replication catastrophe which can be prevented by checkpoint signalling through regulation of origin firing (Toledo et al., 2013).

A major role of FPC is to protect replication fork integrity through linking helicase and polymerase during fork progression. Chromatin association of FPC components requires interaction with RPA. RPA consists of three subunits: RPA70, RPA32 and RPA14 which are conserved in eukaryotes. It contains four DNA binding domains and binds to DNA in different conformations depending on the length of nucleotides and domains involved (Bastin-Shanower and Brill, 2001). Conformational change of RPA leads to varied binding affinity to FPC components Timeless/Tipin, a heterodimeric complex which specifically binds to RPA in the 30nt-binding mode, whereas the

interaction is compromised when RPA is in the 8nt-binding mode. The variation in binding affinity suggests a model where Timeless/Tipin is loaded between helicase and polymerase by RPA in the 30nt-binding mode, whilst RPA dissociates from replisome by transforming to the 8nt-binding mode. Checkpoint activation in the presence of ssDNA promotes RPA association in the 30nt-binding mode, thus recruiting Timeless/Tipin to help mediate checkpoint signaling (Witosch et al., 2014).

An important effector protein in fork protection is Werner syndrome protein (WRN), a member of RecQ helicase family which regulates replication fork stability and recovery in two steps. At an early stage of fork arrest, ATR phosphorylates WRN on multiple C-terminal residues and triggers WRN re-localization and interaction with RPA on stalled forks. The recruitment of WRN stabilises replication fork through preventing DSBs formation. However, when DSB is generated from the collapsed fork, WRN dissociates from nuclear foci in an ATM-dependent manner which allows DNA repair mediated by recombinase RAD51 (Ammazzalorso et al., 2010). BLM, another RecQ helicase, promotes fork restart under the regulation of ATR through phosphorylation at T99 and T122 (Davies et al., 2004). FANCD2 is an effector protein in FA pathway and associates with MCM under the control of ATR. The recruitment of FANCD2 at stalled replication fork restrains DNA synthesis and ssDNA accumulation which further avoids p21 induction and cell senescence (Lossain et al., 2013).

Replication fork regression is the process that fork moves backward and newly synthesised DNA strands anneal to form a Holliday junction. It is considered as a replication fork stabilization mechanism under the regulation of activated checkpoint kinase ATR. Consequences of replication regression include reducing ssDNA formation, allowing DNA lesion repair and promoting lesion bypass which is beneficial to fork stabilization and DNA damage repair (Cortez, 2015). SMARCAL1 is a DNA translocase which catalyses fork reversal at stalled replication fork through the interaction with RPA. Moderate replication fork regression improves genome

stability while unregulated fork regression generates substrates of SLX-4-dependent endonucleases which generate DSBs and fork instability. ATR phosphorylates SMARCAL1 at S652 which inhibits its activity and regulates SMARCAL1 activity at a proper level which promotes fork stability (Couch et al., 2013).

1.2.7 Recovery from checkpoint activation

Cells need to recover from cell cycle arrest and resume cell cycle progression when DNA damage is eliminated. Checkpoint recovery involves checkpoint termination and cell cycle resumption. Failure in checkpoint recovery may result in replication fork instability which generates DNA breaks or abnormal DNA structures. S phase checkpoint recovery also needs to be coupled with cell cycle restart otherwise genome instability is generated when cell progresses to cell cycle with under-replicated DNA (Chaudhury and Koepp, 2016). Termination of checkpoint response is mediated through degradation of checkpoint-related proteins. Phosphorylation at S345 of Chk1, which is essential to its activation, also marks it for ubiquitin-directed proteasomal degradation at a later time. It is speculated that phosphorylation on S345 leads to exposure of a degron motif which stimulates ubiquitination by Cull1/Cul4A-containing E3 ligases (Zhang et al., 2005). In unperturbed conditions or upon DNA damage, Chk1 is protected by Ataxin-3 (ATX3), a deubiquitinase which antagonizes Cull1/Cul4A-containing E3 ligases. After prolonged replication stress, the interaction between activated Chk1 and ATX3 weakens, which leads to the proteasomal destruction of Chk1 and resumption of the cell cycle (Tu et al., 2017). Recovery from checkpoint activation induced by hydroxyurea is regulated by SCF-mediated Claspin destruction. A DSGxxS degron located at N-terminus of Claspin is phosphorylated by Plk1 which leads to Claspin ubiquitination by SCF^{βTrCP} (Peschiaroli et al., 2006), in turn reducing Chk1 activation and thus inhibiting checkpoint signaling. Another mechanism of checkpoint termination involves γH2AX dephosphorylation by the p53-induced phosphatase 1 (Wip1), a serine/threonine phosphatase which recognises a consensus substrate sequence of pS/TQ.

Dephosphorylation of γ H2AX eliminates its function in recruiting DNA repair factors after checkpoint signalling and thus contributes to cell cycle restart (Macurek et al., 2010). Furthermore, cell cycle resumption is regulated by Plk1 which deactivates Wee1 and in turn reactivate CDKs which drives cell cycle progression (Vugt et al., 2004).

1.2.8 DDR and cancer therapy

DDR safeguards genome stability in response to DNA damage and ensures genome information is passed to next generations with high fidelity. When cell accumulates large scale of severe damaged DNA, DDR induces cellular senescence and apoptosis. In the case of erroneous repair or replication bypass, mutations can be introduced to daughter cells which can lead to cancerous transformation if the mutation is located on oncogene or tumour suppressor genes. Effective DNA repair is thus important to prevent cancer. Meanwhile, the DDR pathway has been a target of cancer therapy because impaired DDR leads to accumulation of DNA lesions which reduces cancer growth and induces apoptosis of cancer cell (Torgovnick and Schumacher, 2015). Platinum compounds, such as cisplatin, carboplatin, and oxaliplatin, are widely used chemotherapeutic drugs which modify DNA structure through introducing inter- and intrastrand crosslinks. The platinating agents are effective to some cancer types while resistance can be developed via varying mechanisms including upregulated DDR components (Rabik and Dolan, 2007). Combined treatment with DDR inhibitor is used to cope with the resistance while the toxicity remained as a challenge. The development of synthetic lethality enhances the efficacy and specificity of cancer therapy. It is based on observations that the inactivation of two genes from different DDR pathways leads to cell death while mutation on either of the single gene does not influence cell viability. Cancer cells often carry impaired DDR components and treatment using synthetic lethality methodology leads to selective killing when those cancer cells rely on the remaining DDR pathways to survive (Minchom et al., 2018). One well developed synthetic lethality therapy is using poly(ADP-ribose)-polymerase

(PARP) inhibitors to treat BRCA1/2-deficient cancer cells. PARP1 and PARP2 are sensors of SSB and are an essential regulator of base excision repair (BER). Inactivation of PARP leads to impairment of SSB repair which finally turns into DSB. Repair of DSB usually depends on HR which is mediated by BRCA1/2. The cancer cells carrying these deficient genes are defective in DSB repair which in turn go to apoptosis (Turner et al., 2005). Olaparib is a PARP1 inhibitor and is considered a promising drug to treat BRCA-deficient ovarian and breast cancer (Gelmon et al., 2011; Tutt et al., 2010).

Oncogene activation induced replication stress is considered to be a major source of genome instability in cancer cells (Hills and Diffley, 2014). ATM gene mutations are common for cancer cells, leaving cells to rely on the ATR-Chk1 pathway in DDR (Choi et al., 2016). Deletion of ATR or Chk1 protects cells from being tumorigenic, indicating cancer cells rely on this efficient DDR pathway to survive from heavy replication stress. ATR-Chk1 signalling pathway suppresses origin firing, which reduces replication pressure under replication stress and thus prevents cancer cell death. Inhibitors targeting the ATR-Chk1 pathway, therefore, are sensible anti-cancer drug candidates. Given by the function of ATR/Chk1 in cancer cell survival, initial ATR/Chk1 inhibitors were designed as a sensitizer of chemotherapy or radiotherapy. In combination with DNA damage agents, ATR/Chk1 inhibitors enhance killing of cancer cells through inhibiting cell cycle checkpoint. ATR/Chk1 inhibitors are also developed as single agents which target on replication stress in tumour cells. VX-970 is an ATR inhibitor which showed tumour control in monotherapy and in combination with carboplatin (O'Carrigan et al., 2016). It is also found to be effective to advanced solid tumour suppression in combination with cytotoxic regents including gemcitabine and cisplatin (Plummer et al., 2016; Shapiro et al., 2016). An oral ATR inhibitor, AZD6738, showed promising potential in suppressing non-small cell lung cancer as a monotherapy or in combination with gemcitabine and cisplatin (Vendetti et al., 2015).

Drug development on ATR inhibitor is challenged by several characteristics including large-size of the protein, S-G2 phase-specific activity and similar active site to other PIKK family proteins. The Chk1 inhibitor is better developed than ATR because ATR has broader biological functions than Chk1 which makes ATR inhibitors more aggressive to normal cells (Qiu et al., 2017).

Many Chk1 inhibitors are invented and several of them have reached clinical phase I/II trials. UCN-01, XL844 and CBP501 are a set of inhibitors which have a broad range of the target and their clinical applications are restrained because of a lack of specificity. AZD7762 is an ATP-competitive inhibitor which made promising progress in killing HR-deficient cancer cells while the clinical trial has been terminated because of toxicity and side effects. PF-00477736 is also an ATP-competitive inhibitor which has high selectivity but the development was stopped for business reasons. Other inhibitors, such as LY2603618, MK-8776, and LY2606368, are selective Chk1 inhibitors and efficacy of which remain to be learnt. Development of Chk1 inhibitors for monotherapy or in combination with other therapies is still in progress and identification of biomarkers will be helpful to improve the progress (Qiu et al., 2017).

1.3 Enzymatic and structural characterization of Chk1

1.3.1 Brief overview of protein kinase superfamily

Protein kinases catalyse the phosphoryl transfer from γ -phosphate of an ATP molecule to the hydroxyl group on a serine, threonine or tyrosine residue. Phosphorylation results in a conformational change which is a cause of function changes leading to the substrate activation or deactivation (Swulius and Waxham, 2008). It is thus an important post-translational modification involved in cellular signalling. 518 putative kinase genes have been identified which accounts to 1.7% of the whole human genome (Manning et al., 2002). The protein kinase superfamily can be categorised into 9 groups which are further divided into 134 families (Manning et al., 2002).

Activity of a kinase is regulated by various factors. Some kinases, such as PKA, CDK2 and MAPK, require phosphorylation on its activation loop to become active. The phosphorylation is usually performed on a conserved threonine, which positions the catalytic loop into an active position by interacting with other amino acids (Hunter, 1995). Regulatory subunit/domain interaction is another common factor which regulates kinase activity. PKA remains inactive in complex with a regulatory subunit which interacts and inhibits the catalytic subunit. Dissociation of the regulatory subunit from the catalytic subunit is stimulated by binding to cAMP (Walsh et al., 1968). The release of the regulatory subunit leads to the activation of PKA but not all regulatory subunit has a negative effect on kinase activity. For example, CDK2 remains unphosphorylated and inactive when it is in a monomeric form. Upon binding to a cyclin subunit, T160 on its activation loop becomes accessible and phosphorylation on this residue leads to CDK2 activation (Solomon et al., 1993). Kinase phosphorylates a substrate based on the residues flanking the site of phosphorylation. Phosphate receptor residues are anchored differently to the catalytic cores depending on the interactions formed between the substrate and the kinase backbone (Taylor et al., 1995). Kinases thus can be categorised into serine/threonine-specific kinase and tyrosine-specific kinase. Some kinases, such as

Wee1, are dual-specificity kinase which is capable of phosphorylating both serine/threonine and tyrosine residues (Lindberg et al., 1992). Despite different regulation mechanism and protein size, all eukaryotic kinases share a conserved ~250-300 amino acid catalytic core, consisting of a β -strand rich N-terminal lobe and an α -helix rich C-terminal lobe with a linker in between (Talor et al., 1992). cAMP-dependent protein kinase (PKA) is introduced as an example for structural and functional studies of kinase.

1.3.2 PKA is a prototype of kinase studies

The first kinase structure solved was the catalytic subunit of PKA in 1991 by Knighton et al. (Knighton et al., 1991). The catalytic subunit is a 350-amino-acid polypeptide, which can be expressed in *E.coli* in an active form (Talor et al., 1992). PKA has a simple activation mechanism and the above-mentioned features make it a prototype of the kinase family for studies (Talor et al., 1992). It provides a good example on substrate recognition and kinase catalysis procedure. PKA forms an inactive holoenzyme consisting of two catalytic subunits and two regulatory subunits. Upon cAMP binding to the regulatory subunit, the catalytic subunit dissociates from the complex and becomes active (Walsh et al., 1968). The structure of the catalytic subunit of PKA has been determined as an apoenzyme (PDB#1J3H), in binary complex with adenosine or a phosphopeptide (PDB#1BKX and 1JLU), in ternary complex with ATP and peptide inhibitor or with ADP and substrate peptide (PDB#1ATP and 1JBP), and in transition state complex with ADP, aluminium fluoride (AlF₃) and substrate peptide (SP20) (PDB#1L3R). By comparing the structures from different states, PKA catalysis mechanism is interpreted. The apo catalytic subunit adopts an open conformation with an accessible ATP binding site and the overall molecule in solution is dynamic (Madhusudan et al., 2003). The most conserved motif in the N-terminal lobe is a glycine-rich motif (GxGxxG) on the first two β strands. This is a dynamic region and is responsible to stabilise nucleotide in the ATP-binding pocket (Taylor and Kornev, 2011). Two conserved amino acid residues, K72 and E91,

form an ion pair and function in combination with the glycine loop in stabilising the ATP molecule from the N-terminal lobe (Talor et al., 1992). A hydrophobic core is formed at the centre region between the two lobes which anchors the catalytic loop (residues 166-171) and magnesium-positioning loop (residues 184-187) through interactions with the hydrophobic side chains on these loops (Taylor et al., 2004). Invariant residues D166 and N171, as well as the highly conserved residues R165 and K168, locate in the catalytic loop where the major catalysis event is processed (Talor et al., 1992). The hydrophobic core not only provides an ATP and substrate binding site but also maintains residues R165 and D166 in a correct orientation to catalyse phosphoryl transfer (Madhusudan et al., 2003). Instead of the hydrophobic interaction, the activation loop (residues 184-208) is positioned in an active conformation through hydrogen-bonds and ionic interactions generated by a phosphorylated T197 (Smith et al., 1999). Upon ATP binding, residues on the N-terminal lobe are flexible and the glycine-rich loop (residues 48-57) moves towards the active site. The critical step in catalysis is having the glycine-rich loop firmly engaged to the active site while at this intermediate stage, the tip of the loop remains dynamic and the kinase is not in catalysis structure (Taylor et al., 2004). On the other side, residues on the C-terminal lobe are mostly preformed and these include the conserved residues D166 and K168 which directly interact with the γ -phosphate during catalysis and Mg^{2+} coordinating residues N171 and D184 (Madhusudan et al., 2003). Conformational change on substrate binding residues (E127, R133, and F239) is introduced by ATP binding which prepares the residues to a substrate binding orientation (Madhusudan et al., 2003). AlF₃ mimics the structure of a γ -phosphate molecule and it was crystallized in complex with PKA catalytic subunit, ADP and SP20 to mimic a transition state of catalysis. At this stage, γ -phosphate is oriented for nucleophilic attack through hydrogen bonding with backbone amide of S53 (Madhusudan et al., 2002) (Figure 1.5). The conserved residue in the catalytic loop, K168, forms hydrogen bonds with the P-site serine and γ -phosphate, indicating an important role in phosphoryl transfer. Another conserved residue is D166, which functions in orienting nucleophile and catalysing phosphoryl transfer to the recipient serine through hydrogen bonding

nucleated from its carboxylate group (Madhusudan et al., 2002). Water molecules are excluded from the active site in this closed kinase conformation, allowing maximal catalysis efficiency through bringing phosphate donor and acceptor in close proximity (Taylor et al., 2004).

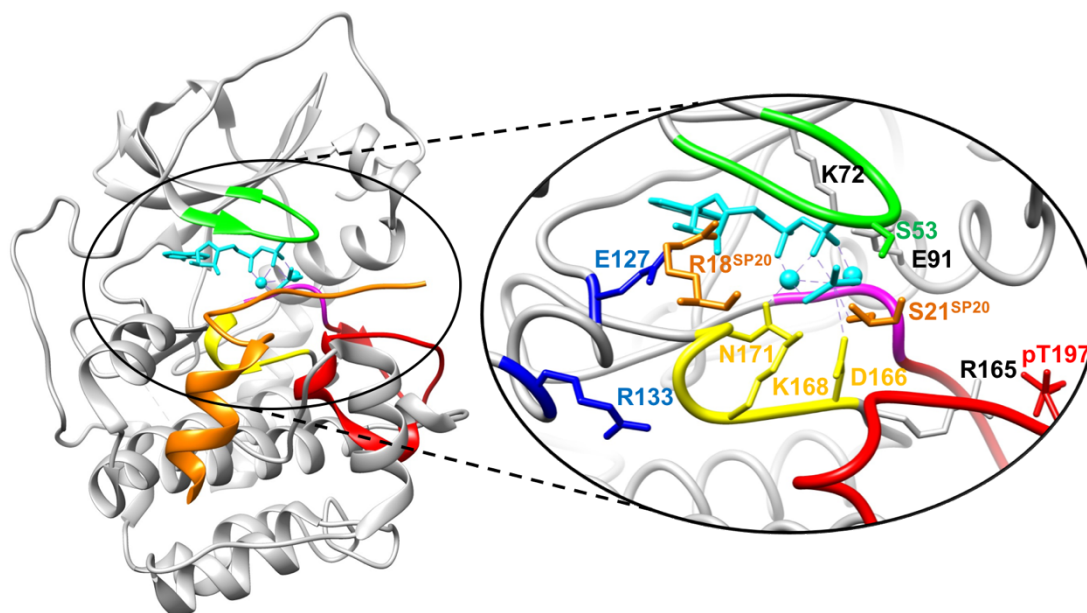


Figure 1.5 Structure of PKA in complex with ADP, AlF₃ and SP20 highlighting the ATP positioning and catalysis related amino acid residues

The structure of the transition state PKA in complex with ADP, AlF₃ and SP20 is shown in grey ribbon. The glycine-rich loop, catalytic loop, magnesium-positioning loop and activation loop are shown in green, yellow, magenta and red. ADP, AlF₃ and magnesium ions which mimic the ATP at the transition state are shown in cyan. The substrate SP20 is shown in orange. The key amino acid residues involved in ATP-positioning and structure stabilising are annotated. More detailed description is in the main text. Figure of the protein structure was generated in Chimera (Pettersen et al., 2004).

1.3.3 Structural features and activation mechanism of Chk1

Human Chk1 is a 476-amino acid serine/threonine kinase which belongs to the Ca²⁺/calmodulin-dependent kinase-like (CAMKL) family. Chk1 consists of a conserved N-terminal kinase domain, a linker with varying length and a C-terminal kinase associated 1 domain (KA1) (Figure 1.6). Crystallization structure of Chk1 N-terminal kinase domain (Chk1KD) shows it adopts an open conformation and Chk1KD has higher kinase activity than full-length Chk1 (Chk1FL) (Chen et al.,

2000). Chk1KD consists of a small N-terminal β -strand-rich lobe and a C-terminal α -helix-rich lobe. Unlike PKA, apo Chk1KD has the same conformation with its binary complex with ATP analog AMP-PNP and no intermediate conformation was observed upon nucleotide binding (Chen et al., 2000). Chk1 activation does not require a phosphorylation modification on its activation loop. The positioning of Chk1 activation loop is oriented by secondary structure and side chain interactions with the core of the C-terminal lobe which keeps the activation loop at an active state in apo structure (Chen et al., 2000). This arrangement of the activation loop indicates the activation of Chk1 is likely regulated by inter- or intramolecular interactions. Chk1 constructs with mutations on its C-terminal kinase association domain (KA) which induces conformational change on KA have higher kinase activity than wild-type (WT) and the increase on the activity does not require phosphorylation on S345. This suggests a model of Chk1 activity regulation that the C-terminal domain has an inhibitory role in its activity which is reversed by the introduction of mutations on KA. The phosphorylation on S317 and S345 by ATR is proposed to result in conformational change on Chk1 and removes the auto-inhibition effect. Structural analysis on Chk1 KA1 shows the C-terminal 100-amino-acid domain forms a similar fold as KA1 identified in other proteins including human MARK1 and MAPK. Chk1 KA1 consists of four β -sheet flanked by two α -helices which form a hydrophobic core with an overall basic surface (Emptage et al., 2017). The interaction between Chk1KD and KA1 is supposed to be partially directed by charge-charge interactions and phosphorylation on linker residues may form a shield on Chk1KD domain thus disrupt the Chk1KD and KA1 interaction (Emptage et al., 2017). Two motifs in KA1 domain are identified as conserved motifs (CM1 and CM2) which functions as a nuclear export sequence (NES) and nuclear localization sequence (NLS) respectively. Translocation of Chk1 is supposed to be important to checkpoint signalling at the level of the whole cell (Wang et al., 2012a).

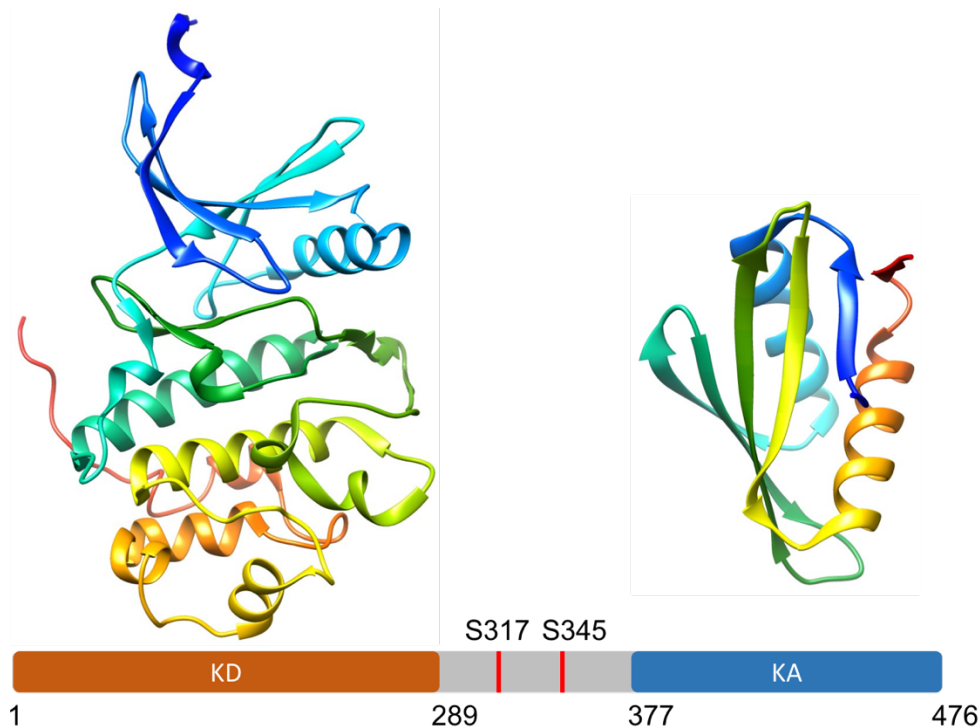


Figure 1.6 Domain structure of human Chk1

Structure of Chk1 kinase domain (pdb#1IA8) and Chk1 kinase association domain (pdb#5WI2) was solved by crystallographic technique. The N-terminal kinase domain adopts an open conformation and remains active when expressed alone. It is followed by a linker region containing two ATR phosphorylation sites (S317 and S345) and a C-terminal domain. A model extracted from these observations is that the auto-inhibitory effect of Chk1 is driven by charge-charge interaction between the two domains and the intramolecular interaction is disrupted when two serine residues are transformed to negatively charged phosphoserines. Figure of the protein structure was generated in Chimera (Pettersen et al., 2004).

1.3.4 Chk1 functions outside checkpoint signalling

In unperturbed conditions, Chk1 associates to chromatin and low level of phosphorylation on S345 is observed which indicates Chk1 keeps a basal activity in normal cycling cells (Jiang et al., 2003). Chk1 maintains genome stability in several ways and cells treated with Chk1 inhibitors undergo increased CDK2 activity, increased RPA recruitment on ssDNA, increased initiation of DNA replication and increased DNA breakage (Syljuåsen et al., 2005). Chk1 regulates origin firing through directly interacting and phosphorylating Treslin at a C-terminal domain, which disrupts loading of Cdc45 on replication origins and in turn suppress origin firings in

unperturbed cells. Cells with the disrupted interaction between Chk1 and Treslin undergo a higher level of origin firing (Guo et al., 2015).

Chk1 is also a crucial mediator in cell cycle progression. Activation of centrosomal cyclin B/Cdk1 drives cell cycle into early M phase and its activity is regulated by Cdc25B. During S and G2 phase in the normal cell cycle, centrosome-associated Chk1 constantly phosphorylates Cdc25B on S230 and suppresses Cdc25B activity which is essential to avoid premature initiation of M phase (Schmitt et al., 2006). Chk1 undergoes phosphorylation on S280 in M phase which is conducted by PIM2 kinase. This phosphorylation promotes Chk1 activity in mitosis which in turn phosphorylates and activates Plk1 thus promotes M phase progression (Adam et al., 2018). Chk1 functions in cytokinesis and protect chromatin stability in the presence of abnormal chromatin bridges. Formation of actin patch maintains intercellular canal between daughter cells which allows time for incomplete chromatin separation to be resolved. Actin patches are regulated by a nonreceptor tyrosine kinase, Src, a substrate of Chk1. Chk1 activates Src through phosphorylating on S51 which in turn delays cytokinesis and prevents chromatin breakage (Dandoulaki et al., 2018).

1.4 Fork pausing complex and Claspin

1.4.1 Claspin structure and its intermolecular interactions

There are two splicing isoforms of human Claspin, Claspin¹³³⁹ and Claspin¹³³² respectively. The most distinctive difference between these two isoforms is that Claspin¹³³⁹ has an evolutionarily conserved C-terminus which cannot be found in Claspin¹³³² isoform. The two isoforms coexist in human cells and both can facilitate checkpoint activation. However, the conserved C-terminus functions in interacting with other checkpoint proteins which are speculated to be essential to efficient Chk1 activation in response to DNA damage. Claspin¹³³² isoform is found to have a less efficient binding ability to Rad9 and cells contain only Claspin¹³³² isoform undergo a delayed Chk1 activation (Liu et al., 2012). Cryo-EM revealed Claspin is a ring-shaped protein which has a higher binding affinity to branched DNA structures than to ssDNA or dsDNA structures (Sar et al., 2004). Human Claspin is predicted to have a pI of 4.5 while the negative charge is not homogeneously distributed over the protein (Figure 1.7). There are two basic patches (BP1 and BP2) residing in an N-terminal replication fork interacting domain (RFID) and an acidic patch (AP) near C-terminus. The distribution of charged patches is speculated to function in interaction with DNA and different proteins (Smits et al., 2018). AP is likely to inhibit Claspin interaction with chromatin via intramolecular interaction with N-terminus and this interaction is disrupted by Cdc7 recruitment and phosphorylation at AP motif. Cdc7 promotes Claspin association on chromatin through phosphorylation and interruption of this event leads to compromised Chk1 activation though the exact sites of phosphorylation remain unclear (Kim et al., 2007). Cdc7 is a serine/threonine kinase which triggers MCM phosphorylation and origin firing. The interaction between Claspin and Cdc7 is also found important to Cdc7 function in origin firing, indicating Claspin has a function in replication initiation via regulating pre-RC (Yang et al., 2016). As described in 1.1.2, Claspin is a component of FPC and its directing binding sites to Tim1 and Pol ϵ are located in N- and C-terminus respectively (Serçin and Kemp,

2011). Chromatin association of Claspin also relies on interaction with helicase co-factor Cdc45 and the binding site is located at N-terminus of Claspin. Chromatin association of Claspin is independent of RPA, which recruits several replication proteins onto replication fork, indicating Claspin associates with chromatin before DNA synthesis and the process is independent of ATR and Rad17 (Lee et al., 2003). C-terminus of Claspin mainly interacts with DNA damage response related proteins including Chk1 and Rad17-RFC. A Chk1-binding domain (CKBD) was firstly identified in *Xenopus* Claspin, which contains two conserved motifs with a sequence of ExxxLCS/TGxFE. Phosphorylation on the serine or threonine residue inside the motifs is required to interact with XChk1 (Kumagai and Dunphy, 2003). The Chk1-binding motif is conserved in human Claspin, which has three conserved motifs. Phosphorylation on T916, S945, S982 on these motifs is essential to Chk1 activation by ATR. Point mutation studies on XChk1 reveal four amino acid residues at N-terminus are required to interact with XClaspin. Crystal structure of human Chk1 KD shows the four corresponding residues (K54, R129, T153, R162) form a sulphate binding site thus it is postulated that these residues form a phosphate binding pocket which docks phosphorylated Claspin (Jeong et al., 2003) (Figure 1.7). These observations generate assumptions on Chk1-Claspin interaction. A model raised from these observations depicts that Claspin functions as a platform which binds one Chk1 molecule on each phosphorylated motif and thus promotes Chk1 activation by ATR or intermolecular autophosphorylation. The rest of the conserved amino acid residues in the Claspin motif might interact with Chk1 side chains to enhance the binding. Whether there are other Claspin binding sites on Chk1 is unknown.

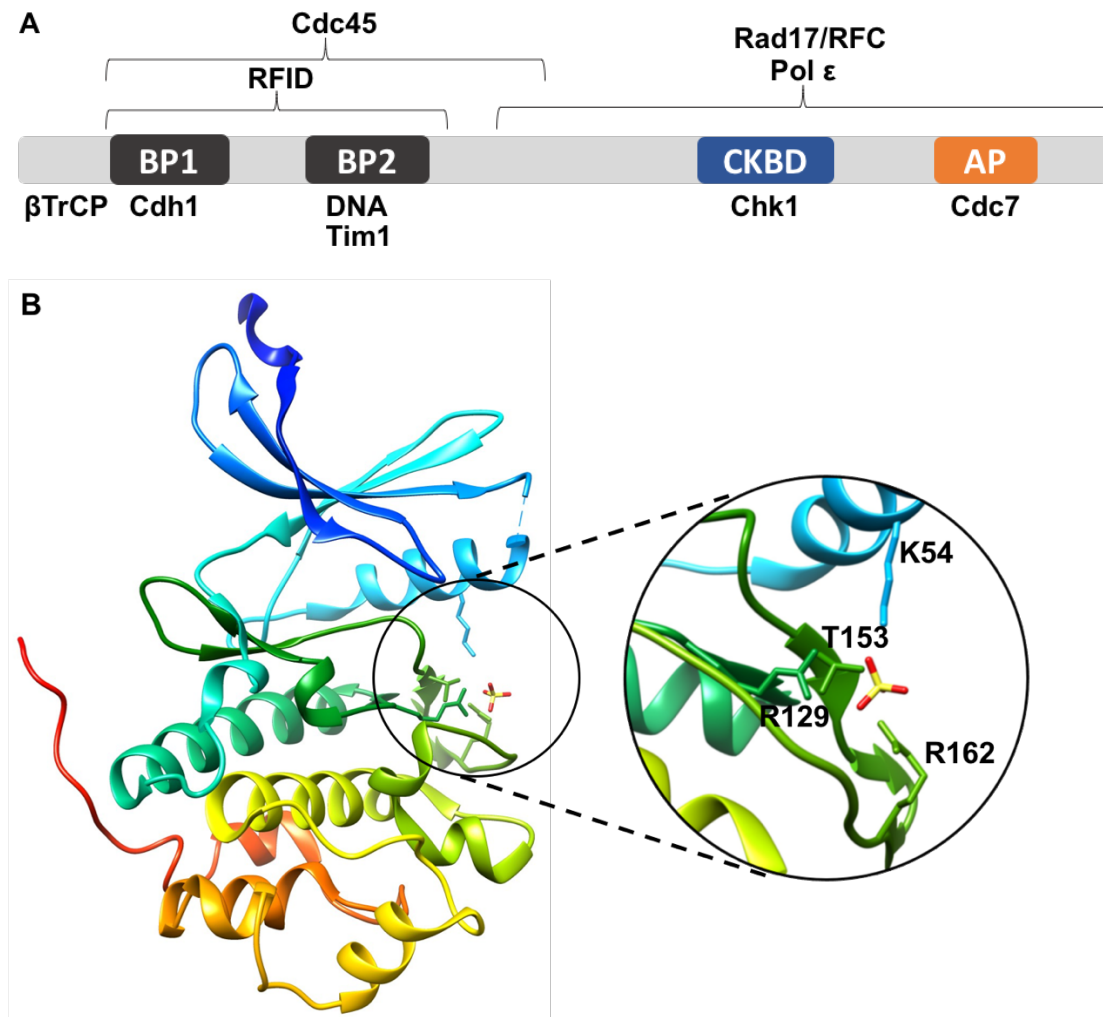


Figure 1.7 Schematic summary of Claspin domains and interactors and putative Claspin binding domain on human Chk1

A: Claspin sequence contains an N-terminal replication fork interacting domain (RFID) with two basic patches (BP), a Chk1-binding domain (CKBD) and a C-terminal acidic patch (AP). These domains interact with proteins involved in Claspin destruction, DNA synthesis and checkpoint signalling. Two degrons at the N-terminus regulate the proteasomal degradation of Claspin through SCF^{βTrCP}-regulated or APC/C^{Cdh1}-regulated ubiquitination. A Cdc45 interacting domain locates at the N-terminus of Claspin. The C-terminus of Claspin interacts with DNA damage response related proteins including Chk1 and Rad17/RFC. As a component of FPC, Claspin interacts with other replisome proteins and the binding sites to Tim1 and Polε locate on BP2 and the C-terminus respectively. Cdc7 promotes the chromatin association through phosphorylating on the AP region. B: Structure of Chk1KD (pdb#1IA8) with the highlight of the four amino acid residues (K54, R129, T153 and R162) which form a putative Claspin binding site where a sulphate ion locates. Figure of the protein structure was generated in Chimera (Pettersen et al., 2004).

1.4.2 Claspin function in FPC

FPC links helicase and polymerase and ensures the integrity of replisome in both unperturbed conditions and DDR. Claspin as well as other two FPC components, Tim1 and Tipin are found to be essential to full activation of Chk1 in response to checkpoint activation (Errico and Costanzo, 2012). Like other components in FPC, Claspin is required to maintain a high rate of replication fork progression (Petermann et al., 2008). It regulates the density of fired origins and prevents progression of replication fork when DNA synthesis is stopped by fork stalling agents. Depletion of Claspin results in increased rate of fork stalling (Scorah and McGowan, 2009).

Claspin function and regulation in unperturbed conditions have also been widely studied in yeast model. Mrc1 (Claspin homolog) forms a heterotrimeric complex and have direct interaction with Tof1 (Tim1 homolog) and Csm3 (Tipin homolog) *in vitro*. Efficient association of Mrc1 to replication fork is dependent on Tof1 and Csm3 and depletion of either of the components lead to compromised Mrc1 association (Bando et al., 2009). Apart from a function in late-firing origin regulation in the checkpoint pathway, Mrc1 also regulates early-firing origin in a checkpoint-independent manner. Hsk1, a fission yeast homolog of Cdc7, phosphorylates a Hsk1 bypass segment on Mrc1 and avoid premature early origin firing at normal replication fork in S phase (Matsumoto et al., 2017). Mrc1 functions in protecting genome stability generated by transcription-replication conflicts. Transcription and replication coexist in S phase and progression of two machineries at the same time may generate obstacles which interfere with faithful duplication of DNA. When the transcription dominantly occurs in S phase, Mrc1 is subject to phosphorylation by multiple kinases on its N-terminus which leads to delay of cell cycle thus safeguards genomic integrity (Duch et al., 2018).

1.4.3 Regulation of Claspin stability

Claspin level fluctuates in the cell cycle. It remains at a low level in G0 and G1 phase and accumulates from S phase which is followed by a rapid degradation in late M phase. Expression of Claspin is regulated by E2F1 under growth stimulation while its degradation is mediated by SCF^{βTrCP} and APC/C^{Cdh1} in M and G1 phase respectively (Bennett and Clarke, 2006; Gao et al., 2009; Iwanaga et al., 2006). Deubiquitinase (DUBs) functions oppositely to ubiquitinase to ensure appropriate checkpoint activation by regulating Claspin level. Deubiquitinating enzyme USP7 specifically counteracts degradation mediated by SCF^{βTrCP} in M phase and USP28 is found to regulate Claspin deubiquitination in opposing function to APC/C^{Cdh1} in G2 phase (Bassermann et al., 2008; Faustrup et al., 2009). USP20 stabilises Claspin in S phase by removing K-48 linked polyubiquitination on Claspin. USP20 is suppressed by HERC2 in unperturbed cells and undergoes phosphorylation by ATR during checkpoint activation. Phosphorylation on USP20 leads to its dissociation from HERC2 and stabilises USP20 which in turn promote checkpoint activation through stabilising Claspin (Zhu et al., 2014). The reversible ubiquitination on Claspin plays an essential role in checkpoint activation and genome stability.

1.5 Perspective and aims

Chk1 is a critical messenger of checkpoint signalling stimulated by DNA damage. It is a 476-amino-acid serine/threonine kinase consisting of an N-terminal kinase domain, a C-terminal regulatory domain and a linker in between. Crystallographic studies have revealed the structures of the two domains separately, leaving the linker region with about 100-amino-acid-length unresolved. The intact full-length Chk1 structure remains unknown and the intramolecular interaction between the two Chk1 domains is unclear. Although the features of the catalytic domain are conserved among all protein kinases, the regulation of kinase activity varies. Understanding on the structural information from an atomic level will shed light on kinase activity regulation and activation mechanism. Biophysical and biomedical studies were applied on Chk1KD and Chk1FL to acquire the overall structural information of full-length Chk1 and the intramolecular binding interface between the two domains. The results shape an auto-inhibition model of Chk1FL activity regulation through a direct intramolecular interaction. The auto-inhibitory effect was studied by Chk1 kinase assays which indicated the inhibition was generated by blocking of ATP binding site on Chk1KD. The result is helpful to interpret Chk1 activation mechanism *in vivo* where the upstream kinase ATR and other mediators are involved. The result is also helpful to the invention of selective kinase inhibitor in cancer therapy.

Chk1 activation requires phosphorylation on S317 and S345 by ATR in checkpoint activation and the adaptor protein Claspin is essential to this process. Depletion of Claspin from *Xenopus* egg extracts abolishes Chk1 activation and leads to a strongly compromised cell cycle arrest in response to DNA replication blocks (Kumagai and Dunphy, 2000). Chk1-binding domain has been identified on *Xenopus* Claspin and human Claspin containing a tandem repeat of two or three Chk1-binding motifs respectively (Kumagai and Dunphy, 2003). Phosphorylation on a site-specific threonine or serine on those motifs is essential to Claspin's interaction with Chk1 but the structural basis of the interaction remains unclear. Direct interaction between

Claspin and Chk1 was visualised by co-immunoprecipitation assays where phosphoserine was incorporated into the target site using amber codon suppression technique. The binding kinetics and affinity was studied using bio-layer interferometry and fluorescence polarization assays, which showed the three motifs on Claspin contribute equally to Chk1 binding. The quantitative measurement provides direct evidence on the intermolecular interaction between Claspin and Chk1, which sheds light on the interpretation of the dynamic molecular interaction during Chk1 activation. Essential residues on the Claspin motif to Chk1 binding was analysed using alanine scanning which revealed that among the phosphoserine flanking residues, only the phenylalanine at the +3 position of the critical phosphoserine was crucial to Chk1 binding. The effect of Claspin binding on Chk1 activity was analysed by kinase assay and the preliminary result showed an increased activity of Chk1 in the presence of a phosphorylated Claspin peptide with the sequence of one Chk1-binding motif. This *in vitro* study indicates the Claspin motif is enough to elevate Chk1 activity even in the absence of the Chk1 upstream kinase ATR. A Chk1 activation model interpreted from this result is that binding of Claspin leads to an activating conformational change of Chk1 and the active status of Chk1 might be further maintained by the phosphorylation on S317 and S345 in the linker region by ATR.

Collectively, this work demonstrated the auto-inhibitory regulation of Chk1 activity and the intramolecular interaction between Chk1KD and Chk1RD in the aim of understand the molecular mechanism of Chk1 activity regulation. In perspective of understanding the role of the adaptor protein Claspin in Chk1 activation, the Claspin-Chk1 interaction was quantitatively characterised and the critical amino acids were defined, which provided evidence on the interpretation of the adaptor-mediated Chk1 activation mechanism.

CHAPTER 2 BIOPHYSICAL STUDIES ON CHK1

2.1 Results

2.1.1 Chk1 constructs and purification

Chk1 sequence consists of a conserved N-terminal catalytic domain, a conserved C-terminal end and a less conserved linker region in between (Figure 2.1). Expression of active Chk1 full length (Chk1FL) and its kinase domain were well established in insect cells and mammalian cells (Chen et al., 2000; Okita et al., 2012) which, however, are more complex expression systems than bacteria system. The bacterial expression has an advantage of easy to culture, fast growth and high yield. Expression of Chk1 in *E.coli* was attempted at the beginning of this project, however, no expression was detected for a 6xHis-GST-Chk1¹⁻²⁸⁹ construct or a 6xHis-GST-Chk1FL construct. It is speculated that a more physiologically related expression system is required for native Chk1 folding and post-translational modifications. Chk1¹⁻²⁸⁹ consisting of the catalytic domain (1-265) and a short linker was selected as the expression construct of the kinase domain (Chk1KD). Chk1KD and Chk1FL with a C-terminal TEV cleavage sequence (ENLYFQ) followed by an 8xHis-tag was expressed in *Sf9* cells. Target protein was purified using Ni-NTA agarose column and size exclusion chromatography (Figure 2.2).

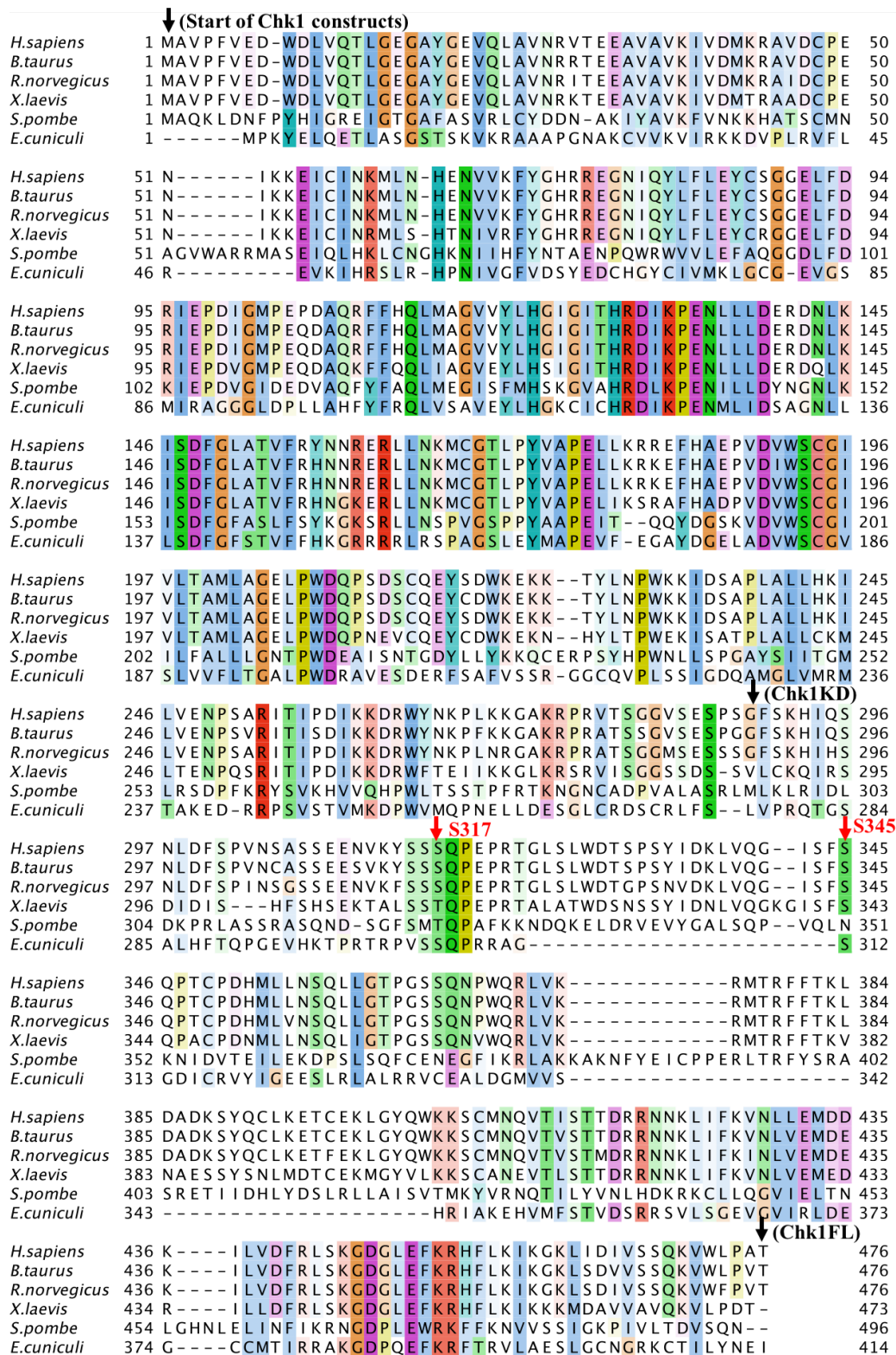


Figure 2.1 Sequence alignment of Chk1

The alignment of Chk1 from human to yeast is coloured by conservation (threshold 30%) with the ClustalWS colouring scheme and is formatted in Jalview (Larkin et al., 2007; Waterhouse et al., 2009). Phosphorylation sites by ATR and regions for expression (Chk1KD and Chk1FL) are marked by red and black arrows respectively.

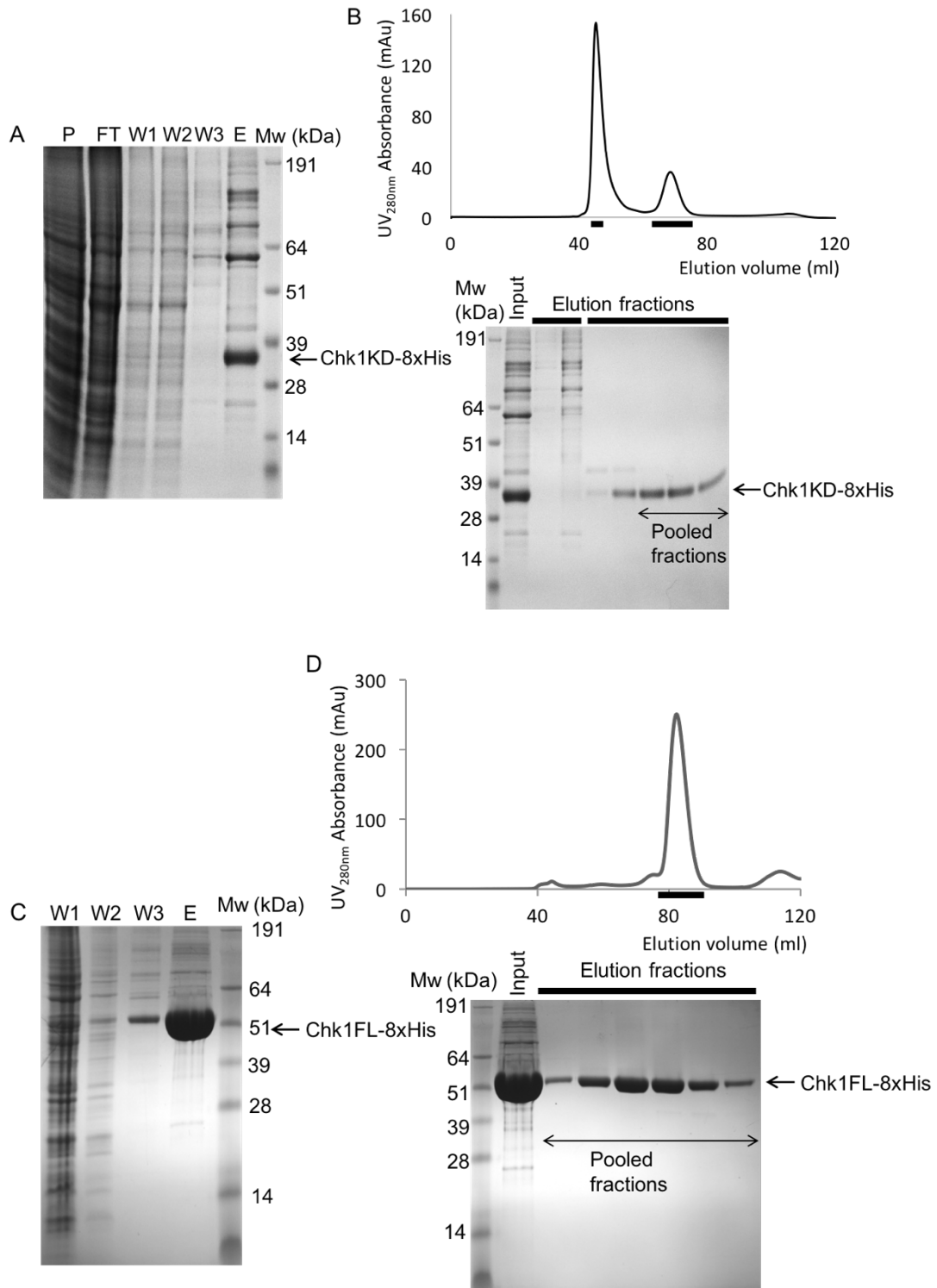


Figure 2.2 Purification of Chk1KD and Chk1FL

Cell lysate was applied on Ni-NTA agarose beads column as an initial purification step for Chk1KD (A) and Chk1FL (C). P: pellet, FT: flow through, W: wash, E: elution. Elution from Ni-NTA column was concentrated and applied on a size-exclusion chromatography using Superdex 75 16/60 column or Superdex 200 16/60 column for Chk1KD (B) and Chk1FL (D) respectively.

Chk1KD appeared as double bands on SDS-PAGE gel thus mass spectrometry analysis was performed to identify the species in Chk1KD. It showed that the purified protein sample consisted of the first methionine truncated Chk1KD constructs, with and without an acetylation modification (Figure 2.3).

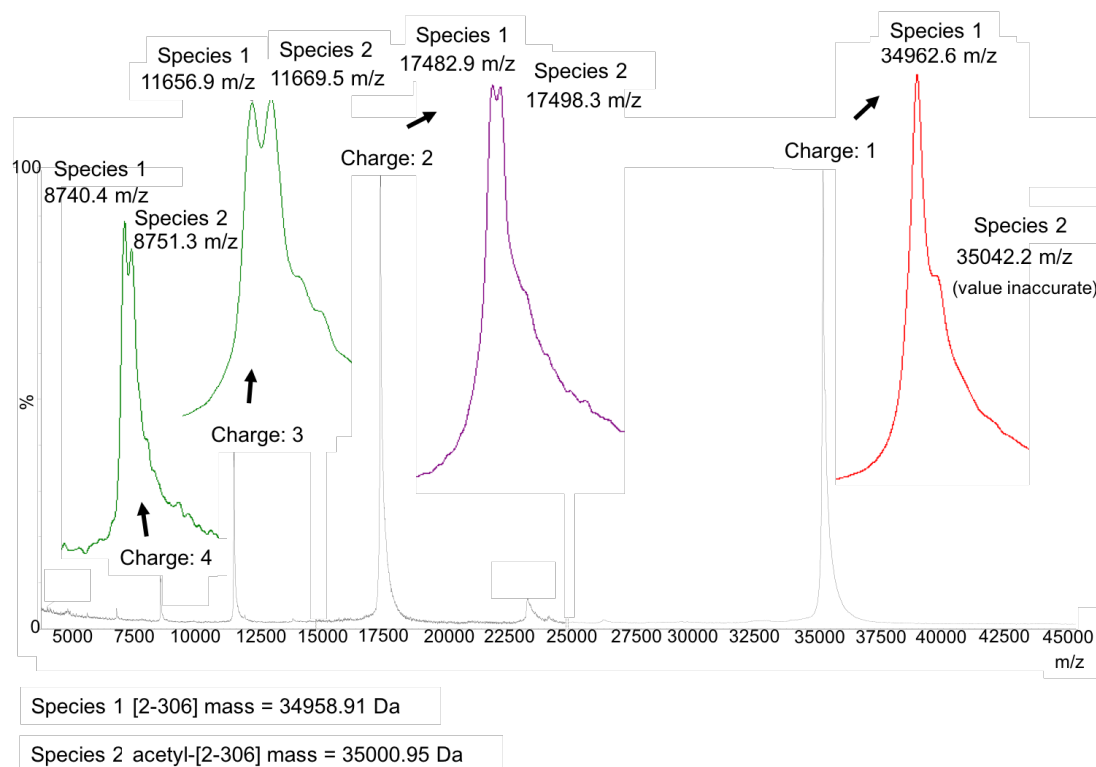


Figure 2.3 Mass spectrometry analysis of Chk1KD

MALDI-TOF (Matrix-assisted laser desorption/ionization-time of flight) mass spectrometry showed the purified Chk1KD sample consisted of two species. The observed mass of the species agreed with the molecular weight of a methionine truncated Chk1KD with and without an acetylation modification (expected molar mass: 35000.95 Da and 34958.91 Da). Analysis was performed by Dr. Len Packman at the Protein and Nucleic Acid Analysis Facility at the University of Cambridge.

2.1.2 Post-translational modifications of recombinant Chk1

Recombinant proteins expressed in eukaryotic expression system can undergo post-translational modifications. Phosphorylation is one of the most common modifications and it might play a role in enzyme activity regulation. To understand if

the Chk1 constructs expressed in *Sf9* cells undergo phosphorylation and to what extent, the recombinant samples of Chk1KD and Chk1FL were analysed by MALDI fingerprinting mass spectrometry. Phosphorylation sites were identified on both of the constructs with different abundance (Figure 2.4). Two phosphorylation modifications were identified in the region preceding the Chk1 linker region on both Chk1KD and Chk1FL. The abundance of these phosphorylated species was at a low level for both constructs. A region containing a phosphorylation site with the highest phosphorylation abundance was identified on Chk1FL with an abundance of 15.47%. Multiple phosphorylation sites were identified from the C-terminal region of Chk1FL with an abundance below 10%. The mass spectrometry results indicated that both Chk1 constructs underwent phosphorylation when expressed in *Sf9* cells, either due to endogenous kinases or Chk1 auto-phosphorylation or both. Phosphorylation introduces inhomogeneity of protein samples and may alter the kinase activity of Chk1. The characteristic of phosphorylation on Chk1 during expression was considered in crystallization and kinetic assays.

| | | | |
|---------------|-----|---|-----|
| <i>Chk1KD</i> | 1 | MAVPFVEDWDLVQTLGEGAYGEVQLAVNRVTEEAVALVKIVDMKRAVDCPE | 50 |
| <i>Chk1FL</i> | 1 | MAVPFVEDWDLVQTLGEGAYGEVQLAVNRVTEEAVALVKIVDMKRAVDCPE | 50 |
| <i>Chk1KD</i> | 51 | NIKKEICINKMLNHENVVKFYGHRREGNIQYLFLEYCSGGELFDRIEPDI | 100 |
| <i>Chk1FL</i> | 51 | NIKKEICINKMLNHENVVKFYGHRREGNIQYLFLEYCSGGELFDRIEPDI | 100 |
| <i>Chk1KD</i> | 101 | GMPEPDAQRFHQLMAGVVYLHGIGITHRDIKPENLLDERDNLKISDFG | 150 |
| <i>Chk1FL</i> | 101 | GMPEPDAQRFHQLMAGVVYLHGIGITHRDIKPENLLDERDNLKISDFG | 150 |
| <i>Chk1KD</i> | 151 | LATVFRYNNRERLLNKMCGTLPYVAPELLKRREFHAEPVDVWSCGIVLTA | 200 |
| <i>Chk1FL</i> | 151 | LATVFRYNNRERLLNKMCGTLPYVAPELLKRREFHAEPVDVWSCGIVLTA | 200 |
| <i>Chk1KD</i> | 201 | MLAGELPWDQPSDSCQEYSDWKEKKTYLNPWKKID ^{5.76%} SAPLALLHKILVENP | 250 |
| <i>Chk1FL</i> | 201 | MLAGELPWDQPSDSCQEYSDWKEKKTYLNPWKKID ^{0.03%} S ^{0.87%} APLALLHKILVENP | 250 |
| <i>Chk1KD</i> | 251 | SARITIPDIKKDRWYNKPLKKGAKRPRVTSGGVSESPSG | 289 |
| <i>Chk1FL</i> | 251 | SARITIPDIKKDRWYNKPLKKGAKRPRVTSGGVSESPSGFSKH ^{15.47%} IQSNLDF | 300 |
| <i>Chk1KD</i> | | | |
| <i>Chk1FL</i> | 301 | SPVNSASSEENVKYS ^{9.34%} SQPEPRTGLSLWDTSP ^{2.33%} SYIDK ^{4.48%} LVQGISFSQPTCP | 350 |
| <i>Chk1KD</i> | | | |
| <i>Chk1FL</i> | 351 | DHMLINSQLLGT ^{6.56%} PGSSONPWORLVKRMTRFFTKLDADKSYQCLKETCEKL | 400 |
| <i>Chk1KD</i> | | | |
| <i>Chk1FL</i> | 401 | GYQWKK ^{4.34%} SCMNQV ^{9.06%} T ^{1.33%} IS ^{1.33%} TTDRRNKLI ^{1.33%} FKVNLL ^{1.33%} EMDDKILVDFRLSKGDGLE | 450 |
| <i>Chk1KD</i> | | | |
| <i>Chk1FL</i> | 451 | FKRHFLKIKGKLIDIVSSQKVWLPAT | 476 |

(Caption on next page)

Figure 2.4 Post-translational phosphorylation mapping of Chk1KD and Chk1FL

Multiple phosphorylation modifications with different abundance on both constructs were detected. Phosphorylation sites are marked with blue (Chk1KD) and red (Chk1FL) boxes, together with their abundance. Peptides marked with dash line indicate a phosphorylation modification was detected on the peptide but the exact site could not be determined. The MALDI fingerprinting mass spectrometry analysis was performed by Dr. Mike Deery at Cambridge Centre for Proteomics at University of Cambridge.

2.1.3 Size-exclusion multi-angle laser scattering (SEC-MALS)

SEC-MALS experiments were performed to establish the molecular mass and oligomerisation status of Chk1 constructs in solution (Figure 2.5). SEC-MALS combines measurements of refractive index (RI), UV absorbance and light-scattering (LS) to determine the molecular mass (MM) and oligomeric state. Medium concentration of salt (300 mM NaCl) was used because of the unstable nature of Chk1FL under low salt condition. Both Chk1FL and Chk1KD at a concentration of 1.5 mg/ml were applied to Superdex 200 10/30 column for analysis. Both samples are monodispersed and the MM of Chk1FL and Chk1KD were measured at 56.88 kDa (0.2% error) and 35.65 kDa (0.1% error) respectively, which corresponded to their calculated molecular mass of 56.31 kDa and 34.89 kDa, respectively. The result of the SEC-MALS analysis shows that Chk1FL and Chk1KD are monomeric in solution.

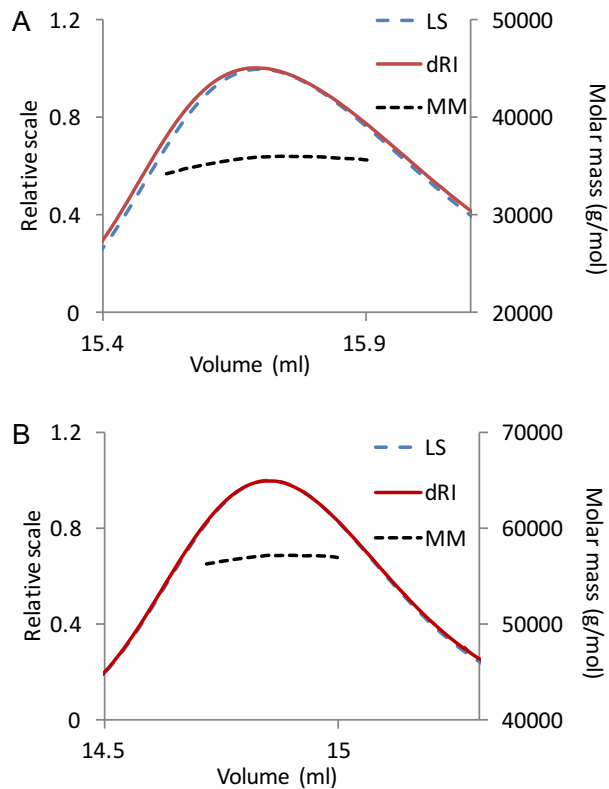


Figure 2.5 SEC-MALS analysis of Chk1KD and Chk1FL

Light scattering (LS), refractive index (dRI) and molecular mass (MM) of Chk1KD (A) and Chk1FL (B) are shown. LS and dRI overlap well in both experiments and the calculated MM was homogenous in selected peaks of both constructs.

2.1.4 Small Angle X-ray Scattering (SAXS)

To obtain structural information about Chk1 in solution, SAXS experiments were performed for Chk1KD and Chk1FL at the SWING beamline of the SOLEIL synchrotron (Gif-Sur-Yvette, France). Buffer subtracted data was analysed using ScÅtter software (Bioisis). Guinier analysis was used to estimate the radius of gyration (R_g). Low- q data in the range of $q \times R_g < 1.3$ was used for R_g estimation which aims to produce a value within 10% of the true value. Guinier analysis of the linear range of low- q data yielded R_g values of 29.06 Å for Chk1KD and 29.54 Å for Chk1FL, indicating that the two Chk1 constructs have very similar hydrodynamic radii. Thus, the SAXS data showed that the overall dimension of Chk1FL was close to Chk1KD, suggesting that the Chk1FL adopts a compact structure in which the

Chk1RD binds tightly to Chk1KD. Further shape information can be extracted from inspection of the KRATKY plot, which provides information about the folding status of the particle: a bell-shaped curve indicates that the sample adopts a globular shape while a rise to a plateau indicates unfolding properties. Both KRATKY plots showed the bell-shape profile expected of a globular particle. Pair-distance distribution function ($P(r)$) describes paired-set of distances between all electrons within a macromolecule and it is useful to investigate a conformational change between two datasets. Fitting of $P(r)$ generates a maximum dimension (D_{max}) which describes the maximum distance between two points within the protein molecule. A well-fitted of $P(r)$ curve is smooth and non-negative, approaching to zero at D_{max} . D_{max} of Chk1KD and Chk1FL was determined at 88 Å and 100 Å respectively, showing that the presence of about 200 amino acid at C-terminus did not increase D_{max} substantially, thus further supporting the hypothesis that the Chk1RD interacted intramolecularly with the Chk1KD to give a compact overall shape.

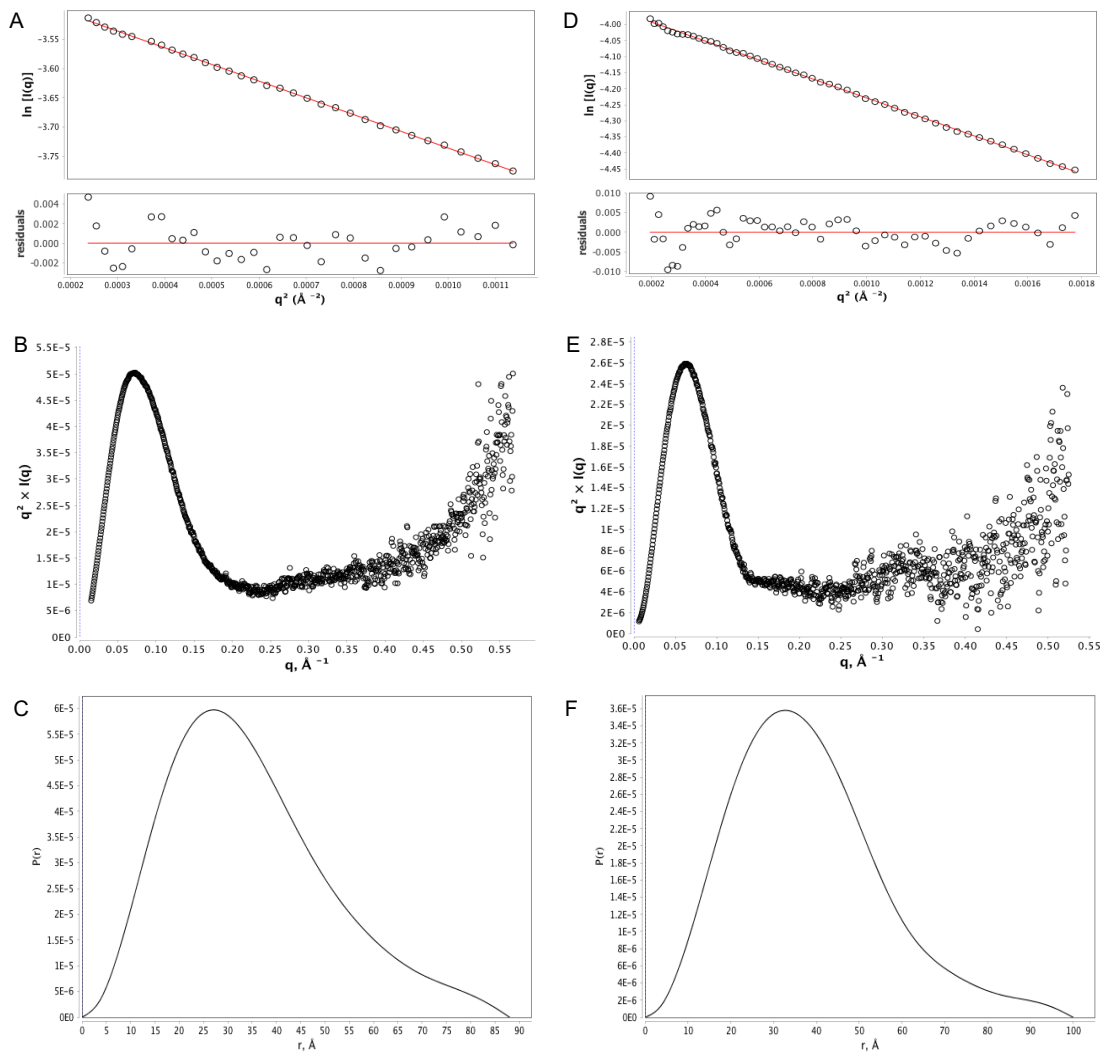


Figure 2.6 Guinier analysis, KRATKY plot and $P(r)$ distribution of Chk1KD and Chk1FL

Initial low- q region was selected in Guinier analysis for Chk1KD (A) and Chk1FL (D). Points randomly distributed on the two sides of the linear regression line. KRATKY plots for Chk1KD (B) and Chk1FL (E) showed bell-shaped curve. D_{max} was determined in $P(r)$ distribution for Chk1KD (C) and Chk1FL (F).

2.1.5 Attempts towards crystallization of Chk1FL

The compact structure of Chk1FL provided a preliminary rationale to structural determination using crystallography. Initial crystallization condition screenings (Materials and Methods 2.3.9) were set up using native Chk1FL but no suitable crystallisation conditions could be determined. One approach to the problem, which

had been previously demonstrated to be successful for many kinase structures, was co-crystallizing with known high-affinity inhibitors in an attempt to stabilise Chk1FL in a single conformation and increase the chance of crystal formation. Several Chk1FL inhibitors including UCN-01, AZD7762 and CHIR-124 (Ni et al., 2006; Oza et al., 2012; Zhao et al., 2002) were used for co-crystallization with Chk1FL but no hit was produced. A further attempt towards producing a suitable Chk1FL sample for crystallization was made by generating a catalytic-dead D130A Chk1FL mutant, in an effort to eliminate or reduce heterogeneity due to Chk1 autophosphorylation during protein expression. SAXS analysis was applied on this construct and the result showed that Chk1FL^{D130A} had the same dimension with wild-type Chk1FL, indicating the introduction of a single mutation did not lead to huge conformational change (Figure 2.7). No hit was identified in initial screening trays for this construct.

As the presence of the C-terminal tag might be responsible for the failure to crystallise the protein, a new Chk1FL construct was prepared that had an N-terminal 8xHis tag followed by a TEV cleavage site, and the new construct was successfully expressed in *Sf9*. Following successful purification and tag removal after TEV treatment, SAXS analysis showed that the tag-cleaved construct adopted similar shape and dimension consistent with what observed previously for the C-terminally tagged Chk1FL (Figure 2.7). Crystal screening of the new Chk1FL sample produced no hit.

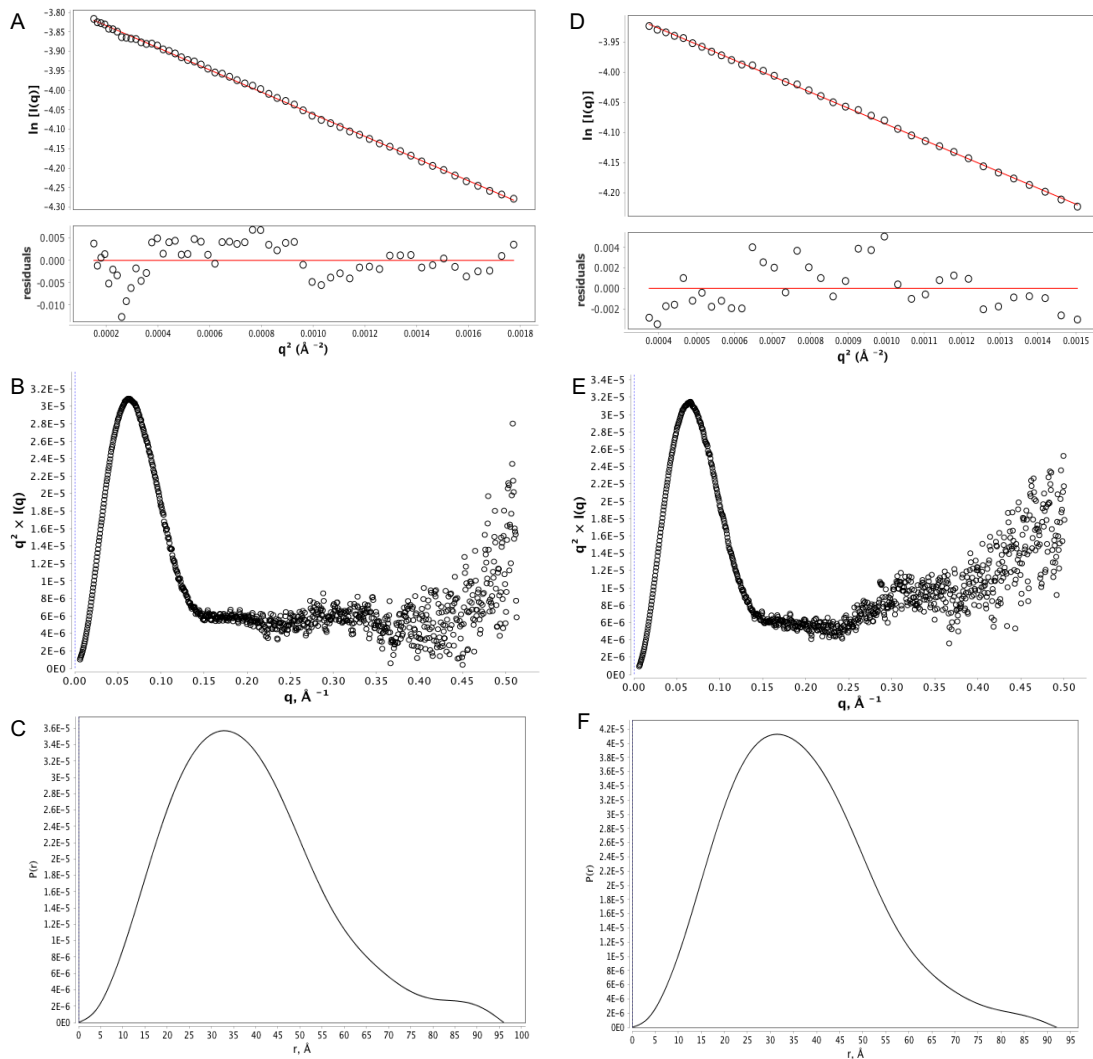


Figure 2.7 Guinier analysis, KRATKY plot and P(r) distribution of Chk1FL^{D130A} and Chk1FL^{notag}

Initial low-q region was selected in Guinier analysis for Chk1FL^{D130A} (A) and Chk1FL^{notag} (D). Points randomly distributed on the two sides of the linear regression line. KRATKY plots showed a bell-shaped curve of Chk1FL^{D130A} (B) and Chk1FL^{notag} (E). Dmax was determined in P(r) distribution at 96 Å for Chk1FL^{D130A} (C) and 92 Å for Chk1FL^{notag} (F).

As recombinant Chk1FL was phosphorylated at multiple sites at varying abundance, possibly interfering with crystallisation, dephosphorylation was thus performed on Chk1FL using λ phosphatase. However, no hit was identified in the crystallisation screening of the dephosphorylated protein. Whether phosphorylation of the recombinant Chk1FL had an influence on crystallization remains debatable, because recombinant Chk1KD samples consistently produced high-quality crystals which

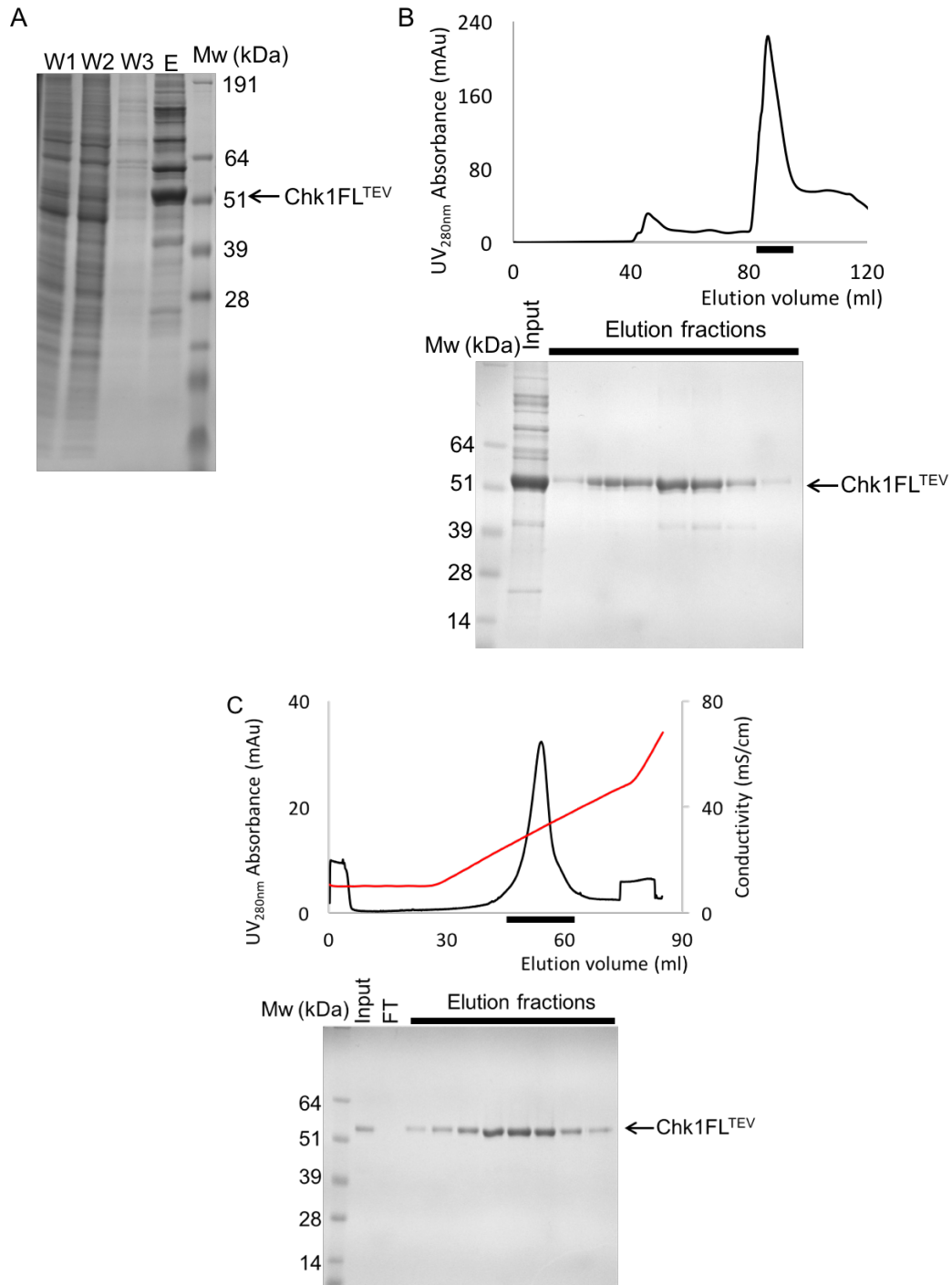
diffracted to high resolution, despite the presence of phosphorylation.

As all approaches towards crystallizing human Chk1FL has been unsuccessful, it was reasoned that the flexible linker between Chk1KD and the C-terminal 100 residues (referred as KA domain in (Emptage et al., 2017)) may be responsible for difficulties in crystallisation. A well-known strategy for protein crystallisation is to switch the species of origin of the protein under investigation. We chose to attempt expression and purification of the Chk1 orthologue from the eukaryotic intracellular parasite *Encephalitozoon Cuniculi* Chk1 (EcChk1). At 414 amino acids, EcChk1 is considerably smaller than its human counterpart. Sequence alignment (Figure 2.1) shows that the N-terminal kinase domain and the C-terminal domain have good sequence similarity with the human kinase, whereas the linker region is less conserved with EcChk1 having a shorter linker. The EcChk1 open reading frame with either an N- or a C-terminal cleavable polyhistidine-tag was cloned into the pFBDM vector and expressed in *Sf9* cells, and the protein was purified using Ni-NTA agarose column and size exclusion chromatography, as for the human protein. EcChk1 was eluted in the void peak during size-exclusion chromatography which indicated it was likely to be in a highly aggregated state. The yield of recombinant protein as judged from SDS-PAGE was much lower than that of hChk1, which indicated the *Sf9* expression of EcChk1 constructs was not a feasible approach.

2.1.6 The kinase and regulatory domains of Chk1 co-elute in size-exclusion chromatography

The result of the SAXS experiments showed that Chk1FL and Chk1KD behaved like particles with similar shape and conformation in solution, suggesting a stable intramolecular association between Chk1's kinase and regulatory domains. To verify the interaction between the two domains, a TEV cleavage sequence (ENLYFQ) was introduced between Chk1KD and the linker region in Chk1FL (between G289 and

F290) to make a Chk1FL^{TEV} construct. Baculovirus infection of *Sf9* cells produced a titer of 2.8×10^8 pfu/ml and expression was performed at MOI = 1:1 for 3 days. Chk1FL^{TEV} was obtained with lower yield and purity comparing to Chk1FL^{WT}, and therefore an extra purification step using Heparin chromatography was added to acquire high purity (Figure 2.8).



(Caption on next page)

Figure 2.8 Purification of Chk1FL^{TEV}

A: Chk1FLTEV was firstly purified by gravity flow Ni-NTA column and the fractions were analysed by SDS-PAGE. W: wash, E: elution. B: Size exclusion chromatography using Superdex 200 16/60 column was performed and elution fractions were analysed by SDS-PAGE. C: Heparin column was the final purification step and target protein was eluted with gradient salt wash. Fractions were analysed by SDS-PAGE and stained by coomassie blue. FT: flow through.

TEV protease cleavage was performed overnight and the sample resulting from the cleavage reaction was analysed by gel-filtration chromatography on a Superdex 200 10/30 column. Gel filtration was performed in the presence of 150 mM NaCl. The chromatography profile showed a single peak. SDS PAGE analysis of peak fractions contained both Chk1KD and Chk1RD in visually stoichiometric ratio, indicating the two domains migrated together during the course of gel filtration, despite their different size (Figure 2.9). A double band appeared on Chk1KD which was speculated as a consequence of *in vivo* acetylation and phosphorylation. A further attempt to separate the two domains was made by loading the peak fractions of the gel filtration chromatography onto a Hitrap Q ion-exchange column: the two domains were eluted together at a concentration of NaCl between 240 and 360 mM. These experiments show that the interaction between the two domains is maintained during different types of chromatographic fractionation and indicate that the intramolecular interaction between Chk1KD and Chk1RD appears to be tight.

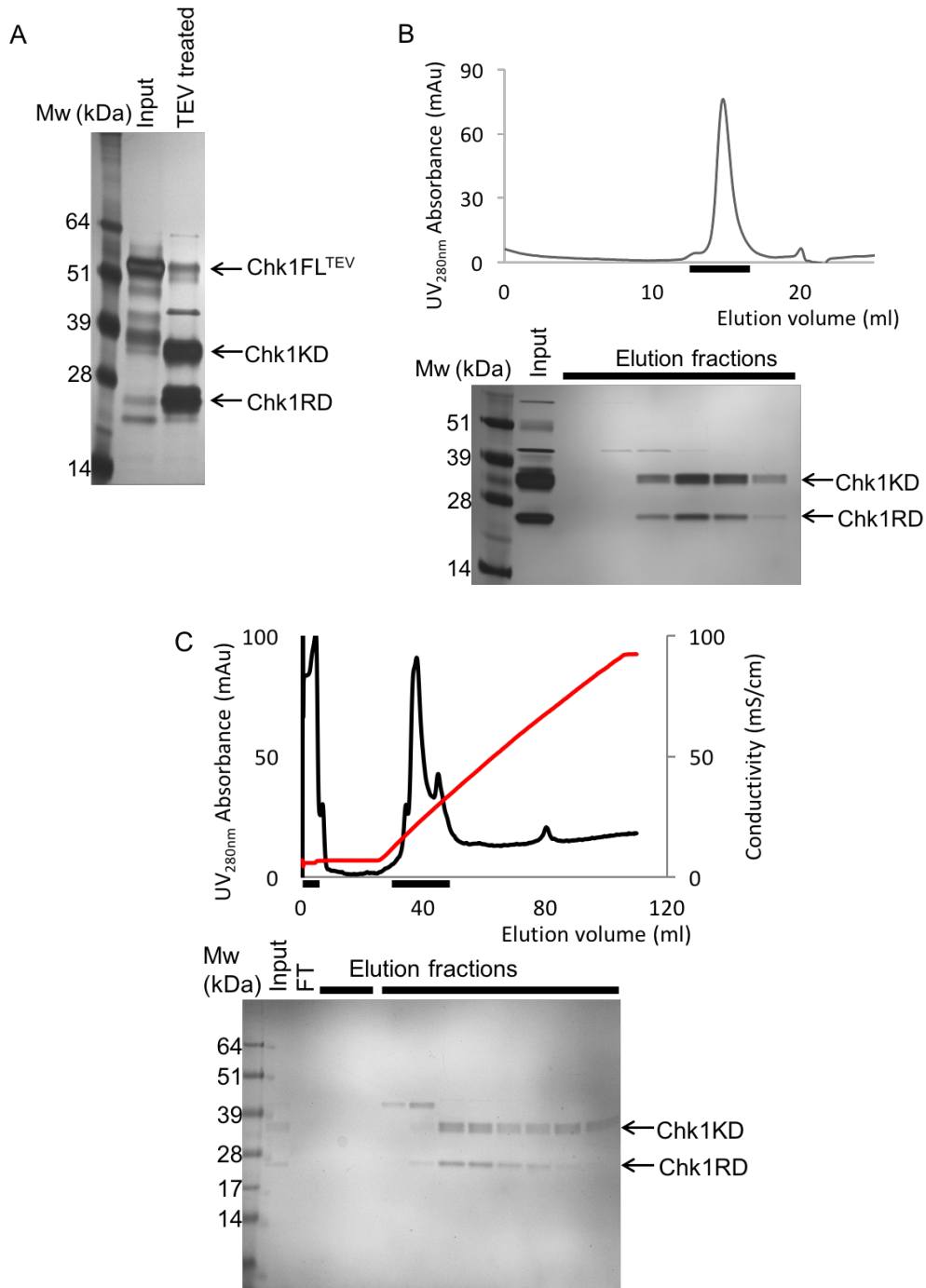


Figure 2.9 Co-migration of Chk1KD and Chk1RD

A: Chk1FL^{TEV} and sample after TEV protease treatment were analysed on SDS-PAGE and stained with silver staining. B: Size exclusion chromatography analysis showed a single and symmetric peak in Chk1KD and Chk1RD co-migration experiment. Silver stained SDS-PAGE analysis of the fractions showed the two domains were co-eluted in visually stoichiometric ratio. C: TEV treated Chk1FL^{TEV} sample was analysed on Hitrap Q column and the two domains were eluted in same fractions during gradient NaCl wash. Fractions were analysed by SDS-PAGE and stained by coomassie blue. FT: flow through.

2.2 Discussion

The experiments reported in this chapter aimed to shed light on the molecular structure of human Chk1, to improve our biochemical understanding of Chk1 function and potentially open up new avenues of Chk1 inhibitor discovery. Biophysical studies including SEC-MALS, SEC-SAXS and crystallization trials were applied to Chk1 constructs which revealed Chk1 characteristics at a molecular level. Both Chk1KD and Chk1FL were identified as monomeric molecules and Chk1FL adopted a very compact structure with a D_{max} of 100 Å, which was 12 Å longer than that of Chk1KD. Chk1FL was thus considered as a suitable candidate for crystallization studies. Crystallization trials, however, did not produce any new perspective on Chk1FL structure determination. A reasonable explanation is the linker region generates a high extent of conformational heterogeneity, which cannot be eliminated by addition of ATP-binding site inhibitors or using a catalytic-dead version of Chk1. Stabilising the linker region is a future direction for Chk1FL crystallization. Alternatively, native structural determination could be achieved by other techniques such as cryo-EM. The linker region accounts for 20% of the full-length Chk1 polypeptide length which restrains the possibility of acquiring interacting interface information by docking the two domains into the SAXS envelope.

Taken together, the results of my experiments suggest that Chk1 adopts an auto-inhibition mechanism, where Chk1RD has an intramolecular interaction with Chk1KD which suppresses its activity. Further studies on this regulatory intramolecular interaction are going to be reported in chapter 3.

2.3 Materials and methods

2.3.1 Generation and expression of Chk1 constructs

IMAGE human Chk1 cDNA was used for the cloning of Chk1¹⁻²⁸⁹ (Chk1KD) and Chk1FL. Chk1KD sequence was amplified by *Chk1KD-f* and *Chk1KD-r* primers (Appendix A) to create an C-terminal TEV cleavage sequence (ENLYFQ) followed by an 8xHis-tag and NotI and HindIII restriction sites. Chk1FL sequence was amplified by *Chk1FL-f* and *Chk1FL-r* primers (Appendix A) to create the same tag and restriction sites for insertion in to pFBDM vector. The amplified sequence was verified on a 1% agarose gel and target band was cut and extracted using geneJET gel extraction kit (Thermo Scientific). Double digest using NotI and HindIII restriction enzymes was applied to the amplified Chk1KD and Chk1FL PCR product and pFBDM vector. The digested DNA was verified by 1% agarose gel and purified. 50 ng vector and three-fold molar excess of digested insert was ligated using quick ligation kit (NEB labs). 2 µl ligated plasmid was transformed into 20 µl DH5α competent cells. After 30 min incubation on ice, cells were incubated in water bath at 42°C for 45 s. 700 µl LB medium was added to the cells and recovery took place at 37°C with shaking at 220 rpm for 1 h. Cells were plated on an agar plate containing 7 µg/mL gentamicin and incubated at 37°C overnight. 4 ml culture of single colony was grown and plasmid was extracted using plasmid miniprep kit (Thermo Scientific) and sequence was verified using Department of Biochemistry DNA Sequencing Facility. 100 ng plasmid was transformed to 50 µl DH10Bac competent cells (Geneva Biotech). Transformed cells were incubated on ice for 30 min followed by a heat-shock at 42°C for 45 s. Cells were incubated on ice for 10 min and 1 ml SOC medium (Thermo Scientific) was added to cells followed by a 6 h incubation at 37°C with shaking at 220 rpm. After recovery, cells were plated on blue/white selection LB-agar plate containing 50 µg/mL kanamycin, 7 µg/mL gentamicin, 10 µg/mL tetracycline, 100 µg/mL X-gal and 40 µg/mL IPTG. Colonies containing the recombinant bacmid were white on X-gal agar plate and can be distinguished from blue colonies which

contained unaltered bacmid. After 48 h incubation at 37 °C, single white colonies were picked and re-streaked on a new selection plate and incubated at 37°C for 24 h. Single white colonies from the re-streaked plate were inoculated in 2 ml LB medium containing 50 µg/mL kanamycin, 7 µg/mL gentamicin and 10 µg/mL tetracycline and cells were grown overnight at 37°C with shaking at a speed of 220 rpm. Cells were spun down at 17,000 g for 5 min and the pellet was resuspended in 250 µl resuspension buffer followed by addition of 250 µl lysis buffer and 350 µl neutralization buffer (Thermo Scientific). Samples were spun down at 17,000 g for 10 min and 700 µl supernatant was mixed with 700 µl isopropanol was spun down at 17,000 g for 10 min. Supernatant was removed and 1 ml 70% ethanol was added to wash the pellet which was followed by a 10 min-spin at 17,000 g. The wash step was repeated twice and after the final spin, 100 µl miliQ water was added to dissolve the bacmid pellet. Bacmid concentration was measured on Nano-drop Spectrophotometer (Thermo Fisher) and 50 ng extracted bacmid was used in insertion verification by PCR using the *pUC/M13-f* and *pUC/M13-r* primers (Appendix A). Bacmid containing the insertion of target size was selected for *Sf9* transfection. 1 µg bacmid was transfected into *Sf9* cells in the form of mixture with Cellfectin® II (Thermo Scientific) and incubated at 27 °C for 4 days to produce P1 virus stock. 1 ml P1 was used to infect 25 ml *Sf9* cells with a density of 10⁶ cells/ml to produce P2 virus stock. P2 was harvested after 4-5 days when cell count stopped increasing and viability dropped below 90%. P2 titer was measured using cell growth inhibition assay developed in the laboratory of Prof. Nick Gay (Department of biochemistry, University of Cambridge) with 6.47x10⁸ pfu/ml and 6.92x10⁸ pfu/ml for Chk1KD and Chk1FL respectively. Expression test was performed for P2 virus at three multiplicity of infection (MOI) (1:0.1, 1:1 and 1:10) for four days and a 1 ml cell culture sample was taken every 24 h after infection. Cell culture for expression test was spun down and the pellet was re-suspended in 100 µl 1x SDS-loading buffer (Novex). The expression was analysed by SDS-PAGE and the large-scale expression conditions were selected at MOI at 1:1 for 3 and 4 days for Chk1KD and Chk1FL respectively.

2.3.2 Purification of Chk1 constructs

Cells were harvested by centrifugation at 500 g for 10 mins (Beckman Coulter, JLA 8.1000). Pellet from 1 L growth culture was re-suspended in 15 ml re-suspension buffer (50 mM Hepes pH 7.5, 500 mM NaCl, 1 mM TCEP and 1 EDTA-free protease inhibitor cocktails tablet). Cell pellet re-suspension was sonicated at 25% cycle and 50% power for 3 mins. Lysate was centrifuged at 35000 g and 4 °C for 1 h. Supernatant was collected and loaded onto gravity flow Ni-NTA agarose column (Qiagen). The column was washed twice with 20 ml wash buffer (25 mM Hepes pH 7.5, 500 mM NaCl, 20 mM imidazole, 0.05 % Triton-X100 and 1 mM TCEP). Step wash was performed on the column with wash buffer containing 40 mM and 300 mM imidazole. Elution from the 300 mM imidazole wash was loaded onto a Superdex75 and Superdex200 16/60 gel filtration column (GE Healthcare) for Chk1KD and Chk1FL respectively. The column was pre-equilibrated and the experiment was performed in the gel filtration buffer (25 mM Hepes pH 7.5, 500 mM NaCl and 2 mM DTT). Elution samples were analysed on a 12% acrylamide SDS-PAGE gel and fractions containing target protein were collected and concentrated. The typical yield of Chk1KD-8xHis and Chk1FL-8xHis was in the range of 0.2 - 0.5 and 0.4 - 1 mg per litre expression respectively. 5-10% glycerol was added to protein sample and protein aliquots were flash frozen using liquid nitrogen and stored at -80 °C.

2.3.3 Generation and purification of EcChk1 constructs

EcChk1 gene sequence was synthesised using gBlocks Gene Fragments service (IDT). Primers *EcChk1Ntag-f* and *EcChk1Ntag-r* were used to generate an N-terminal 8xHis tag followed by a TEV cleavage sequence. Primers *EcChk1Ctag-f* and *EcChk1Ctag-r* were used to generate a C-terminal TEV cleavage site followed by an 8xHis tag. NotI and HindIII restriction sites were introduced on both of the constructs and the amplified PCR product was inserted to pFBDM vector. Bacmid generation, expression and purification was in the same way described in 2.3.1 and 2.3.2,

however, both EcChk1 construct eluted from void peak during gel filtration.

2.3.4 Generation of 8xHis-Chk1FL, Chk1^{D130A} and Chk1^{TEV} constructs

N-terminus-tagged Chk1FL construct with an N-terminal 8xHis tag followed by a TEV cleavage site was created using *Chk1FL2-f* and *Chk1FL2-r* primers (Appendix A) based on IMAGE Chk1 cDNA sequence. The amplified sequence was inserted into the pFBDM vector using NotI and HindIII restriction sites. D130A mutagenesis was generated on pFBDM-Chk1KD and pFBDM-Chk1FL templates by site-directed mutagenesis (QuickChange, Stratagene). Primers *Chk1D130A-f* and *Chk1D130A-r* were used to generate the mutation (Appendix A). To create a TEV cleavage site between Chk1KD and Chk1RD, Chk1 cDNA was firstly amplified with primers *Chk1TEV1-f* and *Chk1TEV1-r* to create an N-terminal 8xHis tag and a C-terminal Avi tag without TEV cleavage site. The amplified sequence was inserted to pFBDM vector using NotI and HindIII restriction sites. Primers *Chk1TEV2-f* and *Chk1TEV2-r* were used to introduce a TEV cleavage site between 289 and 290 using site-direct mutagenesis (QuickChange, Stratagene) on the recombinant plasmid to generate the sequence of Chk1FL^{TEV}.

2.3.5 Purification of Chk1^{D130A} and Chk1^{TEV}

Purification steps of the N-terminal 8xHis-Chk1FL and Chk1^{D130A} constructs were the same with the wild-type Chk1 constructs described in 2.3.2. The yield and purity of the new constructs were at the same level as the wild-type constructs. Initial purification steps of Chk1FL^{TEV} construct remained the same as the procedure described in 2.3.2 and an extra purification step using 5 ml HiTrap Heparin HP affinity column (GE Healthcare) was added to improve purity. The Heparin column was equilibrated with 10% buffer B (buffer A: 25 mM Hepes pH 7.5 and 2 mM DTT, buffer B: 25 mM Hepes pH 7.5, 1 M NaCl and 2 mM DTT). NaCl concentration in Chk1TEV elution from previous gel filtration step was diluted to 100 mM using buffer A. Diluted sample was loaded onto the Heparin column and a gradient NaCl

was performed during the experiment.

2.3.6 Purification and tag removal of 8xHis-Chk1FL

Initial purification steps until Ni-NTA agarose column for the N-terminus tagged 8xHis-Chk1FL construct remained the same with the procedure described in 2.3.2. Elution sample from Ni-NTA chromatography was buffer exchanged to 25 mM Hepes pH 7.5, 250 mM NaCl and 10 mM DTT to remove imidazole and lower salt concentration for TEV treatment. 60 μ l TEV protease at 2 mg/ml was added to 8xHis-Chk1FL and the reaction was incubated at 4°C overnight. The TEV treated sample was concentrated to 1 ml and was applied to Superdex 200 16/60 column for gel filtration in a buffer of 25 mM Hepes pH 7.5, 300 mM NaCl and 2 mM DTT. Elution fractions containing target protein was pooled and concentrated.

2.3.7 SEC-MALS

100 μ l Chk1KD or Chk1FL at a concentration of 1.5 mg/ml was applied on Superdex200 increase 10/30 column pre-equilibrated in gel filtration buffer (25 mM Hepes pH 7.5, 300 mM NaCl and 0.1 mM TCEP). Light scattering and refractive index were measured by DAWN HELEOS II MALLS detector (Wyatt Technology) and Optilab T-rEX differential re-fractometer (Wyatt Technology) respectively. Data was analysed using ASTRA 6 program (Wyatt Technology).

2.3.8 Dephosphorylation of Chk1FL

4 μ l λ phosphatase (Santa Cruz) was added to 36 μ l Chk1FL at a concentration of 80 μ M. 10x reaction buffer, 10x MnCl₂ and miliQ was added to make the final volume up to 250 μ l. Reaction was incubated at 4°C overnight and the sample was purified by loading onto Superdex200 10/30 column (GE Healthcare) pre-equilibrated in buffer (25 mM Hepes pH 7.5, 300 mM KCl and 1 mM DTT).

2.3.9 SEC-SAXS

SEC-SAXS data was collected at the SWING beam line of the Soleil Synchrotron. 50 μ l Chk1 samples (8.3 mg/ml Chk1KD, 3.7 mg/ml Chk1FL, 4.3 mg/ml Chk1FL^{D130A} and 4.9 mg/ml tag-cleaved Chk1FL) were applied to a Superdex 200 Increase 3.2/200 column (GE Healthcare) pre-equilibrated in gel filtration buffer (25 mM Hepes pH 7.5, 300 mM NaCl and 0.1 mM TCEP). Buffer subtraction and initial data processing was performed with the FOXTROT software at the SWING beam line. Further data processing and analysis including Guinier analysis, Kratzky-plot generation and Dmax determination was performed with ScÅtter program (Bioisis).

2.3.10 TEV treatment and co-elution of Chk1KD and Chk1RD

60 μ l TEV protease at 2 mg/ml was added to Chk1FL^{TEV} in a buffer containing 25 mM Hepes pH 7.5, 300 mM NaCl and 10 mM DTT. The reaction was incubated at 4 °C overnight. Overnight sample was applied on a Superdex200 10/30 column pre-equilibrated in a buffer containing 25 mM Hepes pH 7.5, 150 mM NaCl and 2 mM DTT. Fractions were analysed on a 12% acrylamide SDS-PAGE gel and stained by silver staining (Thermo Fisher). Cleaved Chk1FL^{TEV} sample was also applied on Hitrap Q ion-exchange column (buffer A: 25 mM Hepes pH 7.5, 2 mM DTT, buffer B: 25 mM Hepes pH 7.5, 1 M NaCl and 2 mM DTT). Chk1KD and Chk1RD were co-eluted during gradient NaCl wash.

2.3.11 Crystallization trials of Chk1FL

Native Chk1FL at a concentration of 140 μ M was applied on protein crystallization condition screening plates JCSG+ (Molecular Dimensions), PACT (Molecular Dimensions), Morpheus (Molecular Dimensions) and PEGSI (Qiagen). 200 nl protein solution + 200 nl well solution was dispensed by Mosquito robot (TTP Labtech). Plates were stored at 19°C and imaged by Rock Imager (Formulatrix). Drop image

was scanned from 12 h until 30 days after dispensing and no crystal hit was produced in the condition tested. Co-crystallization trials for Chk1FL and Chk1 inhibitors were performed. 130-200 μM Chk1FL was mixed with CHIR-124 (Cambiosciences), UCN-01 (Millipore) or AZD7662 (Sigma) at different molar ratio of 1:1.05, 1:1.2 and 1:2. The mixture was incubated at 4°C for 1 h and was applied on screening plates JCSG+, PACT, PEGSI, PEGSII (Qiagen), Protein Complex (Qiagen), AmSO₄ suite (Qiagen), Wizard I&II (Emerald Biosystems), Wizard III&IV (Emerald Biosystems) and Morpheus. Drop dispensing and plate storage condition was the same with that of native Chk1FL. No crystal hit was produced. 140 μM native dephosphorylated Chk1FL or in complex with UCN-01 at a molar ratio of 1:2 was applied on screening plates PEGSI and PEGSII in the same protocol. No hit was produced. Chk1^{NOTAG} at concentrations of 100 and 200 μM was applied on PEGSI, PEGSII, PACT and JCSG+ using the same protocol. No hit was produced. 140 μM native Chk1FL^{D130A} or in complex with CHIR-124 at a molar ratio of 1:1.2 was applied on PACT, Morpheus, PEGSI, PEGSII, JCSG+, Wizard I&II, Wizard III&IV, AmSO₄ suite and Classics (Qiagen) using the same protocol. No hit was produced.

CHAPTER 3 ENZYMATIC STUDIES OF CHK1 ACTIVITY

3.1 Results

3.1.1 S216 is a major phosphorylation site of Chk1 on 14xHis-SUMO-Cdc25C²⁰⁰⁻²⁵⁶

Kinase activity is an essential property of Chk1 and therefore enzymatic studies of different Chk1 constructs may provide a better understanding of its molecular mechanism and cellular function. Chk1 is a serine/threonine kinase with consensus recognition motif: ϕ -X- β -X-X-(S/T)* (* indicates phosphorylated residue, ϕ is a hydrophobic residue, β is a basic residue and X is any amino acid) (Hutchins et al., 2000). Cdc25C is a well-recognised Chk1 substrate, which phosphorylates it at S216. A region of Cdc25C spanning residues 200 to 256 (Cdc25C²⁰⁰⁻²⁵⁶) with a dual N-terminal 14xHis and SUMO tag was expressed in *E.coli*, purified using Ni-NTA column and size exclusion chromatography, and used as a substrate of Chk1 kinase assays in initial experiments. To verify if S216 is the only phosphorylation site in 14xHis-SUMO-Cdc25C²⁰⁰⁻²⁵⁶, a 14xHis-SUMO-Cdc25C^{200-256S216A} mutant was expressed and purified and tested alongside 14xHis-SUMO-Cdc25C^{200-256WT} in Chk1 kinase assays using [γ -³²P]ATP. The ³²P incorporation on 14xHis-SUMO-Cdc25C^{200-256WT} showed higher intensity than the incorporation on 14xHis-SUMO-Cdc25C^{200-256S216A} by Chk1KD and Chk1FL, which indicated S216 was the major phosphorylation site by Chk1 (Figure 3.1). Weak ³²P incorporation signal was observed on 14xHis-SUMO-Cdc25C^{200-256S216A} construct, indicating both Chk1 constructs had non-specific kinase activity towards either other T/S in Cdc25C sequence or the protein tag. A small amount of ³²P incorporation was also observed on Chk1KD and Chk1FL, indicating auto-phosphorylation activity of Chk1.

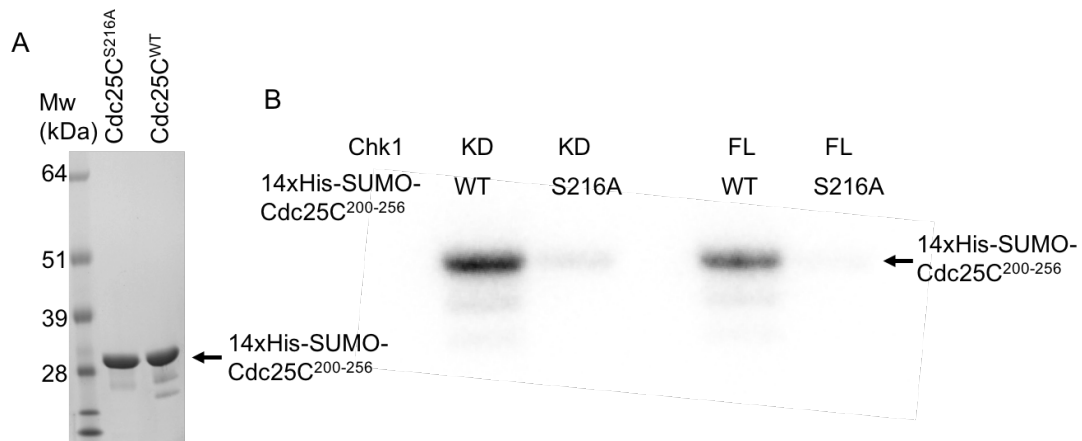


Figure 3.1 ^{32}P incorporation on substrate 14xHis-SUMO-Cdc25C²⁰⁰⁻²⁵⁶

A: The purity of 14xHis-SUMO-Cdc25C^{200-256WT} and 14xHis-SUMO-Cdc25C^{200-256S216A} was shown on SDS-PAGE gel stained with coomassie blue. Unexpected species migrating faster than the target bands were shown on the gel. B: ^{32}P incorporation on substrate was stored in a phosphor screen and the signal was read on an Amersham Typhoon scanner. Signal intensity of each band was read and compared. ^{32}P incorporation on 14xHis-SUMO-Cdc25C^{200-256WT} by both Chk1 kinase constructs was more than that on 14xHis-SUMO-Cdc25C^{200-256S216A}.

3.1.2 NADH-coupled assays of Chk1 activity

Chk1 kinase activity was first investigated using an NADH-coupled assay. Briefly, in the assay conversion of ATP to ADP by the kinase is coupled to the oxidation of NADH to NAD⁺ in the presence of pyruvate kinase and lactate dehydrogenase, leading to a reduction in absorbance at 340 nm over the time course of the reaction (Figure 3.2).

As discussed in chapter 2, purified recombinant Chk1FL expressed in insect cells was phosphorylated at multiple sites. Whether these post-translational modifications affect Chk1FL activity was tested in the kinase assay. Dephosphorylation of Chk1FL was performed by λ phosphatase treatment and the dephosphorylated Chk1FL was assayed in parallel with untreated Chk1FL. ATP hydrolysis rate was calculated at 0.27 and 0.68 $\mu\text{M}/\text{min}$ per micromolar enzyme for dephosphorylated and wild type Chk1FL respectively (Figure 3.2). No significant difference between the two Chk1FL samples

was observed, indicating the degree of heterogeneous Chk1FL phosphorylation resulting from its expression in insect cells on did not influence its kinase activity.

The ATR kinase activates Chk1 by phosphorylation at Chk1's S317 and S345. It is speculated that phosphorylation on these two sites leads to a conformational change which results in Chk1 activation. Understanding the biochemical effect of ATR phosphorylation will shed light on Chk1's activation mechanism. One way to mimic the effect of ATR phosphorylation is to introduce phospho-mimic mutations by replacing serine with glutamate. Two point mutations (S317E and S345E) were generated in Chk1FL to produce a Chk1FL^{S317E/S345E} construct. Chk1FL^{S317E/S345E} was purified using the same protocol as wild-type Chk1FL and had similar purification profiles and yield. ATP hydrolysis rate was calculated at 0.46 and 0.65 $\mu\text{M}/\text{min}$ per micromolar enzyme for Chk1FLWT and Chk1S317E/S345E respectively (Figure 3.2C). NADH-coupled assays of Chk1FL^{WT} and Chk1FL^{S317E/S345E} showed no apparent difference between the two reactions, indicating that the phospho-mimic mutations did not impact Chk1FL activity.

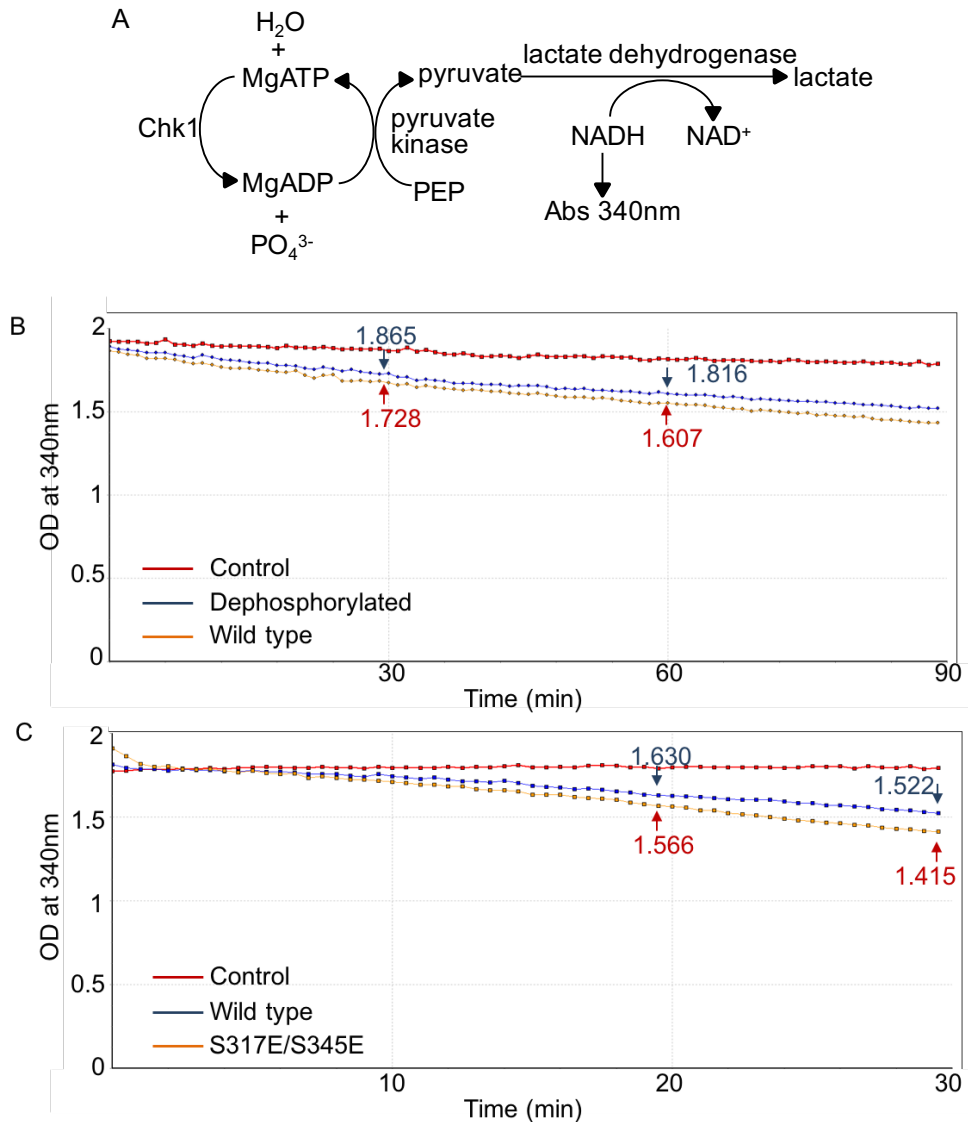


Figure 3.2 Chk1 activity studies using the NADH-coupled assay

A: In the NADH-coupled assay, Chk1 activity was analysed by measuring changes in absorbance at 340nm over time. B: ATP-coupled assay of 1.5 μM dephosphorylated and 1.5 μM untreated (wild type) Chk1FL was performed and absorbance at 340nm was measured at an interval of 1 min for 90 min. A control group with all the reaction ingredients except Chk1 was plotted in red. C: ATP-coupled assay of 6 μM Chk1FL^{WT} and 6 μM Chk1^{S317E/S345E} was performed and the absorbance at 340nm was measured at an interval of 0.5 min for 30 min. A control group with all the reaction ingredients except Chk1 was plotted in red.

The NADH-coupled assay had some disadvantages which made it not suitable for quantitative kinase assays. It measured ATP consumption instead of phosphorylated product formation, making it unsuitable for quantitative studies of kinase activity as not all ATP consumed in the reaction was used as a result of substrate phosphorylation.

For example, Chk1 auto-phosphorylation consumed ATP which cannot be distinguished from the ATP consumed for substrate phosphorylation. The experiment also requires long reaction time and a large amount of kinase to produce a good quality signal, which made it impractical to perform the large number of kinase assays required for quantitative analysis of kinase behaviour. In the following kinase assays, Chk1 activity was therefore studied using radioactive substrate [γ - ^{32}P]ATP.

3.1.3 Determination of ATP concentration for kinase assays

There are several experimental variables that need to be considered in the analysis of kinase activity, including kinase concentration, substrate concentration, ATP concentration and reaction time. ATP concentration should be saturating so it is not rate-limiting in Chk1 kinase assay. The ATP concentration was determined using ^{32}P -ATP based kinase assay (Figure 3.3). The sample was analysed at different time points and the steady state range was selected for reaction rate determination. Reaction rates reached a plateau from 1 mM ATP concentration for both Chk1KD and Chk1FL, indicating that this concentration of ATP was not rate-limiting in the kinase reaction. 1mM ATP was therefore used in subsequent assays.

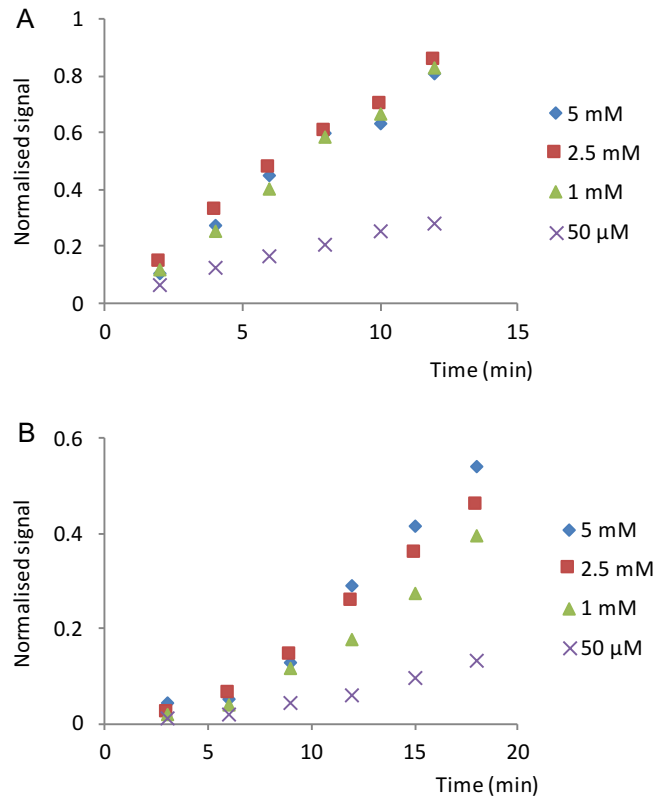


Figure 3.3 Normalised signal of radioactive ^{32}P incorporation on substrate

^{32}P incorporation on 14xHis-SUMO-Cdc25C²⁰⁰⁻²⁵⁶ by Chk1KD (A) and Chk1FL (B) at 50 μM , 1 mM, 2.5 mM and 5 mM ATP. Normalization of signal was performed by running a same sample on all SDS-PAGE gels and the signal of that sample was used as universal reference of all samples for direct comparison. Reactions reached steady-state from 2 min and 12 min in Chk1KD and Chk1FL groups respectively. Slope at 2-8 min of Chk1KD and 12-18 min of Chk1FL was measured as reaction rate.

Initial Chk1 kinase assays were performed using 14xHis-SUMO-Cdc25C²⁰⁰⁻²⁵⁶ as a substrate and reaction samples were analysed on SDS-PAGE gels. The radioactivity signal was stored on a phosphor screen and then was translated to digital density signal in a Typhoon FLA 9500 phosphorimager (GE Healthcare). Kinase reactions with varying substrate concentration in a range of 25 and 150 μM were analysed for 50 or 60 min for Chk1KD and Chk1FL respectively. The steady-state signal was plotted against substrate concentration for initial rate (V_i) calculation. However, the data could not be fit to the Michaelis-Menten model equation. The reason for this remain unclear, but a possible explanation is that kinase reaction did not meet the

single-substrate assumptions of the Michaelis-Menten model, as both Chk1KD and Chk1FL showed some degree of non-specific phosphorylation of the 14xHis-SUMO-Cdc25C substrate.

3.1.4 Chk1 kinase assays at different Cdc25C peptide concentration

To overcome the difficulties encountered with the gel-based analysis, a different [γ - ^{32}P]ATP kinase activity assay was adapted from the published protocol by Hastie *et al* (Hastie *et al.*, 2006). In the new design, a substrate peptide was attached to phosphocellulose paper and the ^{32}P signal incorporated on the substrate was read directly through Cerenkov counting. Comparing to the previous procedure, the new design reduced interference from non-specific phosphorylation of the substrate and increased the accuracy of signal counting by eliminating the multiple signal transfer procedures. A peptide with a region of Cdc25C²⁰⁴⁻²²⁵ was used as a substrate (AKVSRSGLYRSPSPMPENLNRPR, the phosphorylation site is underlined). 50 nM Chk1KD and 500 nM Chk1FL were used in kinetic assays because radioactive signals had a good signal to noise ratio at these conditions. Cdc25C peptide titration at final concentration of 50, 75, 100, 200, 400, 700 and 1000 μM was performed in the presence of 1 mM ATP. To select the time point in the steady-state period, sampling at different time points of kinetic reactions with the lowest and the highest Cdc25C peptide concentration was performed (Figure 3.4).

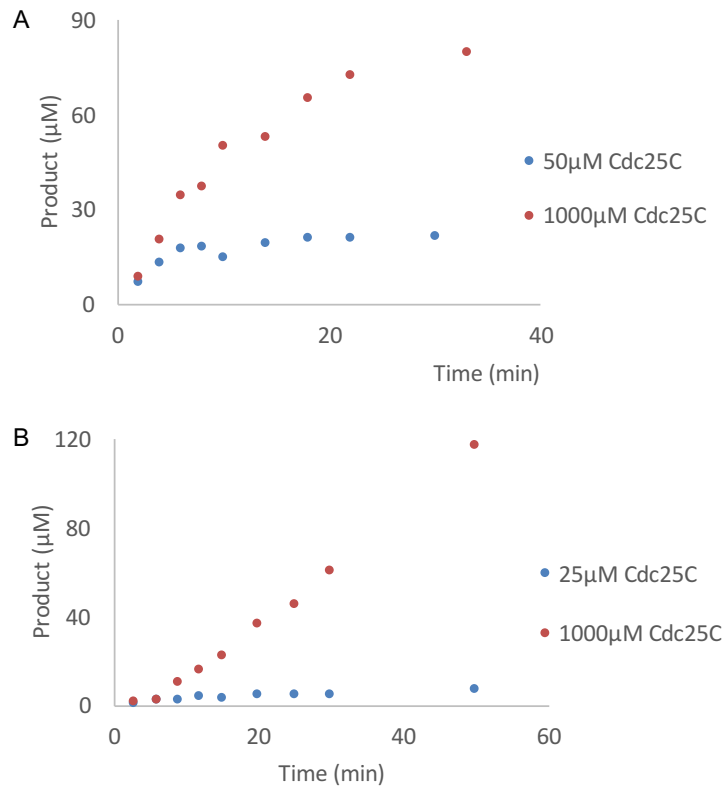


Figure 3.4 Reaction progress curves of Chk1KD and Chk1FL at different Cdc25C concentration

A: Product concentration was plotted against time for Chk1KD at Cdc25C concentration of 50 and 1000 μM. B: Product concentration was plotted against time for Chk1FL at Cdc25C concentration of 25 and 1000 μM. Steady-state reaction velocity (V_i) = slope of the linear range on the progress curve.

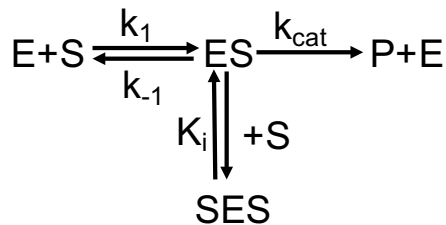
Chk1KD reactions immediately entered steady-state phase after reaction initiation and the time range of 0-5 min was selected for kinase activity analysis. Chk1FL reactions underwent a lag-phase after initiation which was reflected by a slow initial product formation rate in the first 10 min followed by a linear steady-state phase. 10-15 min range was selected for Chk1FL kinase activity analysis. Both datasets were fitted using the Michaelis-Menten equation of steady-state enzyme kinetics (Figure 3.5):

$$V = \frac{d[P]}{dt} = \frac{V_{max}[S]}{K_m + [S]} \quad (\text{Equation 3.1})$$

In the equation, V_{max} represents the maximum reaction rate the system achieves when

the substrate concentration reaches saturation. K_m is the Michaelis-Menten constant, which represents the substrate concentration at which the reaction rate is half of V_{max} .

The kinase assay for Chk1KD showed a departure from the expected trend when Cdc25C peptide concentration exceeded about 200 μM , which was interpreted as due to a substrate inhibition effect. The substrate inhibition effect is led by binding of a second substrate molecule to the ES (enzyme and substrate) complex which forms an inactive SES complex:



A dissociation constant of the inhibitory ternary complex K_i is used in Michaelis-Menten model to account for this inhibition effect:

$$v = \frac{V_{max}[S]}{K_m + [S] \left(1 + \frac{[S]}{K_i}\right)} \quad (\text{Equation 3.2})$$

Conversely, Chk1FL did not show substrate inhibition and the data was normalized and fitted into Michaelis-Menten model with two variables: V_{max} and K_m . V_{max} for Chk1KD and Chk1FL was measured at 18.5 (standard deviation $\Delta=8.3$) and 4.2 ($\Delta=0.7$) $\mu\text{M}/\text{min}$ respectively; K_m was measured at 151 ($\Delta=96$) and 155 ($\Delta=53$) μM . K_i for Chk1KD was measured at 185 ($\Delta=109$) $\mu\text{M}/\text{min}$. K_m of Chk1KD and Chk1FL to Cdc25C peptide was close, which indicated the binding efficiency of both kinases towards the substrate was at the same level.

The catalytic rate constant (k_{cat}) describes the number of substrate molecules turned

into products by the enzyme in one unit time:



k_{cat} can be extracted from V_{max} and enzyme concentration ($[E]$):

$$k_{cat} = \frac{V_{max}}{[E]} \text{ (Equation 3.3)}$$

Given the enzyme concentration of 0.05 μM for Chk1KD and 0.5 μM for Chk1FL, their corresponding catalytic rate k_{cat} was calculated at 370 ($\Delta=166$) and 8.4 ($\Delta=1.4$) min^{-1} , respectively.

The enzyme efficiency describes substrate specificity which is defined as:

$$\text{Enzyme Efficiency} = \frac{k_{cat}}{K_m} \text{ (Equation 3.4)}$$

Kinase efficiency was calculated at 4.1×10^4 ($\Delta=3.2 \times 10^4$) and 903 ($\Delta=343$) $\text{M}^{-1}\text{s}^{-1}$ for Chk1KD and Chk1FL, respectively. The data indicated Cdc25C peptide turnover efficiency of Chk1KD was 45 times of that of Chk1FL. It was intriguing to note the large difference in kinase efficiency between the two Chk1 constructs which showed a similar binding affinity to the Cdc25C peptide. Thus, these results indicated that weaker binding to the peptide substrate was not the reason for the lower efficiency of Chk1FL.

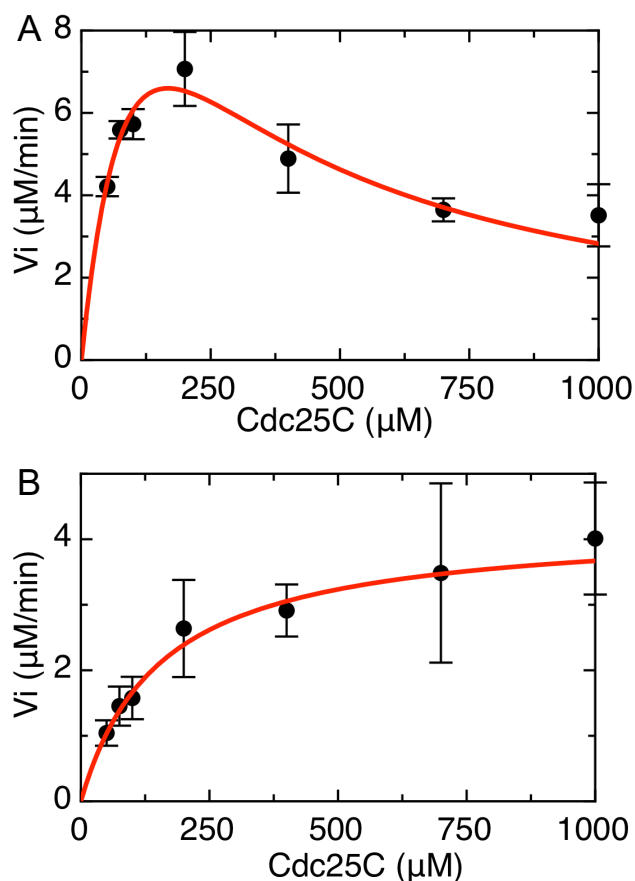


Figure 3.5 Michaelis-Menten plot for Chk1KD and Chk1FL with different Cdc25C peptide concentration

Reaction velocity (V_i) is plotted against Cdc25C peptide concentration for Chk1KD (A) and Chk1FL (B) kinase assays. Data is fitted to Michaelis-Menten model with or without an inhibition parameter K_i using pro Fit (QuantumSoft).

3.1.5 Chk1 kinase assays at different ATP concentration

The Chk1 kinase reaction has two substrates, the Cdc25 peptide and ATP. To study the effect of ATP concentration on the Chk1 enzymatic activity, a series of kinase assays were performed in the presence of increasing amounts of ATP and a constant concentration of Cdc25C peptide. 50 nM Chk1KD and 500 nM Chk1FL were used in the assays, which produced good signal to noise signal. A Cdc25C peptide concentration of 200 μM was selected, as the highest concentration which does not inhibit Chk1KD activity. The steady state of each kinase was verified by plotting product formation versus time (Figure 3.6).

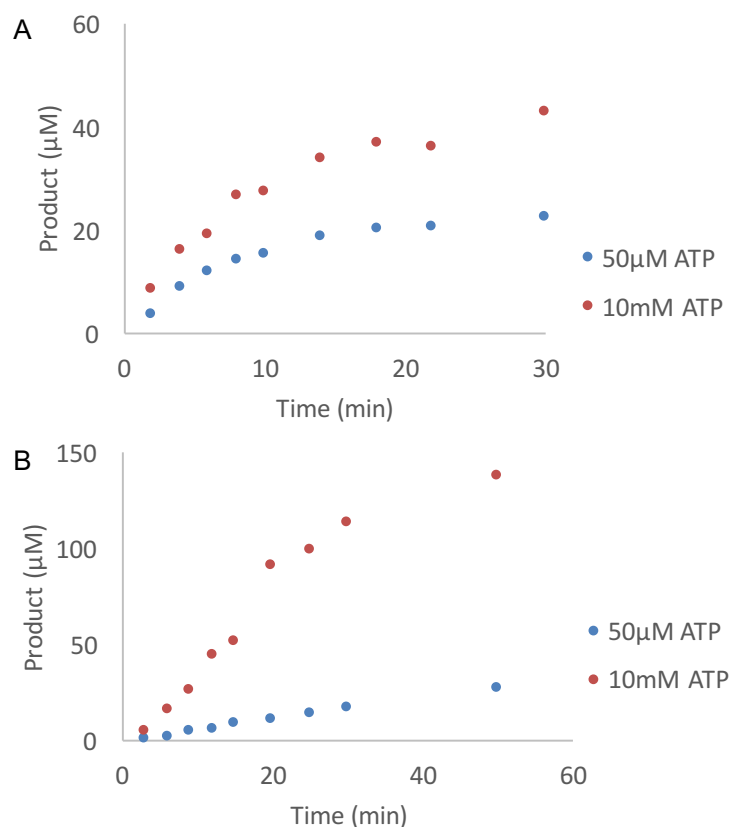


Figure 3.6 Reaction progress curves of Chk1KD and Chk1FL at different ATP concentration

Product concentration was plotted against time for Chk1KD (A) and Chk1FL (B) at ATP concentration of 50 µM and 10 mM. Steady-state reaction velocity (V_i) = slope of the linear range on the progress curve.

Both kinases entered steady-state phase immediately after initiation and 0-4 min and 0-10 min ranges were selected for analysis. Experiments were performed at eight ATP concentrations: 0.0625, 0.125, 0.25, 0.5, 1, 2, 4 and 8 mM. Both sets of data seemed to follow Michaelis-Menten model and were fitted with the V_{max} and K_m variables. V_{max} was fitted at 3.7 ($\Delta=0.1$) and 0.8 ($\Delta=0.2$) µM/min for Chk1KD and Chk1FL respectively; K_m was fitted at 122 ($\Delta=14$) and 330 ($\Delta=190$) µM. The relative measure of ATP binding affinity represented by K_m shows that ATP binding was at a similar level to the two Chk1 constructs. The data could indicate a higher ATP binding affinity to Chk1KD than Chk1FL but the assumption is not conclusive because of the large error in the data. Catalytic rate k_{cat} was calculated at 74 ($\Delta=2$) and 1.6 ($\Delta=0.4$)

min^{-1} for Chk1KD and Chk1FL. Enzyme efficiency was calculated at 1×10^4 ($\Delta=0.1 \times 10^4$) and 81 ($\Delta=51$) $\text{M}^{-1}\text{s}^{-1}$ respectively (Table 3.1). It showed that ATP turnover efficiency of Chk1KD was 123 times of that of Chk1FL, which is more significant than the difference of Cdc25C peptide turnover efficiency between the two constructs. Taken together, these data suggest that Chk1KD is more active than Chk1FL because it has a higher ATP turnover capacity which is a rate-limiting step in Chk1FL kinetic assays. Chk1RD is thus speculated to inhibit Chk1 activity mainly by interfering with ATP binding or catalysis on Chk1KD.

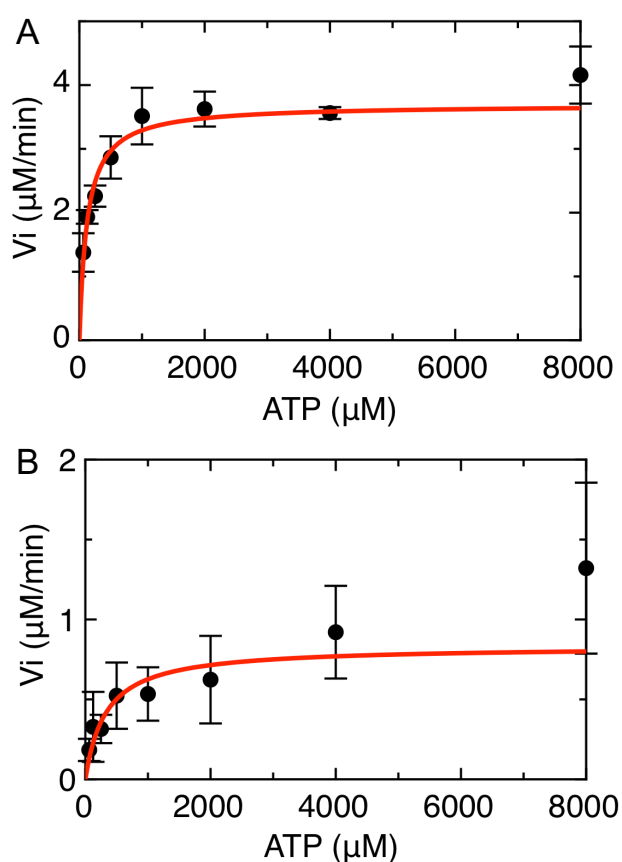


Figure 3.7 Michaelis-Menten plot for Chk1KD and Chk1FL with different ATP peptide concentration

Reaction velocity is plotted against ATP peptide concentration for Chk1KD (A) and Chk1FL (B) kinase assays. Data is fitted to Michaelis-Menten model using pro Fit (QuantumSoft).

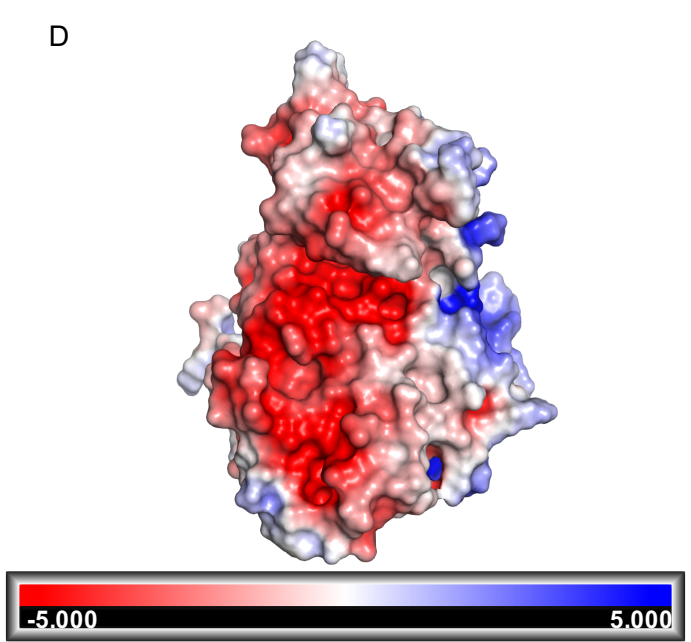
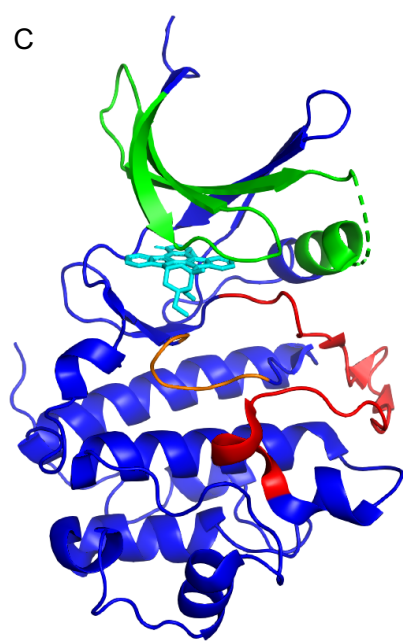
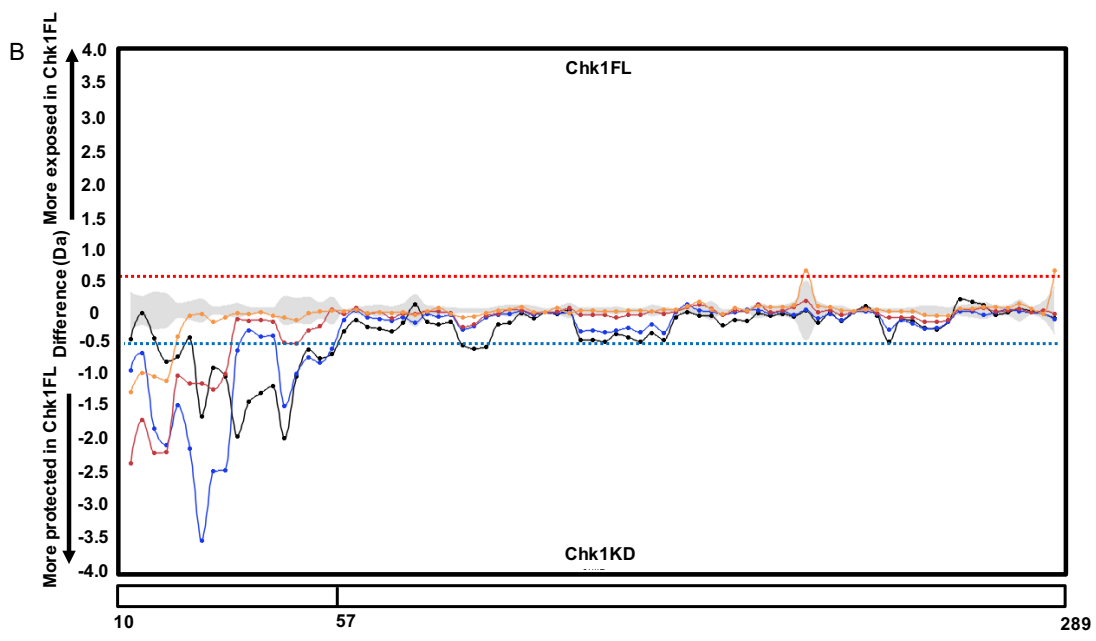
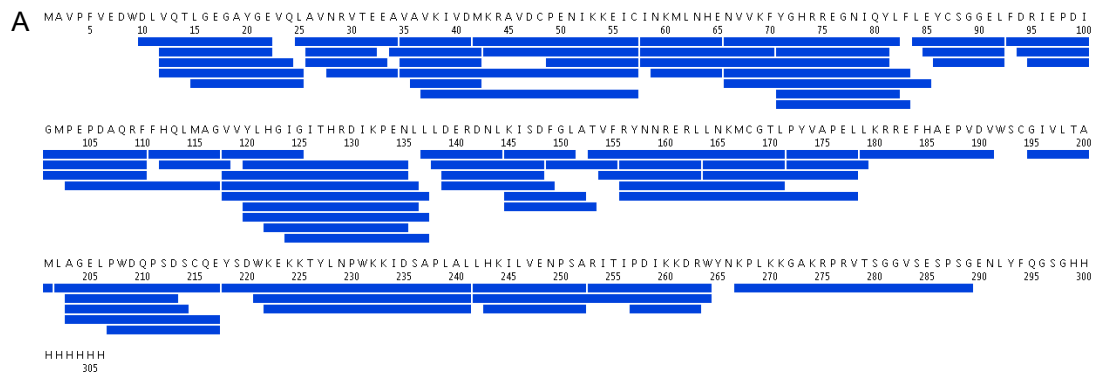
Table 3.1 Michaelis-Menten parameters of Chk1 kinase assays

| | Cdc25C peptide | | | |
|--------|---|----------------------------|------------------------------------|---|
| | V_{max} ($\mu\text{M}/\text{min}$) | K_m (μM) | K_{cat} (min^{-1}) | K_{cat}/K_m ($\text{M}^{-1}\text{s}^{-1}$) |
| Chk1KD | 18.5±8.3 | 151±96 | 370±166 | 4.1x10 ⁴ ±3.2x10 ⁴ |
| Chk1FL | 4.2±0.7 | 155±53 | 8.4±1.4 | 903±343 |
| | ATP | | | |
| | V_{max} ($\mu\text{M}/\text{min}$) | K_m (μM) | K_{cat} (min^{-1}) | K_{cat}/K_m ($\text{M}^{-1}\text{s}^{-1}$) |
| Chk1KD | 3.7±0.1 | 122±14 | 74±2 | 1.0x10 ⁴ ±0.1x10 ⁴ |
| Chk1FL | 0.8±0.2 | 330±190 | 1.6±0.4 | 81±51 |

3.1.6 Chk1 intramolecular interacting interface studies

As shown in chapter 2, a tight binding between Chk1KD and Chk1RD was observed in a size-exclusion co-migration assay. To understand the role of the intramolecular interaction in Chk1 activity regulation, further experiments were performed to study the interaction. Hydrogen-deuterium exchange (HDX) analysis can provide useful information on the presence and extent of inter- and intramolecular interfaces between proteins and protein domains (Koneremann et al., 2011). Comparative HDX experiments were therefore performed on Chk1KD and Chk1FL to investigate the presence of a putative interface between Chk1KD and Chk1RD. The experiments were performed by Drs. Sarah Maslen and Mark Skehel at the Proteomics facility of the MRC-LMB. 40 μM Chk1KD and Chk1FL were diluted in D₂O and labile hydrogen atoms exchanged with deuterium. Incubation in D₂O was performed for 0.3, 3, 30 and 300 seconds and the hydrogen-deuterium exchange was quenched by acidification, followed by proteolytic digestion of the protein samples and MS analysis of the resulting peptides. Sequence coverage of Chk1KD reached 89.9% with

redundancy of 3.71 and 9 N-terminal amino acids and the C-terminal residues spanning the TEV cleavage site and the 8xHis-tag were not covered. Overall the coverage of the region of interest on Chk1KD was good (Figure 3.8). The HDX signal for the Chk1KD was subtracted from that of Chk1FL, to assess what region of Chk1FL was more protected or exposed comparing to Chk1KD (Figure 3.8). The HDX data showed that a region of D10-C57 was significantly more protected in Chk1FL than in Chk1KD, while the rest of the kinase domain sequence showed no difference in the HDX signal (Figure 3.8). Thus, the HDX experiment supported the notion of an intramolecular association between kinase and regulatory domains of Chk1, and indicated that an N-terminal region of Chk1 within its ATP-binding domain was the site of interaction with the with the regulatory domain. Calculation of surface charge using the APBS Electrostatics module in PyMOL (Baker et al., 2001) (Figure 3.8) showed the presence of an acidic patch at the putative interface region on the surface of Chk1KD. In combination with the information gleaned from the structural analysis of the Chk1RD (Emptage et al., 2017), which revealed a substantial basic nature of its surface, it was reasonable to speculate that the intramolecular interaction was driven or partially driven by charge-charge interaction.



(Caption on next page)

Figure 3.8 HDX analysis of Chk1 kinase domain in Chk1FL and Chk1KD

A: Chk1KD was digested by pepsin and the peptide coverage was measured by mass-spectrometry. B: HDX plot of mass differences versus sequence between Chk1FL and Chk1KD, measured at 0.3s, 3s, 30s and 300s (orange, red, blue and black traces, respectively). Error is shown as grey shaded area and significance threshold is marked with red and blue dash lines. Region of D10-C57 is more protected in Chk1FL and other regions does not show significant mass difference in HDX. C: The putative Chk1RD interacting region is shown in green colour on a ribbon representation of the Chk1KD structure (1NVQ). Chk1KD has a bi-lobe structure consisting of a small N-terminal lobe mainly formed by β -strands and a C-terminal lobe mainly formed by α -helices. The activation loop and the catalytic loop is coloured in red and orange, respectively. Chk1 inhibitor UCN-01 coloured in cyan binds to ATP-binding pocket. (Zhao et al., 2002). D: Electrostatics surface of Chk1KD was calculated by APBS Electrostatics in PyMOL in a range of -5 to 5 KT/e with negatively charged surface coloured in red and positively charged surface coloured in blue (Baker et al., 2001).

Within the Chk1 KD-RD interaction region, the exposed V27-A34 sequence forms a β -turn followed by a β -strand (Figure 3.9). To explore if this region of the Chk1KD constitutes the interaction site with Chk1RD, a new construct was designed and tested on kinase activity assay. The 8 amino acids spanning V27 to A34 were replaced with the tetrapeptide TGGS, with the aim to alter the local surface properties whilst avoiding structural disruption of the Chk1KD. The rationale for the mutation was to interfere with the intramolecular association of the regulatory domain with the kinase domain, thus relieving the Chk1RD's inhibition of kinase activity and leading to increased kinase activity of the full-length Chk1 mutant relative to wild-type. The planned mutagenesis was performed on Chk1KD too, as control that the mutation had not affected kinase activity. The new Chk1KD ^{Δ turn} and Chk1FL ^{Δ turn} constructs were successfully expressed in *Sf9* cells and purified using the same protocol with their wild-type constructs. The effect of the mutagenesis targeting the V27-A34 region on enzymatic activity was determined by ³²P-ATP based kinase assay. Unfortunately, both Chk1 ^{Δ turn} FL and KD constructs had lost kinase activity (Figure 3.9), indicating the mutation had disrupted the kinase structure, potentially by interfering with ATP binding.

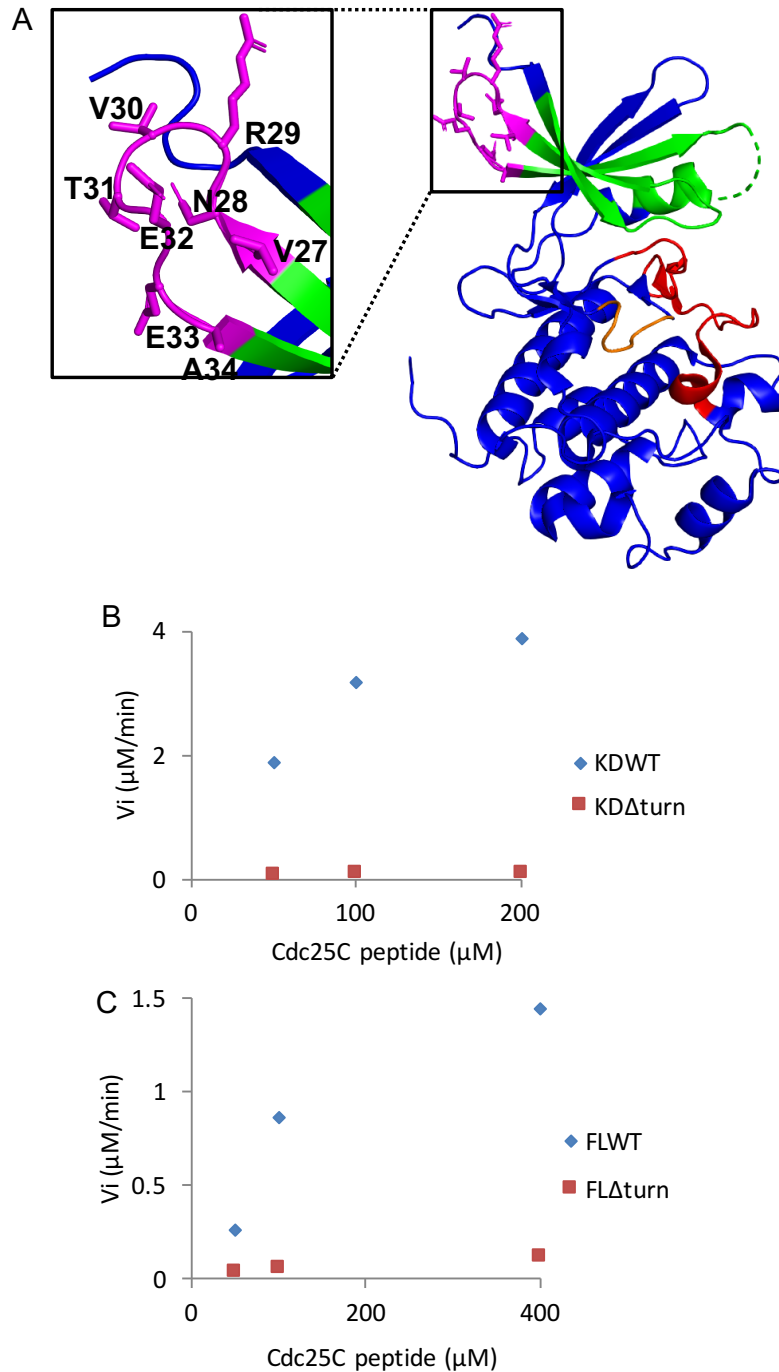


Figure 3.9 Mutant Chk1^{Δturn} and kinase assays

A: The region of V27-A34 (shown in magenta sticks) was replaced by a sequence of TGGGS to make Chk1^{Δturn} mutants. Figure was generated by PyMOL. Kinetic assays were performed in parallel with Chk1^{WT} constructs and both Chk1KD^{Δturn} (B) and Chk1FL^{Δturn} (C) showed abolished kinase activity.

Two other constructs were designed based on the HDX result and the implication from the KA structure (the 91-amino-acid-polypeptide at the C-terminal end) which showed a positively-charged surface (Emptage et al., 2017), and thus indicating that the interaction between Chk1KD and Chk1KA was regulated by electrostatic interaction. Four glutamate residues (E17, E22, E32 and E33) map to the putative Chk1KA interacting interface are exposed on the surface. Two other glutamate residues (E50 and E55) are present at the putative interacting interface: E50 points outward and could have a function in interaction with Chk1KA while E55 points inside towards the N-terminal domain. The HDX rate of these residues was not as strong as the above-mentioned residues so they were not selected for mutagenesis studies. Mutants of Chk1^{E17T/E22T} and Chk1^{E32S/E33T} (Figure 3.10) were introduced on Chk1KD and Chk1FL and all the new constructs were expressed in *Sf9*. These mutants were purified using the same purification protocol with their wild-type counterparts including gravity flow Ni-NTA chromatography, Heparin chromatography and size-exclusion chromatography (Figure 3.11).

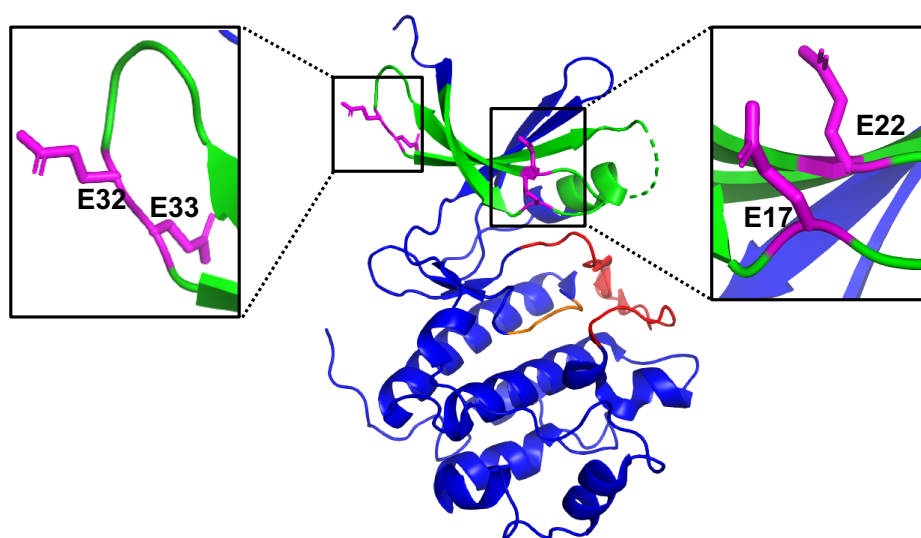
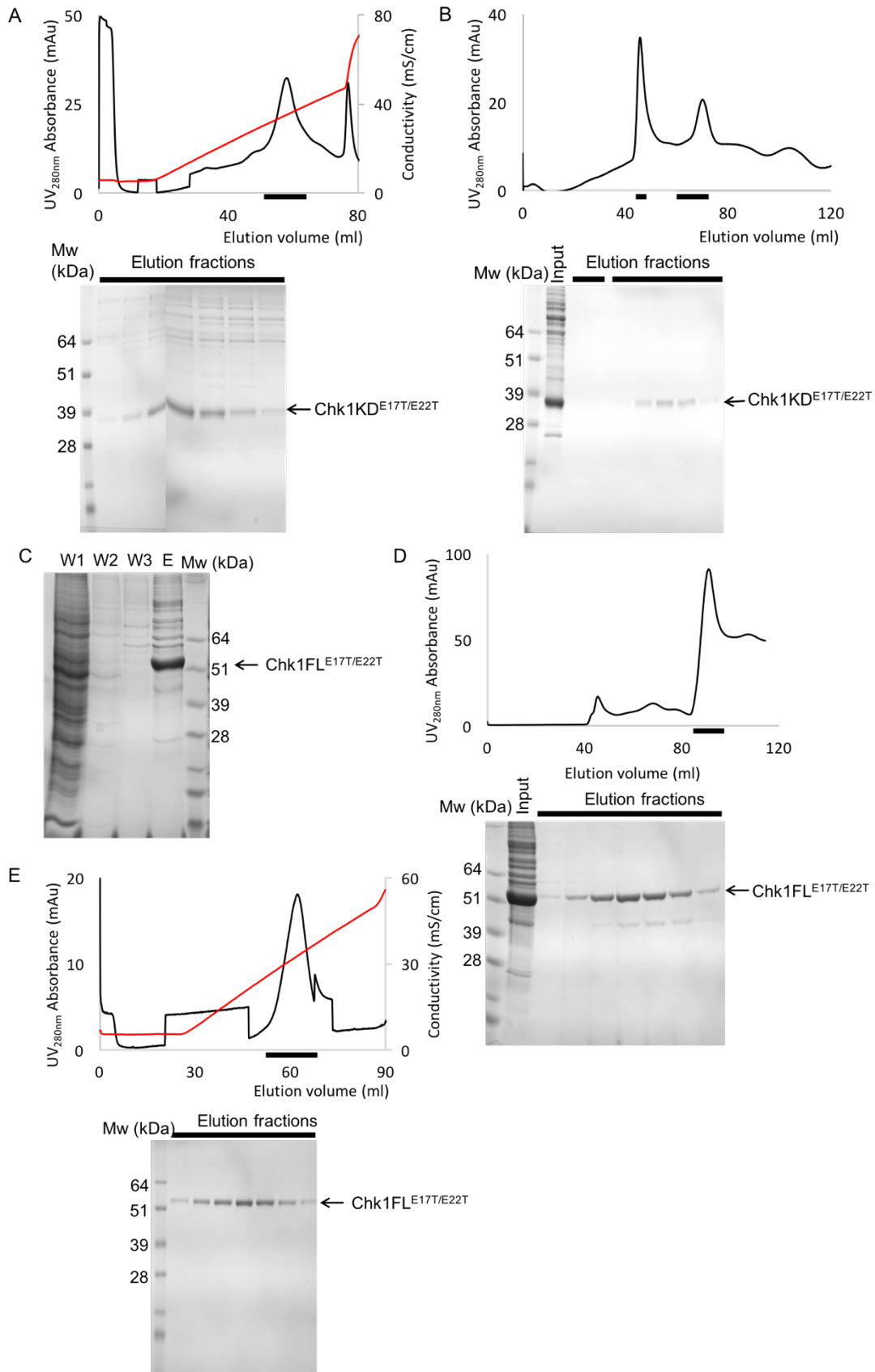


Figure 3.10 Chk1^{E17T/E22T} and Chk1^{E32S/E33T} constructs

Acidic amino acid residues E17 and E22 (shown in magenta) were replaced by threonine to make Chk1^{E17T/E22T} mutants. E32 and E33 (shown in magenta) were replaced by serine and threonine to make Chk1^{E32S/E33T} mutants. Figure was generated by PyMOL.



(Caption on next page)

Figure 3.11 Purification of Chk1KD^{E17T/E22T} and Chk1FL^{E17T/E22T}

A: Cell lysate of Chk1KD^{E17T/E22T} applied on Ni-NTA agarose beads column and the elution was applied onto Hitrap Q ion-exchange column. Protein was eluted with gradient NaCl wash. B: Elution fractions of ion-exchange step was concentrated and applied to a Superdex 200 16/60 column for size exclusion chromatography. C: Cell lysate of Chk1FL^{E17T/E22T} was applied on Ni-NTA agarose beads column and was eluted in 300 mM imidazole. D: Elution was concentrated and applied to a Superdex 200 16/60 column for size exclusion chromatography. E: Fractions containing target protein was applied onto Hitrap Q ion-exchange column and protein was eluted with gradient NaCl wash.

The influence of these mutations was evaluated by ³²P-ATP based kinase assays. All three Chk1KD constructs (WT, E17T/E22T and E32S/E33T) showed a similar level of activity (Figure 3.12), indicating the mutations did not change kinase activity. Chk1FL^{E17T/E22T} was observed to be more active than Chk1FL while Chk1FL^{E32S/E33T} showed a similar level of activity with Chk1FL^{WT} (Figure 3.12).

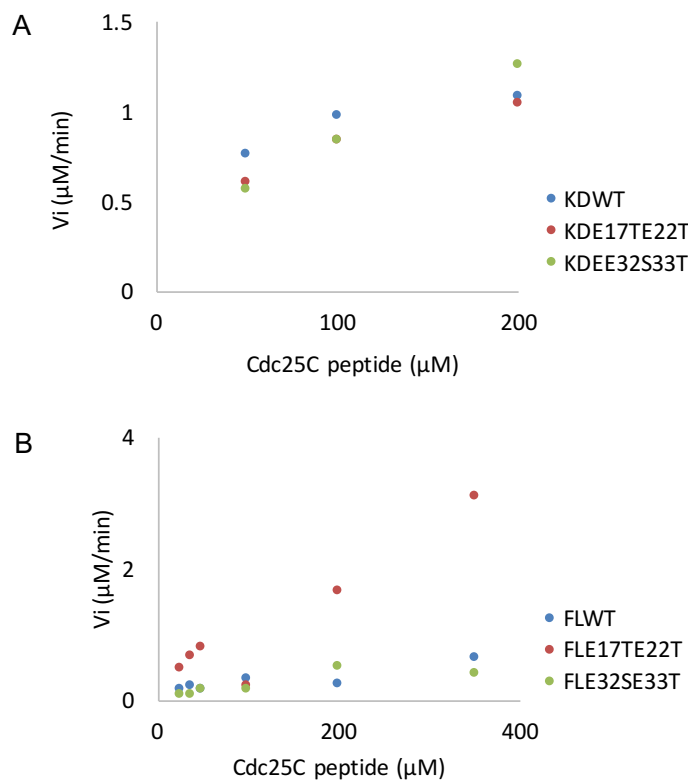
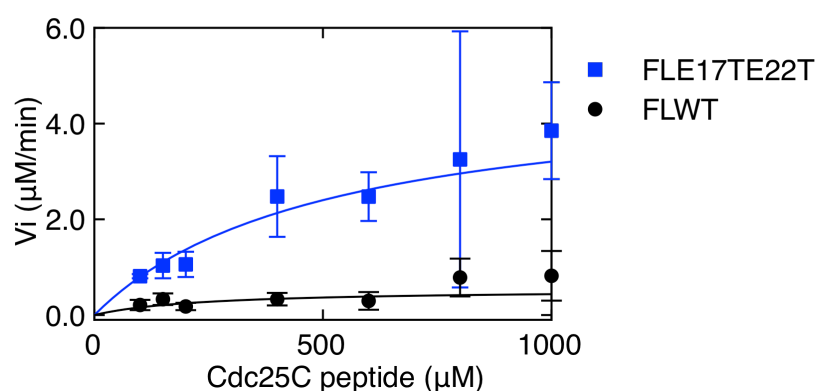


Figure 3.12 Kinase assays of Chk1^{E17T/E22T}, Chk1^{E32S/E33T} and Chk1^{WT}

A: Kinase assays were performed in parallel with Chk1^{WT} constructs and both Chk1KD mutants showed activity at a similar level of Chk1KD^{WT}. B: Chk1FL^{E17T/E22T} showed higher activity than Chk1FL^{WT} and Chk1FL^{E32S/E33T}.

It was intriguing to observe the increased kinetic activity of Chk1FL^{E17T/E22T} in comparison to Chk1FL^{WT} which was an indication of disrupted Chk1KD - Chk1RD interaction. To further investigate kinetic behaviour of the mutant, triplicate kinase assays with Cdc25C peptide titration were performed in parallel with Chk1FL^{WT}. Both datasets were fitted using steady-state enzyme kinetics. V_{max} was measured at 4.8 ($\Delta=1.5$) and 0.5 ($\Delta=0.3$) $\mu\text{M}/\text{min}$ for the Chk1FL^{E17T/E22T} mutant and Chk1FL^{WT} and K_m was measured at 504 ($\Delta=200$) and 236 ($\Delta=313$) μM respectively. Chk1FL^{WT} showed a low level of kinase activity which led to a low signal to noise ratio and thus a higher level of error range.

Enzyme concentration was 0.5 μM for both constructs and k_{cat} was calculated at 9.6 ($\Delta=3.0$) and 1.0 ($\Delta=0.6$) min^{-1} . Enzyme efficiency was calculated at 317 ($\Delta=160$) and 71 ($\Delta=103$) $\text{M}^{-1}\text{s}^{-1}$ for the mutant and the wild-type Chk1FL respectively. These data show that the kinase efficiency of Chk1FL^{E17T/E22T} is four times that of Chk1FL^{WT} (Table 3.2). The observed increase in kinase efficiency did not result from conformational change of active site on Chk1KD because the introduction of the same mutations on Chk1KD did not show a significant difference in kinase activity compared to Chk1KD^{WT} (Figure 3.13). It is thus suggested that the two amino acid residues E17 and E22 are involved in the interacting interface of Chk1KD and Chk1RD and that their mutations and consequent loss of local charge led to disruption of the inhibitory intramolecular interaction and consequent increase in Chk1FL kinase activity.



(Caption on next page)

Figure 3.13 Michaelis-Menten plot of Chk1FL^{E17T/E22T} and Chk1FL^{WT}

Triplicate of kinetic assay between Chk1FL^{E17T/E22T} and Chk1FL^{WT} at varying Cdc25C peptide was plotted and fitted in Michaelis-Menten equation. Fitting and plotting was performed by pro Fit (QuantumSoft).

Table 3.2 Michaelis-Menten parameters of Chk1FL kinase assays

| | Cdc25C peptide | | | |
|-----------------------------|------------------------------|------------------------|--|--|
| | V _{max} (μM/min) | K _m (μM) | K _{cat} (min ⁻¹) | K _{cat} /K _m (M ⁻¹ s ⁻¹) |
| Chk1FL ^{E17T/E22T} | 4.8±1.5 | 504±200 | 9.6±3.0 | 317±160 |
| Chk1FL ^{WT} | 0.5±0.3 | 236±313 | 1.0±0.6 | 71±103 |

3.1.7 Attempts towards understanding binding affinity between ATP and Chk1

Kinase activity mechanism can be better understood in combination with binding affinity information on ATP and substrate. Several biophysical analyses were performed to measure the binding affinity. Isothermal titration calorimeters (iTC) measures heat change introduced by molecule interactions which gives an interpretation of binding parameters including dissociation equilibrium constant (K_d), stoichiometry and enthalpy of interaction. ATP titration was performed with Chk1KD to study the binding event. However, all attempts towards acquiring these binding parameters were unsuccessful because of the uninterpretable signal generated in iTC experiments with a different setup.

An alternative technique, fluorescence polarization (FP), was used to study the interaction between fluorescein labelled ATP (n6-(6-Amino)hexyl-ATP-6-FAM) and Chk1KD. 78 to 0.09 μM Chk1KD titration was performed with 30 nM fluorescein-ATP while no significant anisotropy signal was observed. It was

speculated that the binding affinity between ATP and Chk1FL was beyond the range of Chk1KD titration. Higher Chk1KD concentration at a low salt concentration where the ATP interaction was studied cannot be achieved and thus FP was not an ideal technique to achieve the goal.

Surface plasmon resonance (SPR) was used to measure the binding affinity between ATP and Chk1 constructs. However, response signal generated by ATP titration to Chk1 constructs was extremely weak which showed a poor signal to noise ratio. The binding kinetics thus cannot be determined and the only implication acquired from the experiment was that ATP binds to Chk1 constructs at a sub-micromolar range.

3.2 Discussion

This chapter reported a quantitative analysis of Chk1KD and Chk1FL kinase activity in the presence of the Cdc25C peptide and ATP. Enzyme kinetic parameters were obtained from the fitting to the Michaelis-Menten model and difference was observed in the data between Chk1KD and Chk1FL kinase assays. K_m does not represent but can reflect the binding affinity between the enzyme and the substrate. The data shows that K_m to Cdc25C peptide of both Chk1KD and Chk1FL is at the same level, indicating the two Chk1 constructs have the same binding affinity to the substrate peptide. Because of a large error in K_m on ATP binding to Chk1FL, no conclusive difference on ATP binding to the two Chk1 constructs is seen but an indication of a higher ATP binding affinity to Chk1KD than Chk1FL can be reflected from the data. Chk1KD is 45 times and 123 times as efficient as Chk1FL in terms of Cdc25C peptide and ATP turnover respectively, which supports an assumption that ATP turnover is the rate-limiting step in Chk1FL kinase reaction. In view of the inhibitory role of Chk1RD towards Chk1KD, it is speculated that Chk1RD blocks the ATP binding site on Chk1KD and thus suppresses its efficiency.

To further understand the intramolecular interaction between Chk1KD and Chk1RD from an atomic level, HDX experiment was performed to reveal the interaction interface between the two domains. The N-terminal region spanning residues D10-C57 on Chk1KD was identified as a protected area by Chk1RD. A negatively-charged patch is identified on this region and the intramolecular interaction between the two domains is speculated as an electrostatic interaction. Four glutamate residues in this region expose on the surface of Chk1KD and point mutations to threonine or serine were made to replace these charged residues. The effect of the mutants was verified by kinase assays which showed that the mutant Chk1FL^{E17T/E22T} was four times as efficient as Chk1FL^{WT}. It thus agrees with the assumption that the Chk1 intramolecular interaction is driven by charge-charge interaction between the two domains. The two glutamate residues locate at the glycine-rich loop which is in

close proximity to ATP binding site. The increased activity of the mutant thus supports the assumption that the Chk1RD inhibits Chk1KD activity through interrupting the ATP binding site.

3.3 Materials and Methods

3.3.1 Generation, expression and purification of 14xHis-SUMO-Cdc25C²⁰⁰⁻²⁵⁶

Human Cdc25C²⁰⁰⁻²⁵⁶ gene sequence was synthesised using gBlocks Gene Fragments service (IDT). The Cdc25C²⁰⁰⁻²⁵⁶ sequence was amplified using primers *Cdc25C-f* and *Cdc25C-r* (Appendix A) to create BamHI and HindIII restriction sites. The amplified sequence was inserted to pRSFDuet vector (Novagen) using the two restriction sites. pRSFD-Cdc25C²⁰⁰⁻²⁵⁶ was transformed to Rosetta 2 (DE3) competent cells for expression (procedure is described in 2.3.1). Cells were inoculated to 1 L 2xYT medium and was induced with 1 mM IPTG when OD reached 0.6-0.8. Expression was performed at 37 °C for 4 h. Cell harvest, sonication and centrifugation procedure was the same as described in 2.3.2. The soluble fraction was applied on gravity flow Ni-NTA agarose column and was washed twice with 25 mM Hepes-NaOH pH 7.5, 300 mM NaCl and 50 mM imidazole followed by a 300 mM imidazole elution step. Ni-NTA elution fraction was concentrated to 1 ml and was applied to Superdex 75 16/60 column for gel filtration in a buffer of 25 mM Hepes-NaOH pH 7.5, 300 mM NaCl, 10% glycerol and 2 mM DTT. The elution fraction with highest purity (90%) was concentrated to 243 µM and stored at -80 °C.

3.3.2 Generation of 14xHis-SUMO-Cdc25C^{200-256-S216A}

S216A mutagenesis was introduced to pRSFD-Cdc25C²⁰⁰⁻²⁵⁶ template by site-directed mutagenesis (QuickChange, Stratagene) using primers *Cdc25CS216A-f* and *Cdc25CS216A-r* (Appendix A). Expression and purification procedure of 14xHis-SUMO-Cdc25C^{200-256-S216A} was the same as described in 3.3.1.

3.3.3 Chk1 substrate specificity kinase assays

40 μ l reaction containing 40 μ M 14xHis-SUMO-Cdc25C^{200-256WT} or 14xHis-SUMO-Cdc25C^{200-256S216A}, 50 μ M ATP, 0.05 μ M Chk1KD or 0.5 μ M Chk1FL was performed in reaction buffer with final concentration of 50 mM HEPES-NaOH pH 7.5, 150 mM NaCl, 1mM DTT, 10 mM MgCl₂ and 1 mM beta-glycerolphosphate. Chk1 protein stock was buffer exchanged to Chk1 buffer (50 mM HEPES-NaOH pH 7.5, 500 mM NaCl, 1mM DTT) using protein desalting spin columns (Thermo Fisher). 14xHis-SUMO-Cdc25C²⁰⁰⁻²⁵⁶ were buffer exchanged to 1x reaction buffer. 5x Chk1KD or Chk1FL stock was prepared using the Chk1 buffer. Chk1 stock was added to reaction before the start of the reaction to make the reaction volume to 35 μ l. 1 μ l 10mCi/ml [γ -³²P]ATP (Perkin Elmer, Easytide) was added to 24 μ l cold ATP stock to achieve ATP mixture concentrations of 400 μ M. 5 μ l ATP mixture was added to corresponding reactions to initiate the reaction. The reaction was mixed by shaking briefly was spun down. Reaction was incubated at 37 °C for 40 min. 5 μ l reaction sample was added to 2 μ l 4X protein loading buffer (containing reducing agent) and 1 μ l 0.5M EDTA. The sample was boiled at 80 °C for 10 min. The sample was spun down briefly and was applied on a 12% acrylamide gel for SDS-PAGE analysis. The gel was dried on gel dryer at 80°C for 2h. The dried gel was exposed to a phosphorscreen (GE Healthcare) for 30 min and the signal was scanned and analysed on Typhoon FLA 9500 (GE Healthcare).

3.3.4 NADH-coupled assays of Chk1 activity

200 μ l reaction containing different concentrations of Chk1FL constructs (1.5 μ M dephosphorylated Chk1FL or 1.5/6 μ M untreated Chk1FL or 6 μ M Chk1FL^{3T/SE}), 160 μ M NADH, 2 mM phospho(enol)pyruvate, 50 μ M ATP, 50 μ M 14xHis-SUMO-Cdc25C²⁰⁰⁻²⁵⁶, 1.8-2.8 units of lactate dehydrogenase and 1.2-2 units of pyruvate kinase were performed in reaction buffer (50 mM HEPES-KOH pH 7.5, 150 mM KAc, 8 mM Mg(Ac)₂ and 5 mM β -mercaptoethanol). Reaction was added to

a 96-well assay plate (Corning) and the absorbance at 340nm was read on Pherastar (BMG Labtech) for 30-60 min at an interval of 0.5 or 1 min.

3.3.5 Generation of Chk1^{S317E/S345E}, Chk1^{Δturn}, Chk1^{E17T/E22T} and Chk1^{E32T/E33S}

Chk1 constructs were generated from the pFBDM-Chk1KD and pFBDM-Chk1FL plasmid described in 2.3.1 by site-directed mutagenesis (QuickChange Stratagene). Chk1^{S317E/S345E} was generated using primers *Chk1S317E-f* and *Chk1S317E-r*; *Chk1S345E-f* and *Chk1S345E-r* (Appendix A) based on the Chk1FL plasmid. Chk1^{Δturn} was generated using primers *Chk1Δturn-f* and *Chk1Δturn-r* (Appendix A) based on both construct templates. Chk1^{E17T/E22T} was generated using primers *Chk1E17T-f*, *Chk1E17T-r*, *Chk1E22T-f* and *Chk1E22T-r* (Appendix A) based on both construct templates. Chk1^{E32T/E33S} was generated using primers *Chk1E32T/E33S-f* and *Chk1E32T/E32S-r* (Appendix A) based on both construct templates.

3.3.6 Determination of ATP concentration in kinase assays

50 μl reaction containing 100 μM 14xHis-SUMO-Cdc25C²⁰⁰⁻²⁵⁶, 50 μM, 1 mM, 5 mM or 10 mM ATP, 0.05 μM Chk1KD or 0.5 μM Chk1FL was performed in reaction buffer with final concentration of 50 mM Hepes-NaOH pH 7.5, 150 mM NaCl, 1mM DTT, 20 mM MgCl₂ and 1 mM beta-glycerolphosphate. Chk1 protein stock was buffer exchanged to Chk1 buffer (50 mM Hepes-NaOH pH 7.5, 500 mM NaCl, 1mM DTT) using protein desalting spin columns (Thermo Fisher). 14xHis-SUMO-Cdc25C²⁰⁰⁻²⁵⁶ were buffer exchanged to 1x reaction buffer. 5x Chk1KD or Chk1FL stock was prepared using the Chk1 buffer. Chk1 stock was added to reaction before the start of the reaction to make the reaction volume to 40 μl. 1 μl 10mCi/ml [γ -32P]ATP (Perkin Elmer, Easytide) was added to 14 μl cold ATP stock to achieve ATP mixture concentrations at 250 μM, 5 mM, 25 mM and 50 mM. 10 μl ATP

mixture to corresponding reactions to initiate the reaction and the reaction was mixed by shaking briefly. The reaction was briefly spun down and was incubated at 30 °C. Reaction sample was taken at 2, 4, 6, 8, 10 and 12 min time-point for Chk1KD and 3, 6, 9, 12, 15 and 18 min for Chk1FL. The sample was analysed using the same protocol described in 3.3.3.

3.3.7 Validation of linear ³²P counts range on scintillation counter

Validation of signal detection by scintillator (Beckman Coulter LS6500) was performed by applying serially diluted radiolabelled ATP on phosphocellulose paper and counting the signal of each paper sample. It was shown that a signal above 300 counts per minute was in the linear range of signal detection of the scintillator and therefore the experiments were designed to reach the linear range by varying the ³²P-ATP concentration accordingly.

3.3.8 Time range determination at highest and lowest Cdc25C peptide concentration

50 µl reaction containing 25, 50 or 1000 µM Cdc25C peptide (AKVSRSGLYRSPSPENLNRPR), 1 mM ATP and 0.05 µM Chk1KD or 0.5 µM Chk1FL was performed in reaction buffer at a final concentration of 50 mM HEPES-NaOH pH 7.5, 150 mM NaCl, 1 mM DTT, 20 mM MgCl₂, 1 mM β-glycerolphosphate. Two batches of the Cdc25C peptide with the same sequence was synthesised by Genosphere Biotechnologies (UK) at 5mg at >95% purity. The concentration of the first batch of Cdc25C peptide was determined by Amino Acid Analysis service performed by Dr. Peter Sharratt at the Protein and Nucleic Acid Analysis Facility at the University of Cambridge. The concentration of the second batch of Cdc25 peptide was determined using NanoDrop™ One Microvolume UV-Vis Spectrophotometer (Thermo Scientific) at the wavelength of 205nm and the

concentration was calibrated based on the reading at 205nm of the first batch of the peptide. Chk1 protein stock was buffer exchanged to Chk1 buffer (50 mM Hepes-NaOH pH 7.5, 500 mM NaCl, 1mM DTT) using protein desalting spin columns (Thermo Fisher). Absorbance at 280 nm was measured on Cary 50 UV-Vis Spectrophotometer (Agilent Technologies) and concentration was determined with extinction coefficient at 280 nm. 2.5 μ M Chk1FL or 0.25 μ M Chk1KD (5x) protein stock was prepared using Chk1 buffer. 5 mM (5x) ATP mix was prepared from 100 mM ATP (Thermo Fisher) and 10mCi/ml [γ - 32 P]ATP (Perkin Elmer). 10 μ l ATP mix was added to each reaction. 0.25 μ M Chk1KD 2.5 μ M Chk1FL was added to each reaction to initiate the reaction. The reaction was mixed by shaking the tube briefly which was followed by a quickly spin. The reaction was incubated at 30 °C. A reference reaction containing the same components except Chk1KD or Chk1FL was performed in parallel with the experiment reaction. 5 μ l reaction was spotted on a pre-labelled 1.2 cm x 1.2cm P81 phosphocellulose paper (Reaction Biology Corp.) and the paper was immediately immersed into chilled 75 mM phosphoric acid to stop the reaction. The peptide was positively charged and bound to phosphocellulose paper during the wash in 75 mM phosphoric acid, which washed off free ATP attached to the phosphocellulose paper. The paper was washed in 500 ml phosphoric acid for 10 min with stirring and the old phosphoric acid was replaced by fresh phosphoric acid. The wash step was repeated three times. The paper was briefly rinsed with acetone after the last wash and was left to air dry for 1 h. ATP signal calibration sample was prepared by spotting 5 μ l 10x diluted ATP mix on the phosphocellulose paper and air dried. Dry phosphocellulose paper was sealed in scintillator tubes and the 32 P emission counts was read on a scintillation counter (Beckman Coulter LS6500) using a "32P program". Radioactivity count for one unit of ATP was obtained using the ATP calibration sample which was used to interpret the amount of phosphate incorporated into the substrate (product formation). Product formation rate was acquired which was equal to enzyme catalysis rate. It was plotted against time and steady-state range was acquired.

3.3.9 Chk1 kinase assay at different concentration of Cdc25C peptide

10 μ l reaction for Chk1KD or 14 μ l reaction for Chk1FL containing varying concentration (25, 50, 75, 100, 200, 400, 700 and 1000 μ M) of Cdc25C peptide, 1 mM ATP mix and 0.05 μ M Chk1KD or 0.5 μ M Chk1FL was performed in reaction buffer at a final concentration of 50 mM Hepes-NaOH pH 7.5, 150 mM NaCl, 1 mM DTT, 20 mM MgCl₂, 1 mM β -glycerolphosphate. The remaining procedure was the same with the protocol described in 3.3.8. Sample was taken and stopped at 5 min for Chk1KD. Two time-points (10 min and 15 min) for Chk1FL were taken. The rate of product formation was plotted against Cdc25C peptide concentration. The data was fitted to Michaelis-Menten model with and without a substrate inhibition dissociate parameter using Pro Fit software (<http://quansoft.com>). The error of k_{cat} was acquired from the error propagation analysis: $\Delta k_{cat} = \frac{\Delta V_{max}}{[E]}$. The error of enzyme efficiency

was acquired from the error propagation analysis: $\Delta \frac{k_{cat}}{k_m} = \frac{k_{cat}}{k_m} \sqrt{\left(\frac{\Delta k_{cat}}{k_{cat}}\right)^2 + \left(\frac{\Delta k_m}{k_m}\right)^2}$

3.3.10 Time range determination at highest and lowest ATP concentration

50 μ l reaction containing 200 μ M Cdc25C peptide, 50 μ M or 10 mM ATP and 0.05 μ M Chk1KD or 0.5 μ M Chk1FL was performed in reaction buffer. Assay procedure was described in 3.3.8.

3.3.11 Chk1 kinase assay at different concentration of ATP

10 μ l reaction containing 200 μ M Cdc25C peptide, 0.0625, 0.125, 0.25, 0.5, 1, 2, 4 or 8 mM ATP and 0.05 μ M Chk1KD or 0.5 μ M Chk1FL was performed in reaction buffer. Assay procedure was described in 3.3.9. Sample was taken and stopped at 5 min for Chk1KD and 10 min for Chk1FL. The rate of product formation was plotted against ATP peptide concentration. The data was fitted to Michaelis-Menten model using Pro Fit software (<http://quansoft.com>).

Claspin⁸⁸⁴⁻⁹⁹² with an N-terminal 6xHis and MBP tag were expressed in *E. coli* in 1 L growth medium. 6xHis-MBP-Claspin⁸⁵⁰⁻⁹⁹² produced a higher yield compared to Claspin⁸⁸⁴⁻⁹⁹² and this construct was chosen for large-scale expression (Figure 4.2).

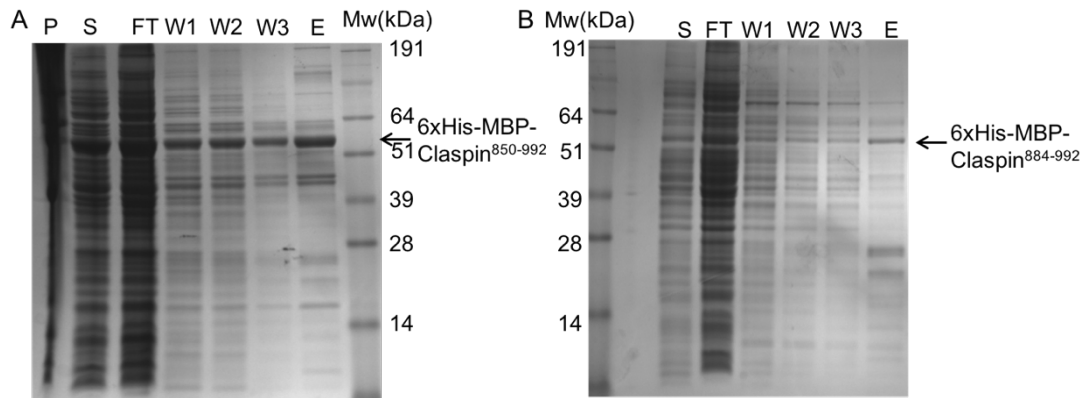


Figure 4.2 Expression of 6xHis-MBP-Claspin constructs

Ni-NTA purification of 6xHis-MBP-Claspin⁸⁵⁰⁻⁹⁹² (A) and 6xHis-MBP-Claspin⁸⁸⁴⁻⁹⁹² (B) was performed to the 1 L expression. 6xHis-MBP-Claspin⁸⁵⁰⁻⁹⁹² showed high yield than 6xHis-MBP-Claspin⁸⁸⁴⁻⁹⁹² in elution fraction. P: pellet, S: supernatant, FT: flow through, W1-W3: wash 1-3, E: elution.

8 L expression of 6xHis-MBP-Claspin⁸⁵⁰⁻⁹⁹² was purified by Ni-NTA chromatography, Hitrap Q ion-exchange chromatography and Superdex 200 16/60 size-exclusion chromatography (Figure 4.3). Full-length protein was separated from most of the impurities and fractions containing target protein was pooled and concentrated.

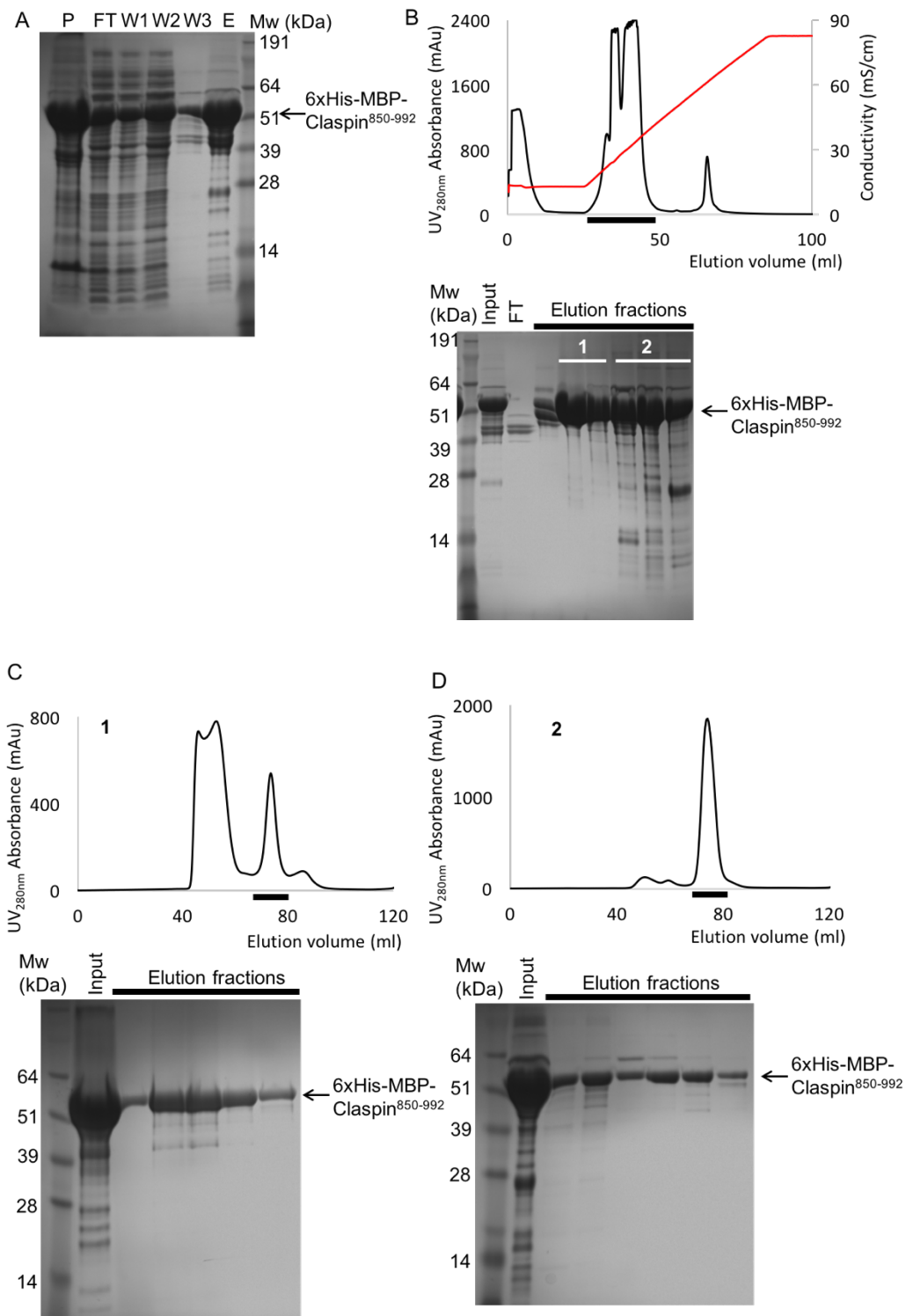


Figure 4.3 Purification of 6xHis-MBP-Claspin⁸⁵⁰⁻⁹⁹²

A: 6xHis-MBP-Claspin⁸⁵⁰⁻⁹⁹² was firstly purified by gravity flow Ni-NTA column and the fractions were analysed by SDS-PAGE. B: Elution from Ni-NTA column was loaded onto Hitrap Q ion-exchange column and protein was eluted with gradient NaCl wash. C: Elution fractions of ion-exchange step were split into two size exclusion chromatography using Superdex200 16/60 column.

4.1.2 Phosphoserine incorporation in Claspin CKBD using amber codon suppression

As described in the Introduction, phosphorylation of Claspin CKBD is essential to Chk1 binding. Quantitative, site-specific phosphorylation of a recombinant protein is a difficult task to accomplish during heterologous protein expression in a host system. Prof. Jason Chin's lab (MRC-LMB, Cambridge) recently developed an engineered bacterial system which can achieve site-specific phosphoserine incorporation exploiting the amber codon suppression approach. The system adopts an orthogonal aminoacyl-tRNA synthetase (SepRS)/tRNACUA pair to incorporate phosphoserine on a target protein site in a SerB (an *E.coli* phosphatase) knockout *E.coli* strain (Rogerson et al., 2016). The engineered SepRS associates with a phosphoserine tRNA and incorporates phosphoserine upon recognition of an Amber codon (Figure 4.4).

Two 6xHis-GST-Claspin constructs spanning the region of 850-992 and 884-992 with single point mutation of T916pS or S945pS were used for expression test in the amber codon suppression strain (Figure 4.3). The system can only incorporate phosphoserine into the target site so a phosphoserine is incorporated into site 916 on Claspin even though the residue in the original sequence is a threonine instead of a serine.

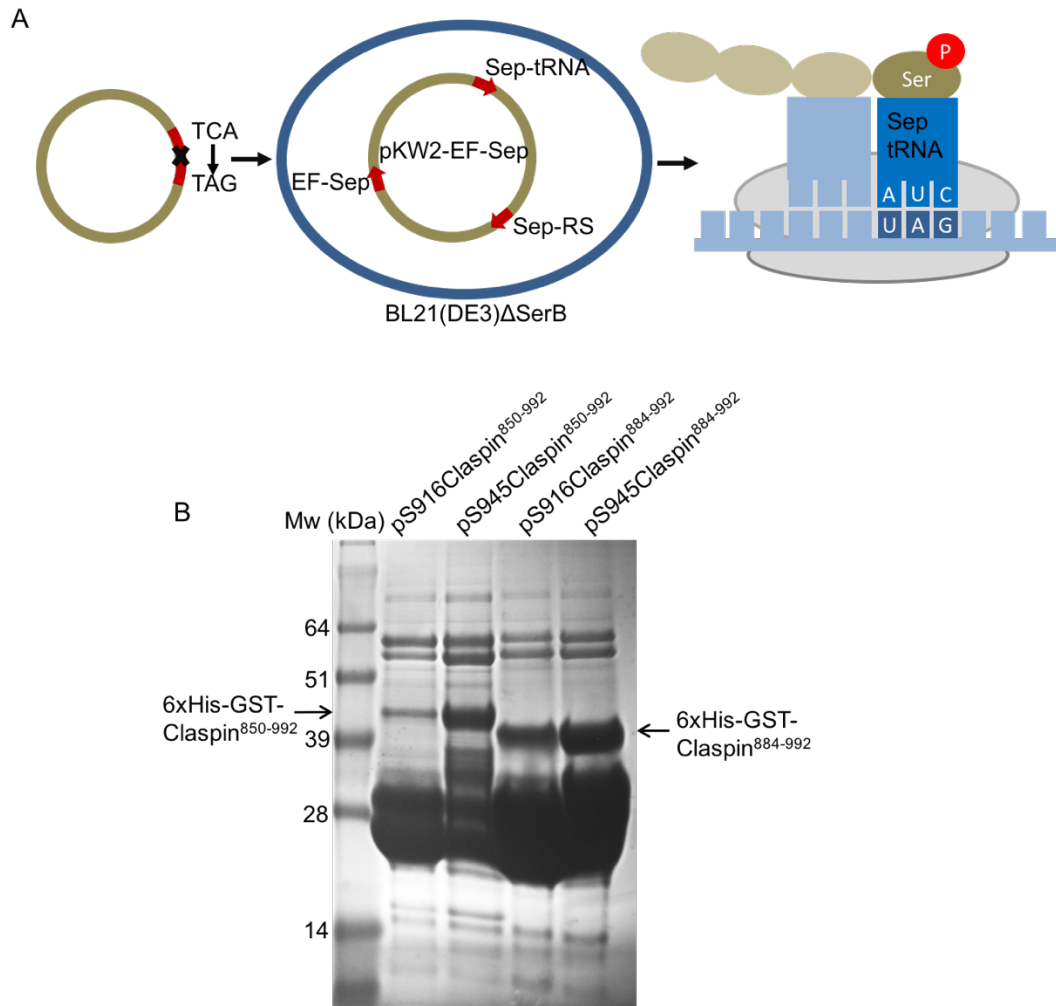
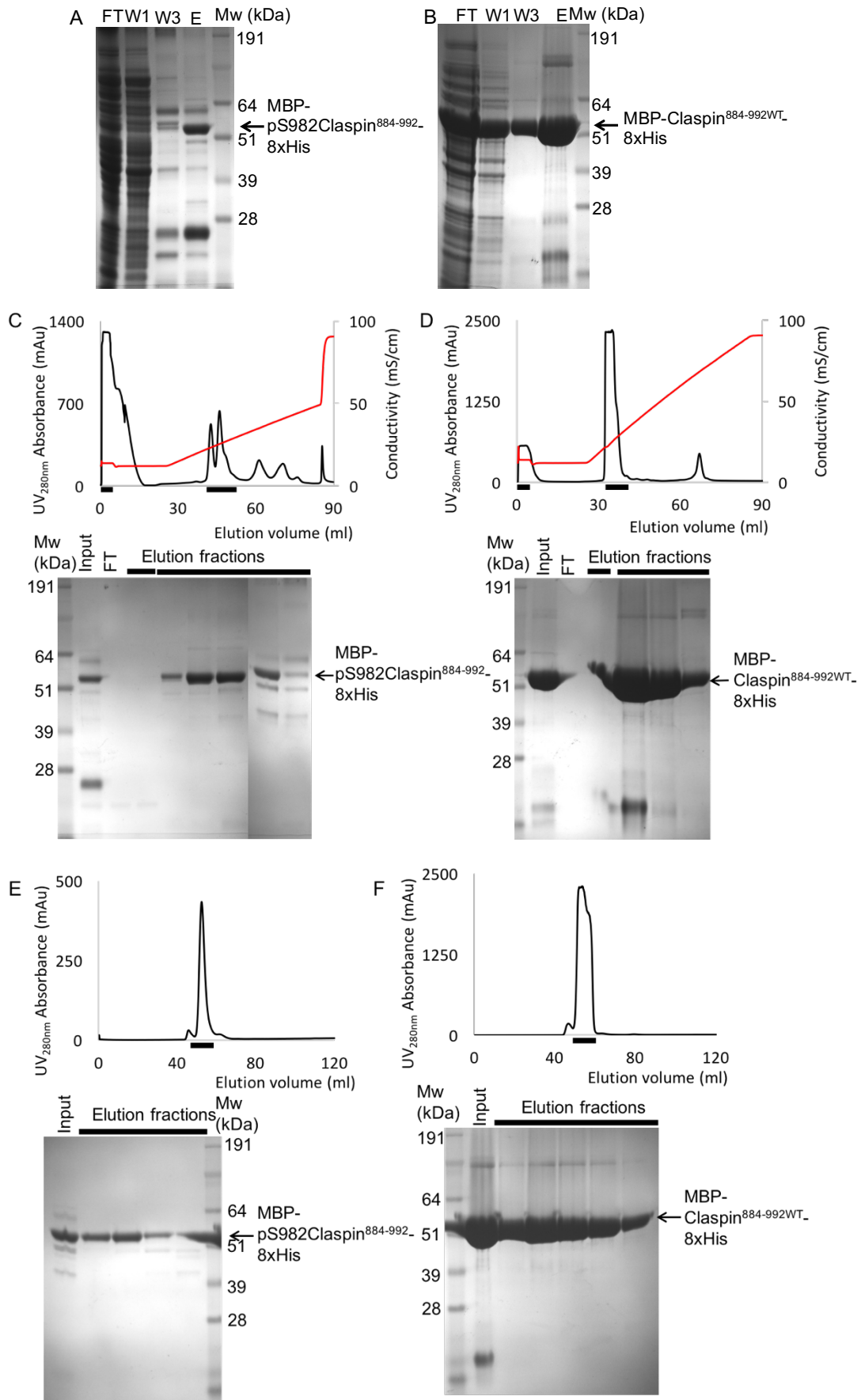


Figure 4.4 Expression test of 6xHis-GST-Claspin constructs expressed in amber codon suppression system

A: A brief schematic description of the Amber codon suppression method used for phosphoserine incorporation. B: 6xHis-GST-Claspin⁸⁵⁰⁻⁹⁹² and 6xHis-GST-Claspin⁸⁸⁴⁻⁹⁹² with phosphoserine incorporated on site 916 or 945 were expressed in the amber codon suppression system. Gravity flow Ni-NTA column was used as an initial purification step for 1 L expression and the elution from the Ni-NTA agarose beads was analysed by SDS-PAGE.

Both the 6xHis-GST-Claspin⁸⁸⁴⁻⁹⁹² constructs showed higher yield than the 6xHis-GST-Claspin⁸⁵⁰⁻⁹⁹² constructs so the 884-992 region was selected for expression in the Amber codon suppression system. Because of the dimerization nature of GST tag, the 6xHis-GST-Claspin⁸⁸⁴⁻⁹⁹² construct showed co-purification of significant levels of truncated protein, likely due to the presence of the amber codon, alongside the full-length protein, which could not be successfully removed. Other tags were

used for recombinant protein expression. Constructs with N-terminal dual 6xHis-MBP tag and a single amber codon for phosphoserine incorporation at positions corresponding to T916, S945 or S982 were expressed. The N-terminally tagged constructs were still difficult to be separated from truncated constructs so the N-terminal 6xHis tag was moved to the C-terminus as an 8xHis tag to facilitate the purification of full-length Claspin constructs. The three mono-phosphorylated Claspin constructs were expressed at the same level and were purified by Ni-NTA affinity chromatography, Hitrap Q ion-exchange chromatography and Superdex 75 16/60 size-exclusion chromatography. Full-length protein was separated from most of the impurities and fractions containing target protein was pooled and concentrated (Figure 4.5). MBP-pS982Claspin⁸⁸⁴⁻⁹⁹²-8xHis was concentrated to 0.4 mg from a 4 L-expression and MBP-Claspin^{884-992WT}-8xHis was concentrated to 16.8 mg from a 2 L-expression. The yield of wild-type protein was about one to two orders of magnitude higher than that of phosphoserine incorporated protein.



(Caption on next page)

Figure 4.5 Purification of 4 L MBP-pS982Claspin⁸⁸⁴⁻⁹⁹²-8xHis and 2 L MBP-Claspin^{884-992WT}-8xHis

Cell lysate was applied on Ni-NTA agarose beads column as an initial purification step for MBP-pS982Claspin⁸⁸⁴⁻⁹⁹²-8xHis (A) and MBP-Claspin^{884-992WT}-8xHis (B). Elution from Ni-NTA column was applied on Hitrap Q column and target protein was eluted along gradient NaCl wash for MBP-pS982Claspin⁸⁸⁴⁻⁹⁹²-8xHis (C) and MBP-Claspin^{884-992WT}-8xHis (D). A size-exclusion chromatography using Superdex 75 16/60 column was used as a final purification step for MBP-pS982Claspin⁸⁸⁴⁻⁹⁹²-8xHis (E) and MBP-Claspin^{884-992WT}-8xHis (F).

Purified Claspin samples were further treated with TEV protease to remove the N-terminal MBP tag. Cleaved Claspin⁸⁸⁴⁻⁹⁹²-8xHis peptide was purified using a Hitrap Q ion-exchange chromatography (Figure 4.6).

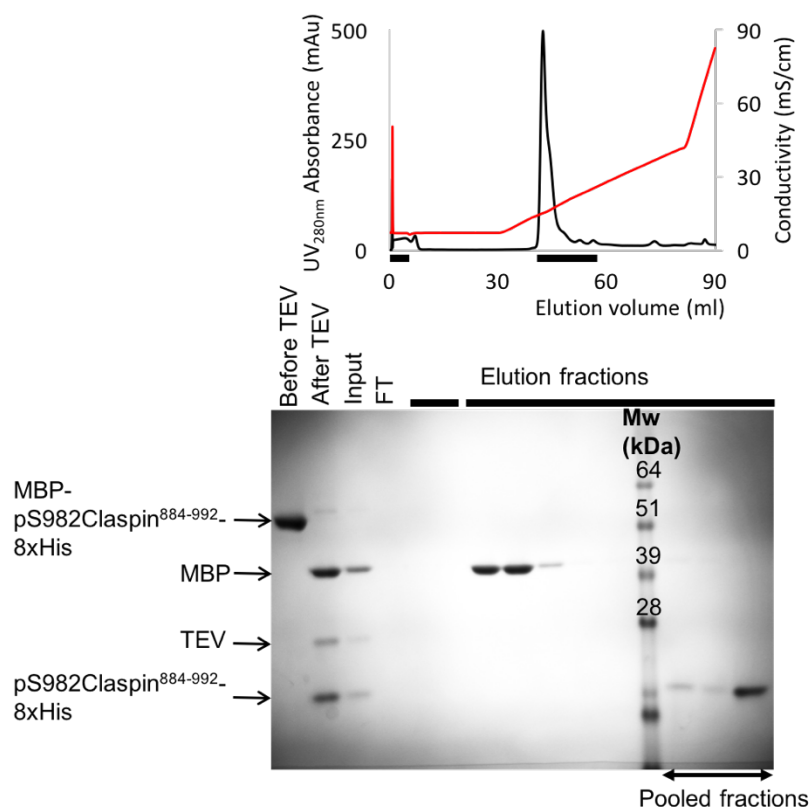
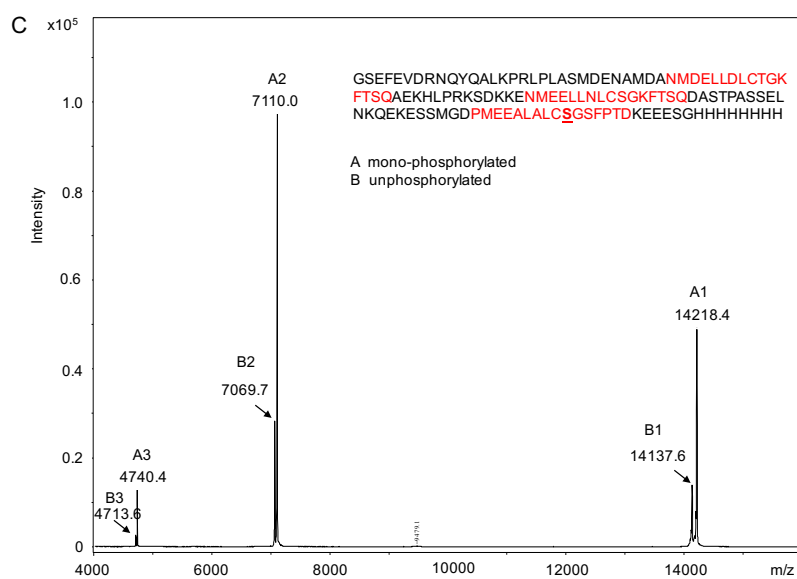
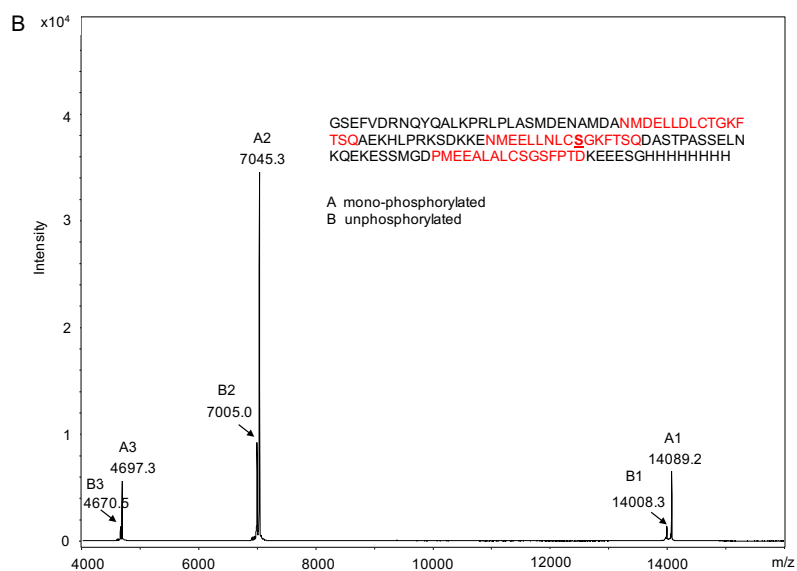
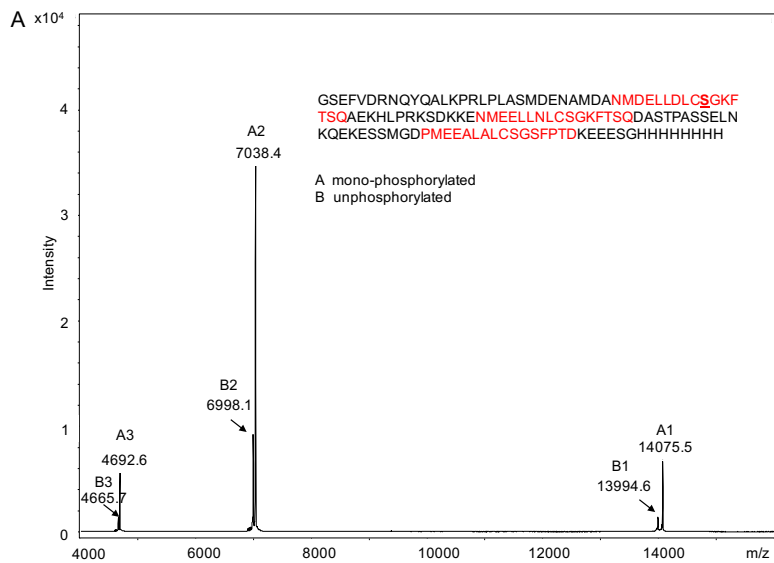


Figure 4.6 Purification of pS982Claspin⁸⁸⁴⁻⁹⁹²-8xHis peptide

The MBP tag was removed from MBP-pS982Claspin⁸⁸⁴⁻⁹⁹²-8xHis after a TEV treatment. The cleaved pS982Claspin⁸⁸⁴⁻⁹⁹²-8xHis was purified by ion-exchange chromatography using Hitrap Q column.

The phosphoserine incorporation to the three cleaved peptide samples was analysed by MALDI-TOF mass spectrometry (Figure 4.7).



(Caption on next page)

Figure 4.7 Mass spectrometry of the Claspin⁸⁸⁴⁻⁹⁹²-8xHis peptides

MALDI-TOF mass spectrometry of cleaved pS916Claspin⁸⁸⁴⁻⁹⁹²-8xHis (A), pS945Claspin⁸⁸⁴⁻⁹⁹²-8xHis (B) and pS982Claspin⁸⁸⁴⁻⁹⁹²-8xHis (C) showed all the three samples formed by a mixture of phosphorylated and unphosphorylated species. The mass spectrometry analysis was performed by Dr. Len Packman at the Protein and Nucleic Acid Analysis Facility at the University of Cambridge.

Mass spectrometry showed the samples were mixtures of phosphorylated and non-phosphorylated species. Addition of phosphatase inhibitor β -glycerolphosphate and NaF during purification did not eliminate the presence of non-phosphorylated species, indicating that dephosphorylation occurred during expression.

Incorporation of phosphoserine into two or three sites on MBP-Claspin⁸⁸⁴⁻⁹⁹²-8xHis constructs was attempted at 1 L-expression. Expression of double phosphoserine incorporated Claspin constructs was detected but at very low yield (Figure 4.8). Expression of triple phosphoserine incorporated Claspin construct from 1 L-expression was not detected. A further purification step using ion-exchange chromatography for the pS916+pS945Claspin⁸⁸⁴⁻⁹⁹²-8xHis construct was performed but no target protein can be detected in Hitrap Q flow through or elution fractions. The incorporation of double- and triple-phosphoserine was low efficient and adequate yield at high purity was not achieved.

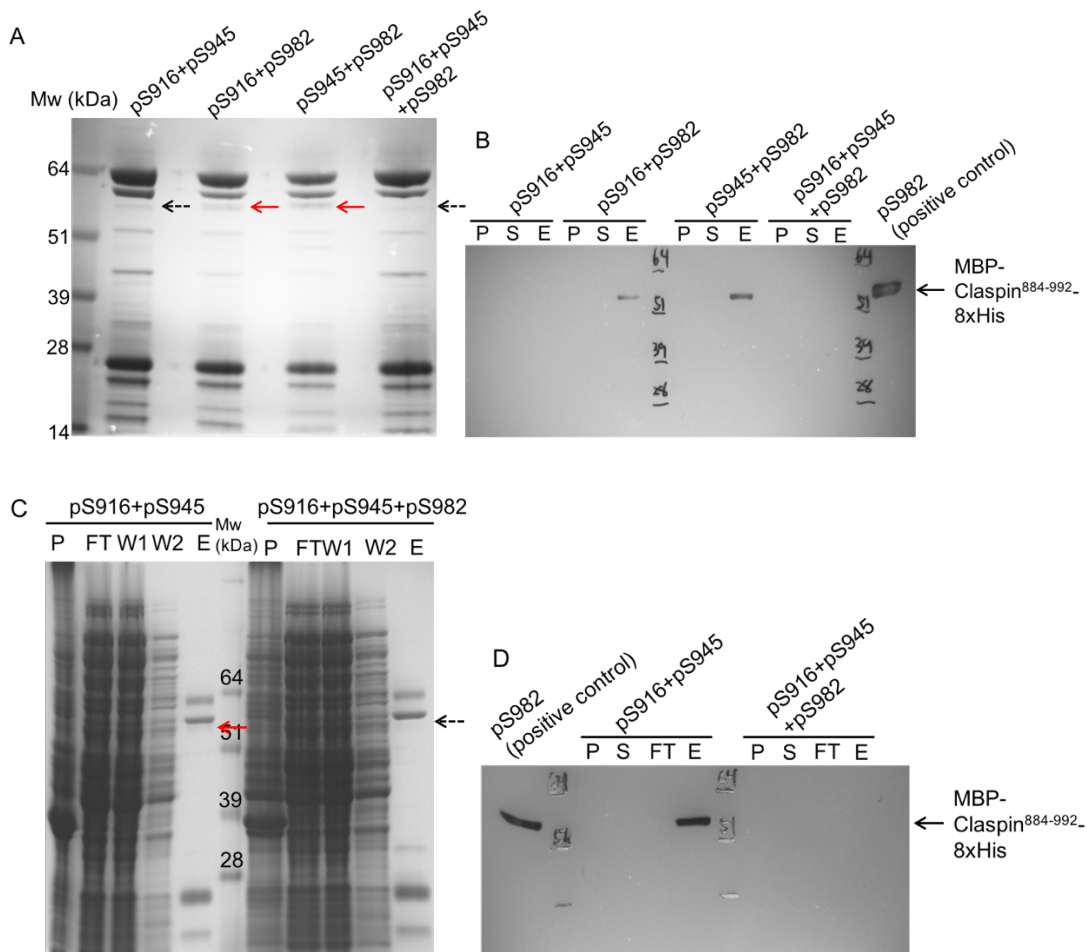


Figure 4.8 Expression of double- and triple- phosphoserine incorporated MBP-Claspin⁸⁸⁴⁻⁹⁹²-8xHis constructs

A: Cell lysate of the four double- or triple- phosphoserine incorporated Claspin constructs from 1L-expression was applied on gravity flow Ni-NTA column. Multiple bands appeared at target molecular weight. B: Western blot using anti-polyhistidine antibody was performed to verify target bands. MBP-pS982Claspin⁸⁸⁴⁻⁹⁹²-8xHis was used as a positive control. Only MBP-pS916pS982Claspin⁸⁸⁴⁻⁹⁹²-8xHis and MBP-pS945pS982Claspin⁸⁸⁴⁻⁹⁹²-8xHis were detected in the corresponding elution fractions. C: Ni-NTA chromatography was performed for MBP-pS916pS945Claspin⁸⁸⁴⁻⁹⁹²-8xHis and MBP-pS916pS945pS982Claspin⁸⁸⁴⁻⁹⁹²-8xHis from a different 1L-expression. D: Western blot using anti-polyhistidine antibody was performed to verify target bands. MBP-pS982Claspin⁸⁸⁴⁻⁹⁹²-8xHis was used as a positive control. Target protein expression was only detected in the MBP-pS916pS945Claspin⁸⁸⁴⁻⁹⁹²-8xHis elution fraction. MBP-pS916pS945pS982Claspin⁸⁸⁴⁻⁹⁹²-8xHis was not detected in any of the expression test. Red arrow: expression confirmed by western blot. Black dash-line arrow: expected band but no target protein expression was detected.

4.1.3 Interaction studies between Claspin and Chk1

Pull-down assays were performed to study the interaction between Chk1 constructs and each of the three mono-phosphoserine Claspin constructs. The MBP-Claspin⁸⁸⁴⁻⁹⁹²-8xHis constructs were used in Chk1KD pull-down assays. Chk1FL migrates at a close region to the MBP-Claspin⁸⁸⁴⁻⁹⁹²-8xHis constructs which makes it difficult to interpret the pull-down results. A new Claspin⁸⁸⁴⁻⁹⁹²-8xHis constructs with a dual N-terminal Strep-SUMO tag was prepared. The three mono-phosphorylated Claspin constructs were expressed at the same level and were purified by Ni-NTA affinity chromatography and Superdex 75 16/60 size-exclusion chromatography. Full-length protein was separated from most of the impurities and fractions containing target protein was pooled and concentrated. The yield of Strep-SUMO-pS945Claspin⁸⁸⁴⁻⁹⁹²-8xHis and Strep-SUMO-Claspin^{884-992WT}-8xHis from a 3 L-expression was 2.5 mg and 14.5 mg respectively (Figure 4.9).

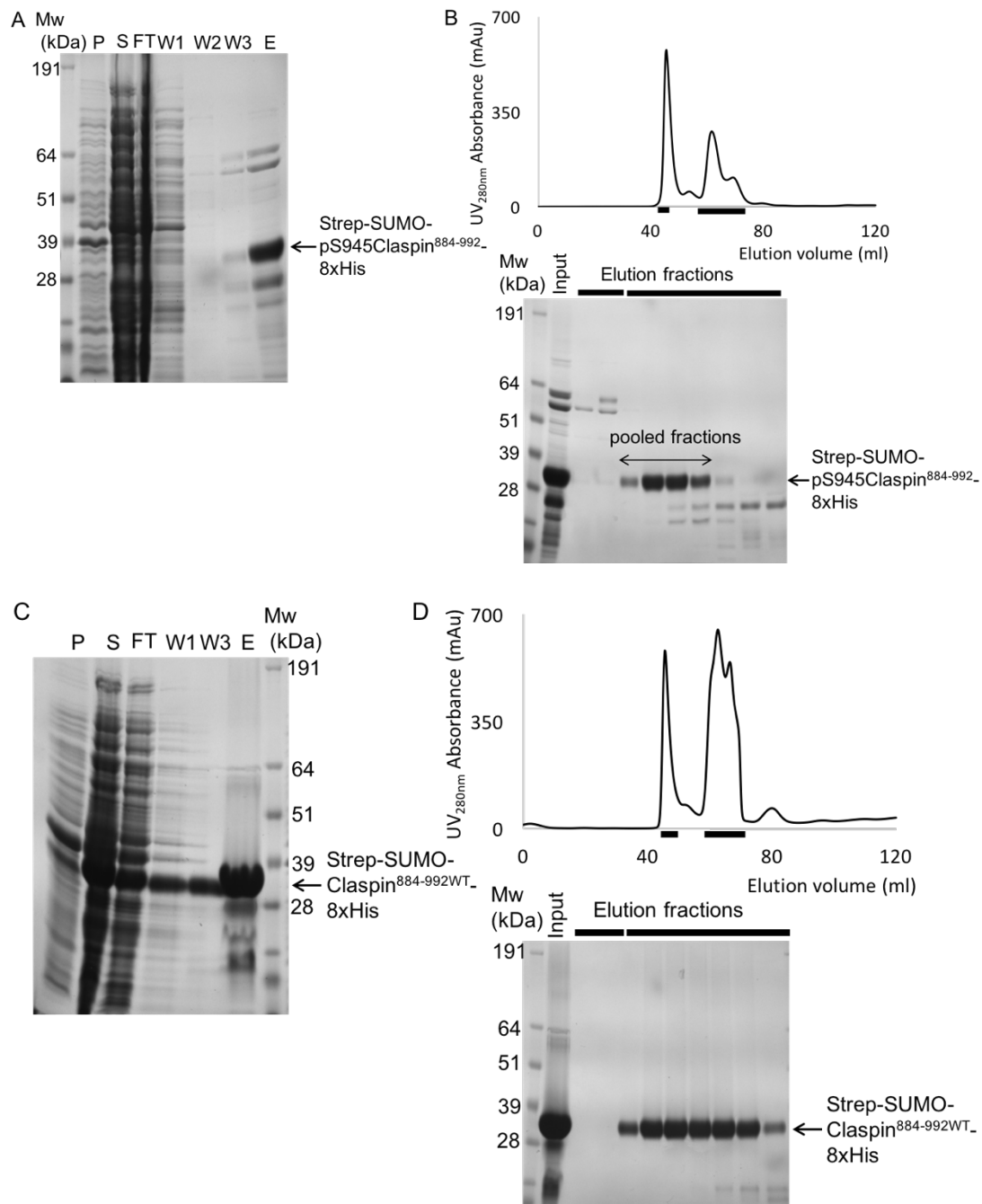


Figure 4.9 Purification of Strep-SUMO-pS945Claspin⁸⁸⁴⁻⁹⁹²-8xHis and Strep-SUMO-Claspin^{884-992WT}-8xHis

Cell lysate was applied on Ni-NTA agarose beads column as an initial purification step for Strep-SUMO-pS945Claspin⁸⁸⁴⁻⁹⁹²-8xHis (A) and Strep-SUMO-Claspin^{884-992WT}-8xHis (C). Elution from Ni-NTA column was concentrated and applied on a size-exclusion chromatography using Superdex 75 16/60 column for a final purification step for Strep-SUMO-pS945Claspin⁸⁸⁴⁻⁹⁹²-8xHis (B) and Strep-SUMO-Claspin^{884-992WT}-8xHis (D).

Mono-phosphorylated and unphosphorylated Claspin constructs were immobilised on

amylose beads or StrepTactin beads and Chk1KD or Chk1FL was applied onto the Claspin constructs. Different tags of Claspin constructs were used in the two pull-down assays to separate Claspin and Chk1 on SDS-PAGE gels (Figure 4.10). All three phosphoserine Claspin constructs successfully pulled down both Chk1KD and Chk1FL with similar binding affinities, whereas unphosphorylated Claspin showed no appreciable binding to Chk1KD and very weak binding towards Chk1FL. No significant difference in binding strength towards Chk1 was observed among the three phosphorylated Claspin constructs.

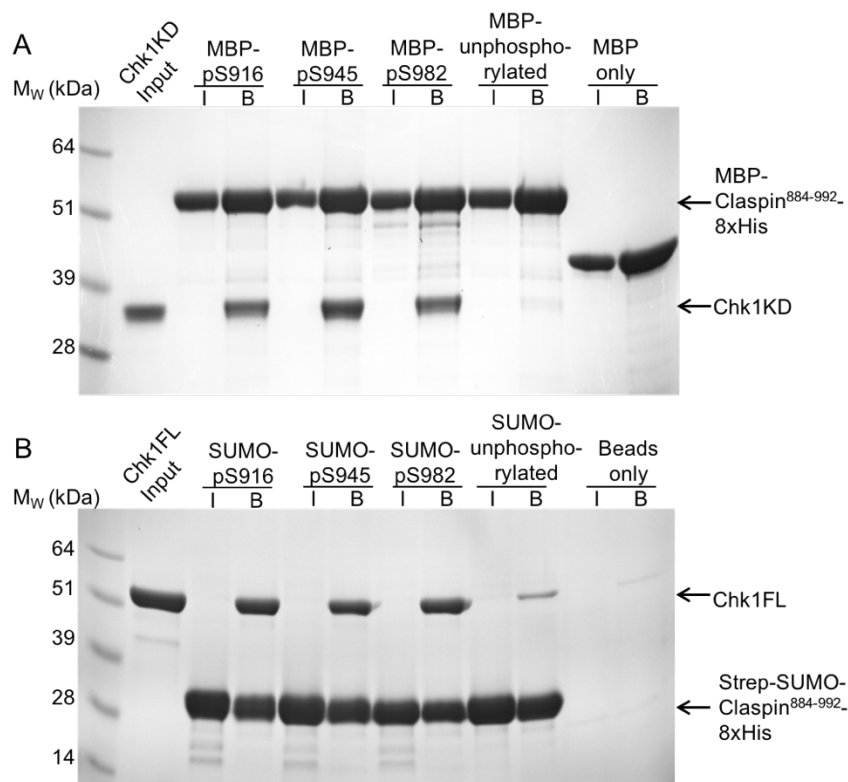


Figure 4.10 Pull-down assays of mono-phosphoserine incorporated Claspin constructs with Chk1KD and Chk1FL

A: Pull-down assays for MBP-Claspin⁸⁸⁴⁻⁹⁹²-8xHis constructs with Chk1KD. B: Pull-down assays for Strep-SUMO-Claspin⁸⁸⁴⁻⁹⁹²-8xHis constructs with Chk1FL. Samples were analysed by SDS-PAGE and the gels were stained with coomassie blue. I: beads sample with immobilised bait input, B: beads sample after pull-down.

One way to test the effect of amino acid phosphorylation is by phospho-mimicry, by mutating threonine/serine to either glutamate or aspartate. Compared to aspartate, glutamate is more similar to phosphoserine in chemical structure and therefore a triple

Claspin^{3T/SE} (T916E/S945E/S982E) mutant construct replacing all serine phosphorylation site with glutamate was prepared. The phospho-mimic mutagenesis was introduced on 6xHis-MBP-Claspin⁸⁸⁴⁻⁹⁹² construct (the 2nd construct described in section 4.1.1). The Claspin^{3T/SE} protein was purified in the same way as a unphosphorylated Claspin construct (MBP-Claspin⁸⁸⁴⁻⁹⁹²-8xHis) described in 4.1.2. In the pull-down experiment, phospho-mimic Claspin (Claspin^{3T/SE}), unphosphorylated Claspin (MBP-Claspin⁸⁸⁴⁻⁹⁹²-8xHis) and mono-phosphorylated pS945Claspin (MBP-Claspin⁸⁸⁴⁻⁹⁹²-8xHis construct with phosphoserine incorporation on 945) were immobilised on amylose beads and the same amount of Chk1KD was incubated with each Claspin constructs (Figure 4.11). Both unphosphorylated Claspin and Claspin^{3T/SE} showed weak binding to Chk1KD which was in contrast to strong binding observed between pS945Claspin and Chk1KD. The mutant with glutamate did not work as an effective mimic replacement of phosphoserine, which indicates that the interaction with Chk1 is not purely based on charge and requires specific stereochemical contacts mediated by the phosphoserine side chain.

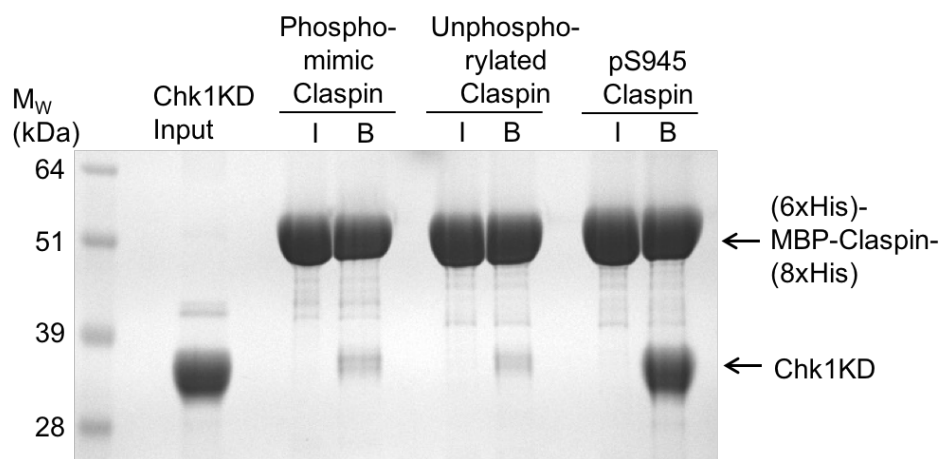
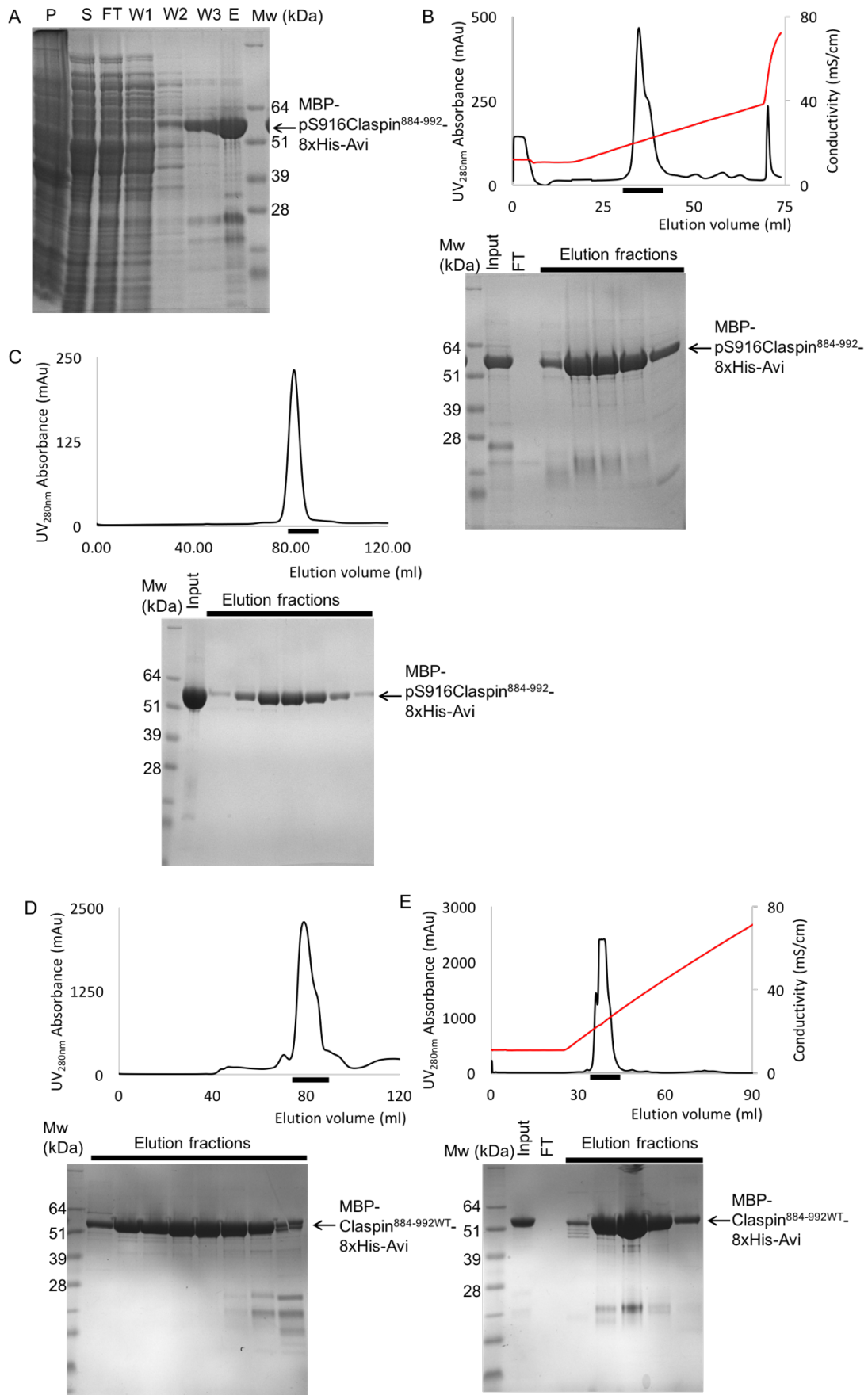


Figure 4.11 Pull-down assays of phospho-mimic Claspin with Chk1KD

Phospho-mimic (T916E/S945E/S982E), unphosphorylated (negative control) and pS945 (positive control) Claspin used for pull-down assays with Chk1KD. Samples of beads were analysed by SDS-PAGE and the gels were stained with coomassie blue. I: beads sample with immobilised bait input, B: beads sample after pull-down.

4.1.4 Quantitative analysis of Chk1-Claspin binding using biolayer-interferometry

To acquire more accurate binding affinity information on the interaction of the mono-serine phosphorylated Claspin constructs with Chk1, biolayer-interferometry was employed using a ForteBio Octet instrument. To be able to attach it to the streptavidin biosensor, a new MBP-Claspin⁸⁸⁴⁻⁹⁹²-8xHis construct was expressed with an Avi-tag sequence (GLNDIFEAQKIEWHE, biotinylation site is underlined) fused to its C-terminus (Figure 4.12).



(Caption on next page)

Figure 4.12 Purification of MBP-pS916Claspin⁸⁸⁴⁻⁹⁹²-8xHis-Avi and MBP-Claspin^{884-992WT}-8xHis-Avi

A: Cell lysate was applied on Ni-NTA agarose beads column as an initial purification step for MBP-pS916Claspin⁸⁸⁴⁻⁹⁹²-8xHis-Avi. B: Elution from Ni-NTA column was applied on an ion-exchange chromatography using Hitrap Q column. FT: flow through. C: Fractions containing target protein were concentrated and applied on a size-exclusion chromatography using Superdex 200 16/60 column for a final purification step. D: Elution from Ni-NTA column of MBP-Claspin^{884-992WT}-8xHis-Avi was applied on an ion-exchange chromatography using Hitrap Q column. E: Fractions containing target protein were concentrated and applied on a size-exclusion chromatography using Superdex 200 16/60 column for a final purification step.

In vitro biotinylation on MBP-pS916Claspin⁸⁸⁴⁻⁹⁹²-8xHis-Avi was performed by recombinant MBP-BirA (from Dr. Joe Maman, Department of Biochemistry, University of Cambridge) and the samples were analysed and compared with the untreated protein. Biotinylation was visualised by western blot using Streptavidin-AP conjugate antibody. The extent of biotinylation on the untreated sample was at the similar level to the BirA treated samples at different time points and different ratios, which showed that the Avi-tag biotinylation took place during expression in *E.coli* (Figure 4.13).

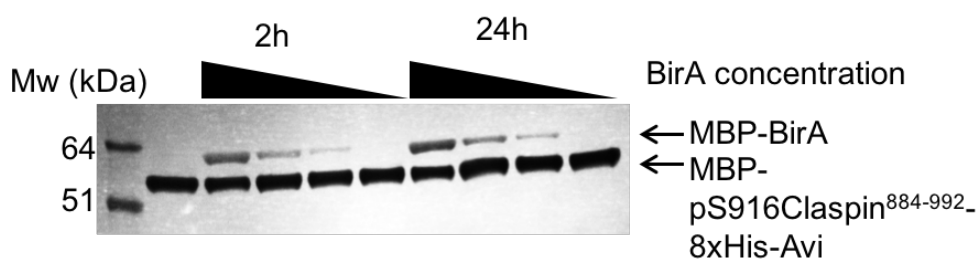


Figure 4.13 *In vitro* biotinylation verification of MBP-pS916Claspin⁸⁸⁴⁻⁹⁹²-8xHis-Avi

Native MBP-pS916Claspin⁸⁸⁴⁻⁹⁹²-8xHis-Avi without treatment (first sample lane) and MBP-BirA treated proteins at molar ratio of 2:1, 1:1, 0.5:1 and 0.1:1 for 2 h and 24 h were analysed by western blot using Streptavidin-AP conjugate antibody. The biotinylation level of MBP-pS916Claspin⁸⁸⁴⁻⁹⁹²-8xHis-Avi was the same in all conditions.

The biotinylated mono-phosphorylated Claspin constructs were immobilised onto the streptavidin biosensor as the ligand and their interaction with Chk1 was tested. A Chk1 titration in the range of 20 and 500 nM was performed for each Claspin

construct. Individual association and dissociation curves were fitted to a 1:1 binding model (Figure 4.14) and K_d was calculated from averaged k_{on} and k_{off} determined from fitting signal curves with high fitting scores (Table 4.1). The data showed all the K_d between the mono-phosphorylated Claspin constructs and Chk1 constructs were at sub-micromolar level, with no significant differences in K_d from different combinations of binding partners. All three mono-phosphorylated Claspin constructs had a similar binding affinity to Chk1, in agreement with the result of the pull-down experiments. Furthermore, Chk1FL and Chk1KD bound the monophosphorylated Claspin CKBD with similar affinities, indicating that their interaction site resides within Chk1's kinase domain. No binding between unphosphorylated MBP-Claspin^{884-992^{WT}}-8xHis-Avi and Chk1KD or Chk1FL was observed (Figure 4.14), which indicated the phosphorylation on Claspin CKBD was essential to Claspin-Chk1 interaction.

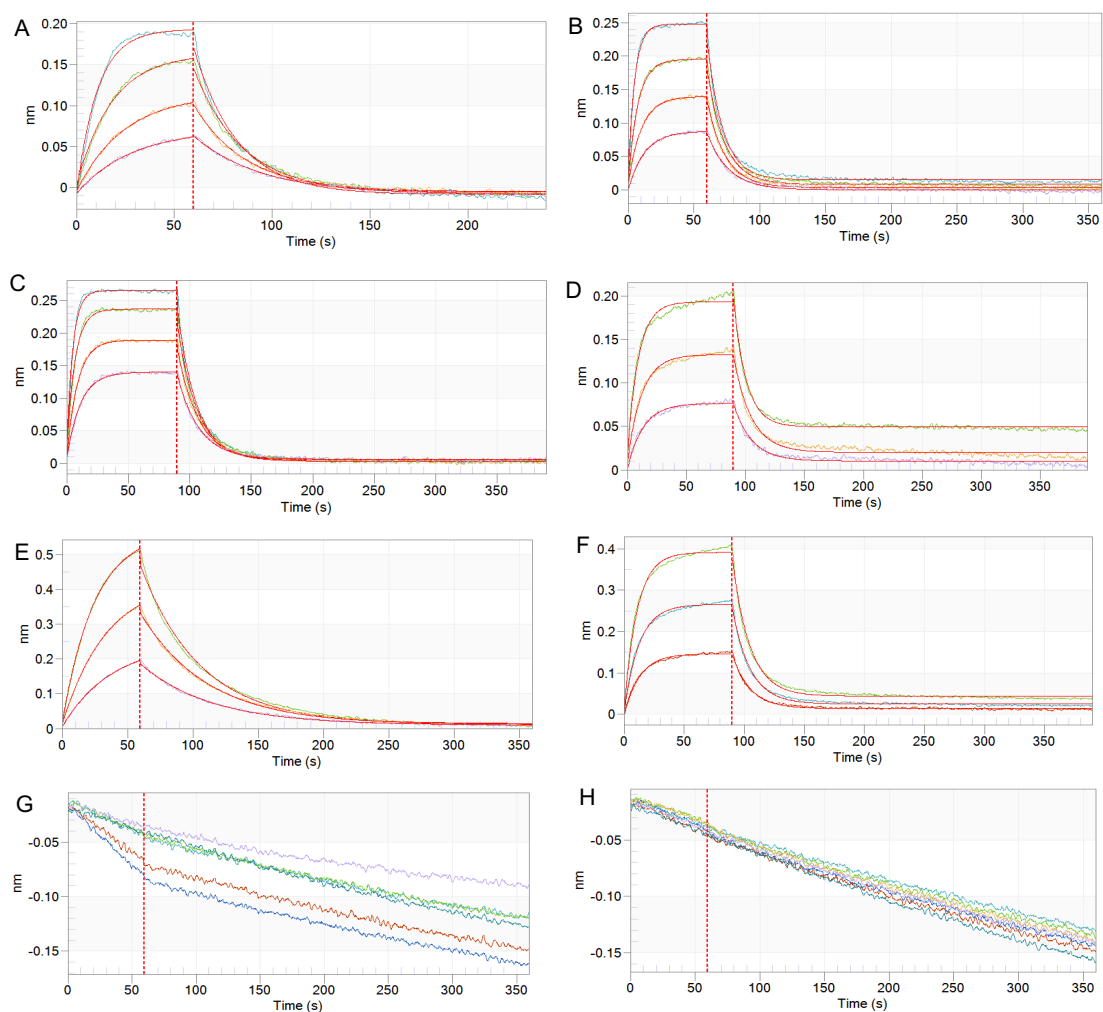


Figure 4.14 Binding curves of Claspin⁸⁸⁴⁻⁹⁹²-8xHis-Avi and Chk1

Association and dissociation steps of binding curves of pS916Claspin⁸⁸⁴⁻⁹⁹²-8xHis-Avi to Chk1KD (A) and Chk1FL (B), pS945Claspin⁸⁸⁴⁻⁹⁹²-8xHis-Avi to Chk1KD (C) and Chk1FL (D) and pS982Claspin⁸⁸⁴⁻⁹⁹²-8xHis-Avi to Chk1KD (E) and Chk1FL (F) were fitted to a 1:1 fitting model. Association and dissociation steps of binding curves of MBP-Claspin⁸⁸⁴⁻⁹⁹²WT-8xHis-Avi to Chk1KD (G) and Chk1FL (H) showed no binding between analyte and ligand.

Table 4.1 Binding parameters of the Claspin⁸⁸⁴⁻⁹⁹²-8xHis-Avi - Chk1 interaction

| Claspin ⁸⁸⁴⁻⁹⁹² - | Chk1KD | | |
|------------------------------|---|---|---|
| 8xHis-Avi | k_{on} (M ⁻¹ s ⁻¹) | k_{off} (s ⁻¹) | K_d (M) |
| pS916 | $2.46 \times 10^5 \pm 1.24 \times 10^5$ | $3.83 \times 10^{-2} \pm 0.69 \times 10^{-2}$ | $1.55 \times 10^{-7} \pm 0.83 \times 10^{-7}$ |
| pS945 | $6.02 \times 10^5 \pm 0.84 \times 10^5$ | $5.96 \times 10^{-2} \pm 0.40 \times 10^{-2}$ | $9.89 \times 10^{-8} \pm 1.53 \times 10^{-8}$ |
| pS982 | $1.77 \times 10^5 \pm 0.26 \times 10^5$ | $1.99 \times 10^{-2} \pm 0.17 \times 10^{-2}$ | $1.13 \times 10^{-7} \pm 0.19 \times 10^{-7}$ |
| Claspin ⁸⁸⁴⁻⁹⁹² - | Chk1FL | | |
| 8xHis-Avi | k_{on} (M ⁻¹ s ⁻¹) | k_{off} (s ⁻¹) | K_d (M) |
| pS916 | $8.17 \times 10^5 \pm 1.00 \times 10^5$ | $7.38 \times 10^{-2} \pm 0.94 \times 10^{-2}$ | $9.04 \times 10^{-8} \pm 1.60 \times 10^{-8}$ |
| pS945 | $2.63 \times 10^5 \pm 0.95 \times 10^5$ | $7.48 \times 10^{-2} \pm 1.60 \times 10^{-2}$ | $2.85 \times 10^{-7} \pm 1.20 \times 10^{-7}$ |
| pS982 | $2.26 \times 10^5 \pm 0.34 \times 10^5$ | $6.76 \times 10^{-2} \pm 0.08 \times 10^{-2}$ | $2.99 \times 10^{-7} \pm 0.45 \times 10^{-7}$ |

Whether the Claspin construct with phosphorylation on two Chk1-binding motifs had different binding kinetics from the mono-phosphorylated constructs was tested using bio-layer interferometry. 5 L-expression of phosphoserine incorporation at 916 and 945 on MBP-Claspin⁸⁸⁴⁻⁹⁹²-8xHis-Avi was performed and purification techniques including Ni-NTA chromatography and size-exclusion chromatography were applied (Figure 4.15).

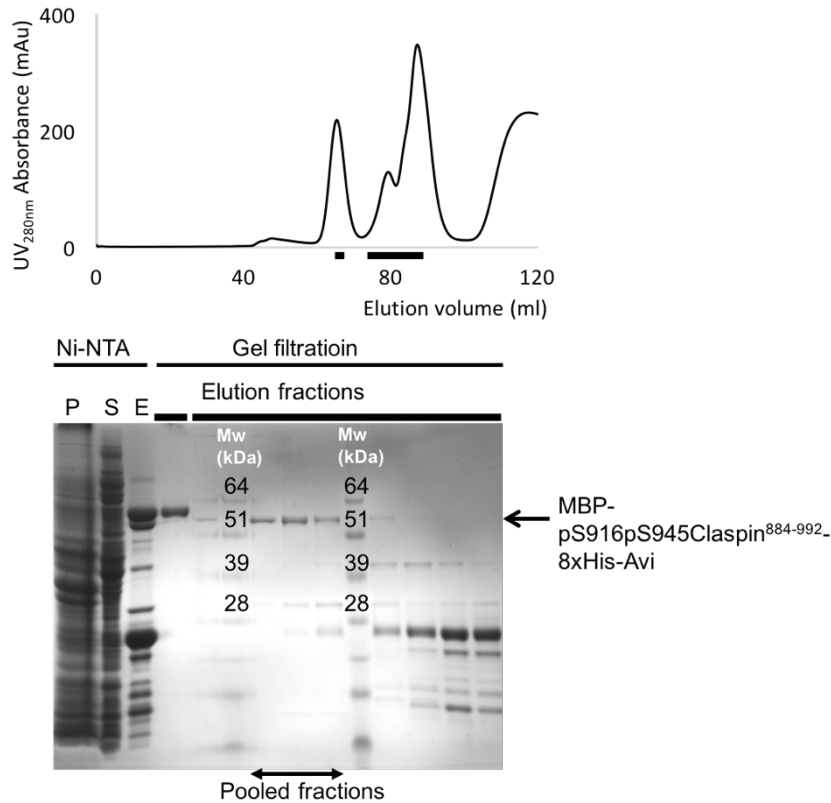


Figure 4.15 Purification of MBP-pS916pS945Claspin⁸⁸⁴⁻⁹⁹²-8xHis-Avi

Cell lysate was applied on gravity flow Ni-NTA column and protein was eluted in 300 mM imidazole. Concentrated elution was applied on Superdex 200 16/60 gel filtration column. Several contamination bands were observed in the target protein fractions.

Mass spectrometry analysis showed the solution sample was a mixture of double-phosphorylated, mono-phosphorylated and unphosphorylated MBP-Claspin⁸⁸⁴⁻⁹⁹²-8xHis-Avi constructs in a biotinylated form. The full-length MBP-pS916pS945Claspin⁸⁸⁴⁻⁹⁹²-8xHis-Avi construct was attached to the Streptavidin biosensor and its binding kinetics to Chk1KD was measured on ForteBio Octet instrument. The averaged k_{on} and k_{off} was measured at $6.12 \times 10^5 \text{ M}^{-1} \text{ s}^{-1}$ and $6.85 \times 10^{-2} \text{ s}^{-1}$ respectively. The K_d was determined at $1.12 \times 10^{-7} \text{ M}$. No obvious difference on binding affinity to Chk1KD was observed on the double-phosphorylated MBP-Claspin⁸⁸⁴⁻⁹⁹²-8xHis-Avi construct comparing to the mono-phosphorylated constructs. Because the phosphorylation status of the Claspin construct was not homogeneous in this experiment, a quantitative conclusion cannot be achieved.

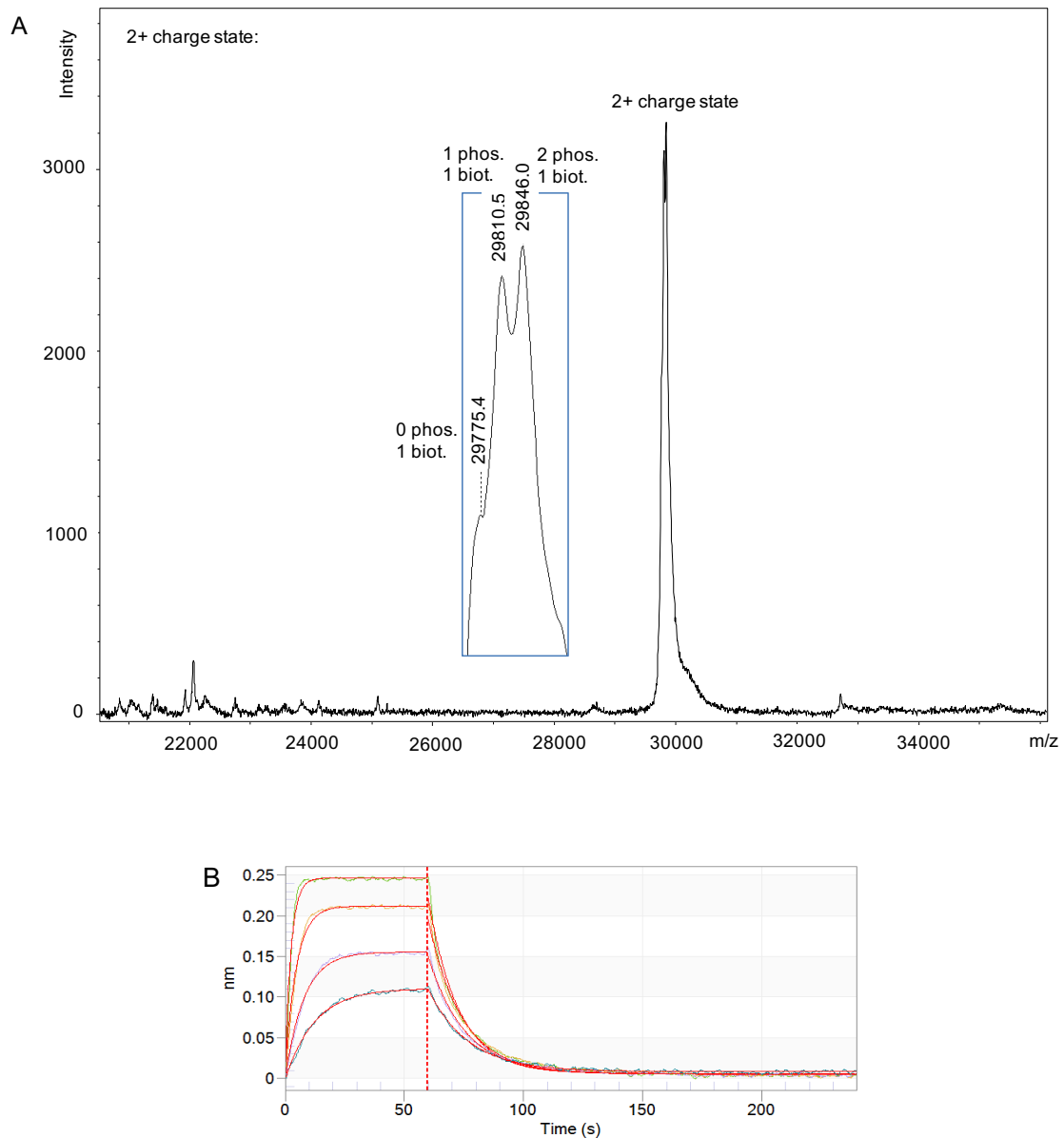


Figure 4.16 Mass spectrometry and bio-layer interferometry of double-phosphorylated Claspin

A: A 2+ charge peak was zoomed in from a MALDI-TOF mass spectrometry analysis. A mixture of double-phosphorylated, mono-phosphorylated and unphosphorylated MBP-Claspin⁸⁸⁴⁻⁹⁹²-8xHis-Avi constructs was detected. The peak indicated all the species was biotinylated. Mass spectrometry analysis was performed by Dr Len Packman from at the Protein and Nucleic Acid Analysis Facility at the University of Cambridge. B: Association and dissociation steps of binding analysis of MBP-pS916pS945Claspin⁸⁸⁴⁻⁹⁹²-8xHis-Avi and Chk1KD on ForteBio Octet instrument. Data was fitted into a 1:1 binding model.

4.1.5 Scanning of kinase responsible to Claspin phosphorylation on CKBD

Although mono-phosphoserine incorporation was successful, the production of double and triple phosphoserine incorporated Claspin using the amber codon suppression approach was not efficient. It would be very useful to be able to produce Claspin that is phosphorylated on all three Chk1 binding motifs, to aid in the elucidation of the structural basis for their specific interaction. Casein kinase 1 γ 1 (CK1 γ 1) and Cdc7/Dbf4 (DDK) were reported to mediate Chk1 activation through Claspin phosphorylation (Chini et al., 2006; Kim et al., 2007; Meng et al., 2011).

Kinase assays were therefore performed to check if they were able to phosphorylate Chk1KD. Recombinant CK1 γ 1 kinase domain (CK1 γ 1⁴³⁻³⁵²) with an N-terminal GST tag was expressed in *E.coli* and purified by Ni-NTA column, ion exchange chromatography and size exclusion chromatography. The Cdc7 ^{Δ 1-36}/Dbf4 complex was supplied by Aji Jatikusumo in our laboratory. Kinase activity of CK1 γ 1 and DDK was checked using ³²P-ATP based kinase assay, using Claspin^{3T/SE} as a negative control for specificity of phosphorylation. ³²P incorporation signals indicated that CK1 γ 1 and DDK did phosphorylate Claspin, but in a non-specific way, as well as undergoing autophosphorylation (Figure 4.17). Whether phosphorylation by these kinases, as well as Chk1 itself, contributes to Claspin interaction with Chk1 was also tested by pull-down (Figure 4.17). CK1 γ 1, Chk1 and DDK treated Claspin only showed weak background binding to Chk1KD as untreated unphosphorylated Claspin, indicating none of these kinases functioned as a direct upstream kinase of Claspin CKBD phosphorylation *in vitro*. Considering the *in vivo* studies which showed evidence on Claspin phosphorylation by these kinases, it was speculated that phosphorylation on Claspin CKBD still could be performed by one of the kinases but possibly the completion of the process required co-operation of other adaptors.

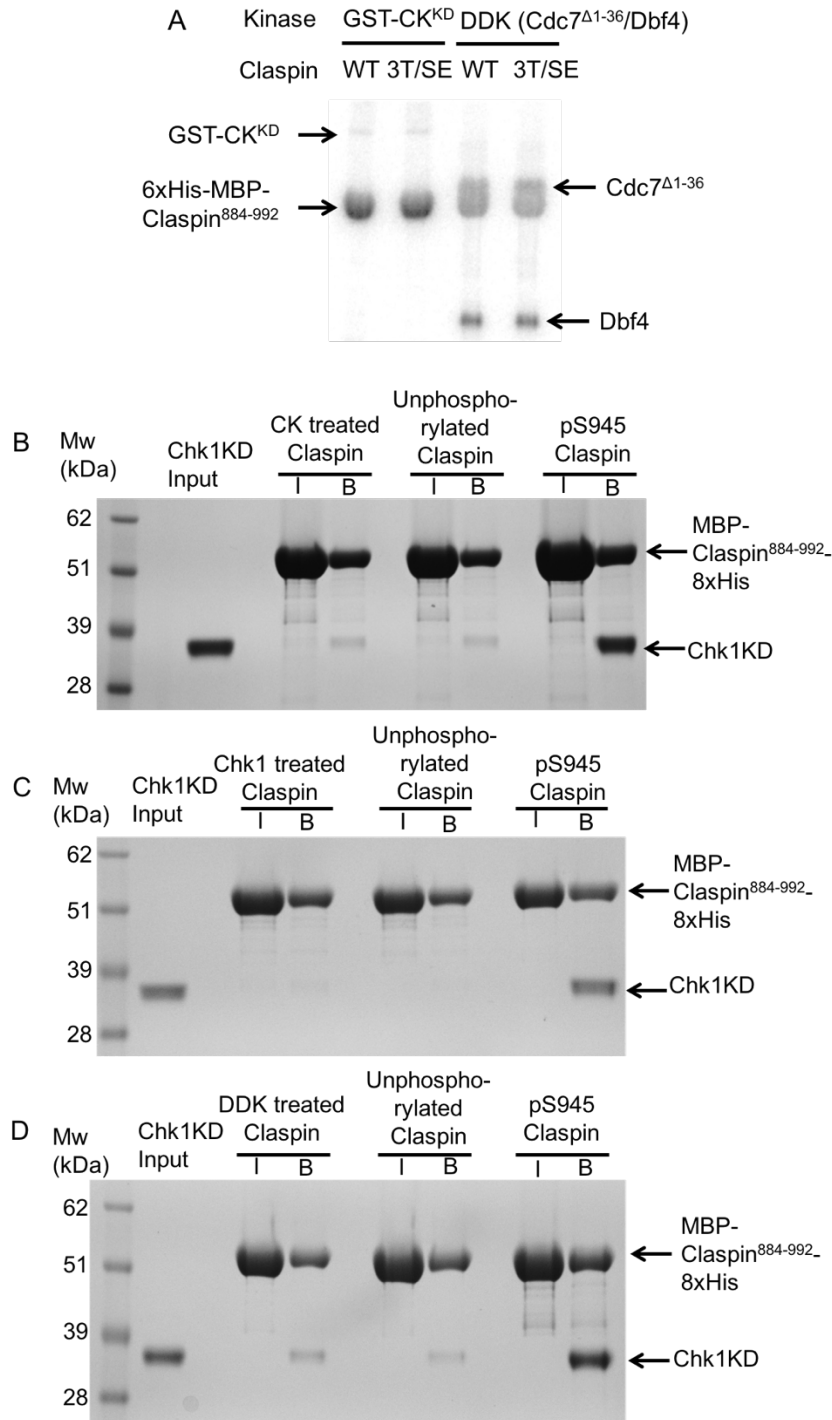


Figure 4.17 Effects of CK1 γ ⁴³⁻³⁵² and Cdc7^{Δ1-36}/Dbf4 phosphorylation on the Claspin-Chk1 interaction.

A: ³²P incorporation signal was detected on kinases (CK1 γ 1 and DDK), Claspin^{WT} and Claspin^{3T/SE}. B-D: Pull-down assays of Chk1KD by CK1 γ 1-, Chk1- and DDK-treated Claspin immobilised on amylose beads. The pull downs were analysed by SDS-PAGE. Unphosphorylated and pS945 Claspin were assayed as negative and positive control respectively. I: Immobilised input, B: Beads sample after pull-down assays.

4.1.6 Alanine scanning of the Claspin Chk1-binding motif

It was shown in the previous section that phosphorylation on T916, S945 and S982 was essential to the interaction of Claspin with Chk1. Sequence conservation in the three Chk1-binding motifs extends beyond the phosphorylated serine and spans approximately 16 amino acids. However, the relative contribution to the interaction with Chk1 of the conserved residues flanking the phosphoserine is unknown. To check if the other conserved amino acid residues have pivotal functions on the Chk1 binding, alanine scanning of the Chk1-binding motif was performed. The second motif has high sequence consensus with the first one so it was chosen for the experiment (Figure 4.18). Fifteen MBP-pS945Claspin⁸⁸⁴⁻⁹⁹²-8xHis-Avi constructs with an alanine substitution to one residue in the region of N936-Q951 were expressed and purified with phosphoserine incorporated on residue 945. The new constructs were expressed with an N-terminal MBP tag so that they could be immobilised on amylose beads for pull-down assays of Chk1KD (Figure 4.18). The alanine-scanning experiment showed that only alanine mutation of F948 abolished binding to Chk1KD, whereas the other fourteen constructs showed the same level of binding as wild-type pS945 Claspin.

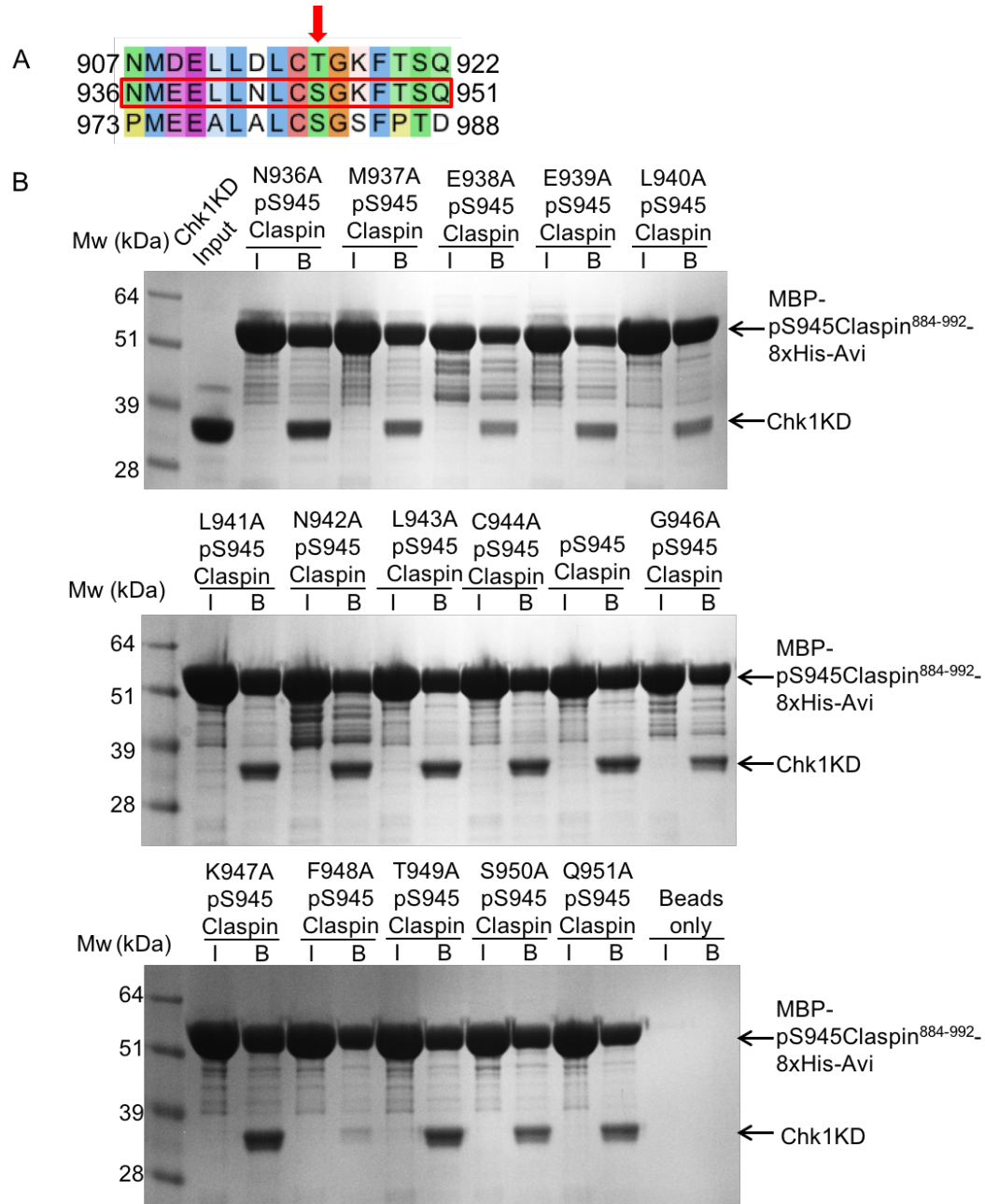


Figure 4.18 Alanine scanning of the Claspin CKBD motif

A: Sequence alignment of three Claspin Chk1-binding motifs. The alignment is coloured by conservation (threshold 30%) with the ClustalWS colouring scheme (Larkin et al., 2007). The phosphorylation site is marked with the red arrow. The sequence used for alanine scanning is marked with a red rectangle. B: Pull-down assays for the 15 alanine mutant constructs, analysed by SDS-PAGE. I: immobilised input, B: beads sample after pull-down assays.

The disruptive effect of the F948A mutation on the interaction between Claspin and Chk1KD was confirmed by Biolayer interferometry (Figure 4.19). To test if the F948A mutation had altered the structure of the Claspin CKBD, circular dichroism

(CD) experiments were performed to compare the putative secondary structure of the wild-type and F948A Claspin constructs. CD measures the difference between the absorption of right and left circularly polarised light at a wavelength range of 190 and 260 nm. α -helices, β -strand and the random coil have different CD spectra, thus providing insight into the secondary structure content of a protein sample. Wild-type (pS945Claspin⁸⁸⁴⁻⁹⁹²-8xHis-Avi) and F948A (pS945Claspin^{884-992F948A}-8xHis-Avi) Claspin polypeptide samples at a concentration of 0.5 mg/ml was analysed on circular dichroism spectroscopy in triplicate. Data was smoothed and buffer-subtracted. CD spectra showed a strong negative signal near 200 nm and weak negative signal above 210 nm for both samples, indicating neither wild-type Claspin nor F948A constructs had significant degrees of secondary structure (Figure 4.19).

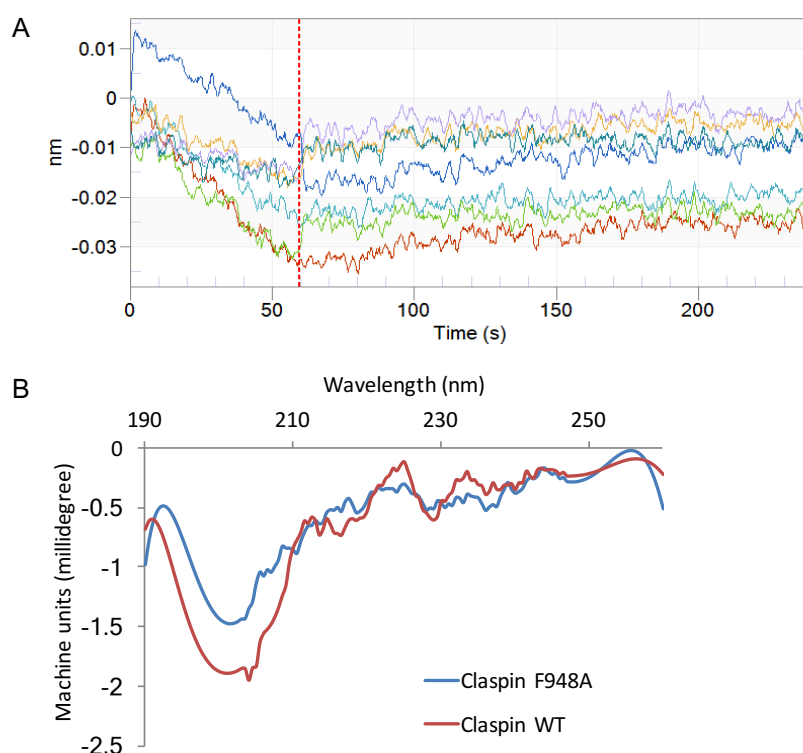
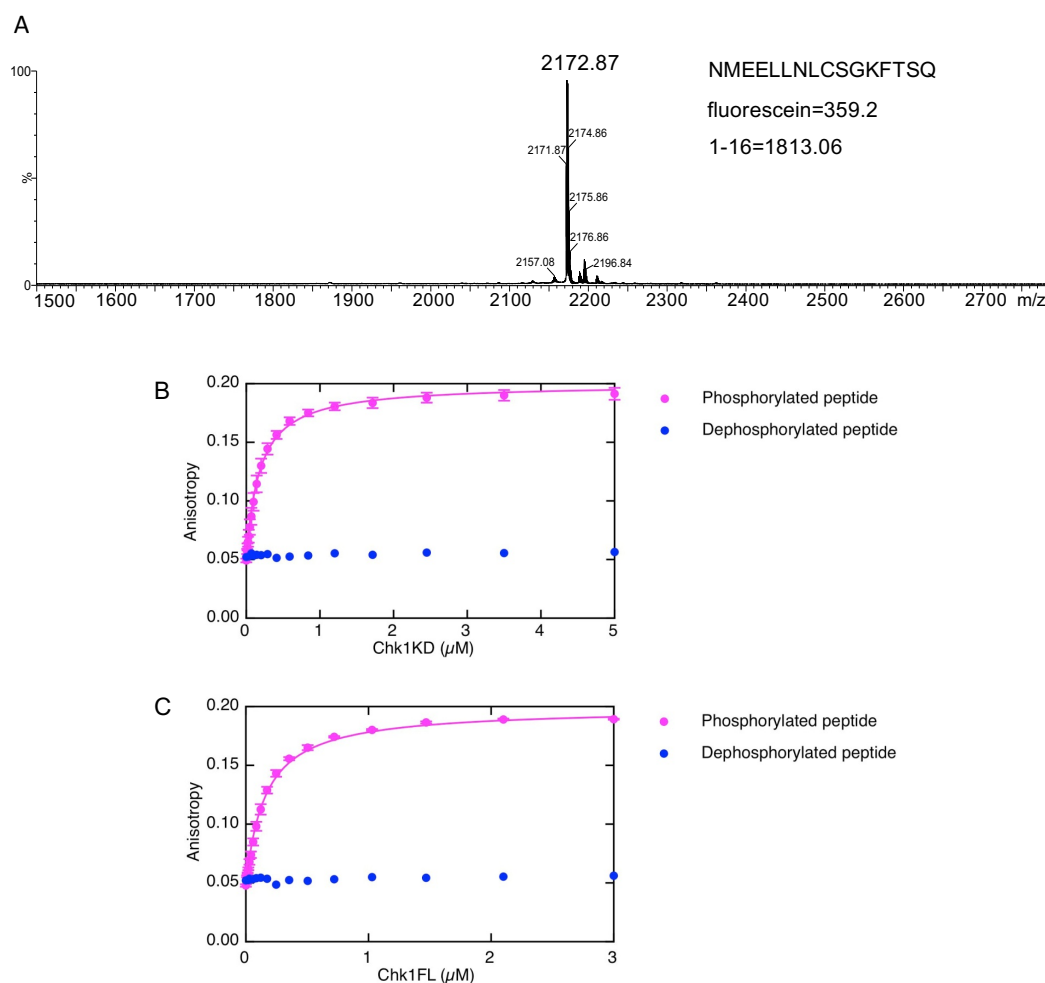


Figure 4.19 Biophysical studies on pS945Claspin^{884-992F948A}-8xHis-Avi

A: Binding curves of Claspin^{F948A} and Chk1KD acquired from Bio-layer Interferometry. Association (0-60 min) and dissociation step (60-240 min) of Claspin^{F948A} (ligand) and Chk1KD (analyte) kinetics study was shown. The association signal showed no binding between the ligand and the analyte. B: CD spectrometry was applied on Claspin^{F948A} and Claspin^{WT}. Machine units were plotted versus wavelength. No secondary structure was observed for either constructs.

4.1.7 Binding affinity determination between Claspin motif and Chk1

A Fluorescein-labelled phosphoserine Claspin⁹³⁶⁻⁹⁵¹ peptide of sequence: NMEELLNLCSGKFTSQ (phosphorylated serine is underlined) was used in fluorescence polarization assays, to determine the binding affinity towards Chk1. Anisotropy data for Chk1KD and Chk1FL binding experiments were fitted to 1:1 binding model, yielding a K_d of 0.18 ($\Delta=0.01$) and 0.16 ($\Delta=0.003$) μ M respectively (Figure 4.20), in agreement with the result of the previous measurements. As a control, dephosphorylation of the Claspin peptide was performed by incubation with λ phosphatase and confirmed by mass spectrometry (Figure 4.20). Anisotropy signal indicates that dephosphorylation of Claspin peptide abolished binding with both Chk1 constructs thus confirming that phosphorylation of S945 of the Claspin peptide is essential to binding.



(Caption on next page)

Figure 4.20 Chk1 titration to Claspin peptide using fluorescence polarisation assays

A: MALDI-TOF mass spectrometry showed a major peak at 2172.87 m/z which corresponded to a fluorescein attached Claspin peptide without phosphorylation, indicating the dephosphorylation treatment was successful. Mass spectrometry analysis was performed by Dr Len Packman from at the Protein and Nucleic Acid Analysis Facility at the University of Cambridge. Chk1KD (B) and Chk1FL (C) titration to fluorescein-labelled Claspin peptide was performed and anisotropy signal was collected by Pherastar. Both phosphorylated and dephosphorylated Claspin peptide was used at concentration of 10 nM in each assay.

4.1.8 Effect of Claspin binding on Chk1 activity

To check the effect of the interaction with Claspin on Chk1 kinase activity, a Claspin⁹³⁶⁻⁹⁵¹ peptide phosphorylated at S945 (NMEELLNLCSGKFTSQ) was titrated in Chk1KD and Chk1FL kinase assays. Endpoint sampling was performed at a range of 0-5 and 10-15 min for Chk1KD and Chk1FL respectively. Reactions were performed with either no pClaspin peptide or with pClaspin peptide at a concentration of 12, 60, 120, 240, 600 and 1200 μM (Figure 4.21).

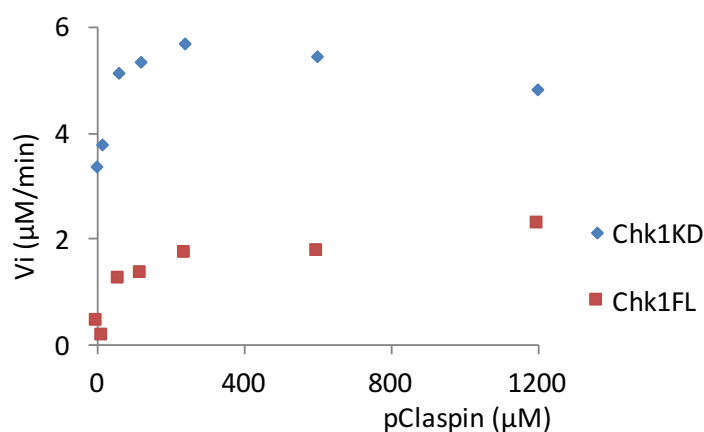


Figure 4.21 Effect of phosphorylated Claspin peptide on Chk1 activity

Initial-rate measurements of Cdc25C peptide phosphorylation by Chk1KD (blue) and Chk1FL (red) were plotted against Claspin peptide concentration. Addition of the phosphorylated Claspin peptide at different concentrations resulted in higher substrate phosphorylation than the reaction without the presence of the Claspin peptide.

Addition of pClaspin peptide at all tested concentration in reaction increased the activity of both Chk1KD and Chk1FL constructs. Intriguingly, kinase activity in the

Chk1KD reaction decreased when the concentration of Claspin peptide exceeded 240 μM , suggesting an inhibitory effect on Chk1KD activity. Conversely, the activity of Chk1FL increased during Claspin peptide titration.

4.1.9 Attempts towards co-crystallization of Chk1KD and phospho-Claspin peptide

Co-crystallization of Chk1KD and the phosphorylated Claspin peptide (NMEELLNLCSGKFTSQ) was attempted to acquire structural information on Chk1-Claspin interaction. Crystals were grown (Materials and methods 4.3.19) and analysed by X-ray diffraction. Although the resolution remained at the same level as for the native unliganded Chk1KD crystals, no Claspin peptide was detected in the electron density map. A second approach to crystallising a Chk1KD-Claspin CKBD complex was therefore adopted. Native wild-type Chk1KD crystals were grown using published conditions (Chen et al., 2000). The phosphorylated Claspin peptide was soaked into the Chk1KD crystals and the soaked crystals were analysed by X-ray diffraction. The resolution remained at the same level as for the native Chk1KD crystals but no Claspin peptide was detected in the electron density map. It is possible that the strong interactions between Chk1KD molecules driving growth of the crystal lattice might disrupt the binding of Chk1KD to the Claspin peptide. I therefore attempted to disrupt Chk1KD crystal growth by mutating amino acid P268, which is involved in a crystal contact in the lattice of Chk1KD crystal. The mutant of Chk1KD^{P268S} was expressed in *Sf9* and the construct was purified using the same purification protocol as Chk1KD^{WT}. The mutant retained normal binding affinity to Claspin which was verified by FP (K_d of 121 μM), but unfortunately failed to co-crystallise with the Claspin peptide.

4.2 Discussion

This chapter describes the characterisation of the interaction of Chk1 with the Claspin CKBD. How Claspin recruits Chk1 to the replisome and how Claspin binding affects Chk1 function at the fork is unclear. The amber codon suppression approach was used to produce three Claspin CKBD proteins, each mono-phosphorylated at one of the three Chk1-binding motifs, and measured their interaction with Chk1KD and Chk1FL using qualitative and quantitative methods.

The mono-phosphorylated versions of the Claspin CKBD bind Chk1 with similar sub-micromolar affinities, in the range of 90 to 289 nM. Thus, no large differences in the strength of the measured Claspin-Chk1 interaction exist among the three repeats, even if the third repeat is considerably less well conserved than the first two. Furthermore, no large difference in affinity towards Claspin was measured between Chk1KD and Chk1FL, indicating that the postulated intramolecular interaction between the kinase and regulatory domains does not interfere or negatively impact the association with Claspin.

ATR phosphorylation at S317 and S345 is a well-characterised step in Chk1 activation. However, whether Chk1 phosphorylation by ATR affects Claspin binding is not clear. Furthermore, an ATR consensus SQ sequence is conserved within all the three motifs in the CKBD of Claspin (Figure 4.1). In my *in vitro* experiments, none of the kinases reported in the literature to be responsible for Claspin phosphorylation were able to phosphorylate the Claspin CKBD. It is possible to speculate that the phosphorylation of the Claspin CKBD leading to Chk1 recruitment might result from a series of phosphorylation events, whereby ATR phosphorylates Claspin on its SQ sequence thus generating an interaction platform for another kinase to conduct the phosphorylation that is required to Chk1 binding.

A peculiar feature of the Claspin-Chk1 interaction is the presence of a tandem repeat

of three contiguous Chk1-binding motifs in Claspin. Although no evidence is available concerning their function, my work has shown that they can all bind Chk1; it is possible that variable degrees of occupancy of the Claspin CKBD might reflect different levels of Chk1 signalling during the replication stress response. It is further possible that adjacent Claspin-bound Chk1 molecules could undergo homotypic regulatory interactions. These hypotheses could be verified by a direct structural determination on the complex or by measuring binding kinetics between phosphorylated Claspin with Chk1. Unfortunately, it was not possible to study the interaction of Chk1 with di- or tri-phosphorylated Claspin CKBD, due to the limitation of the amber suppressor codon method which led to severely reduced expression yields and inhomogeneity of the di- and tri-phosphorylated proteins.

Alanine scanning mutagenesis of Claspin's Chk1-binding motif showed that only one Claspin amino acid in addition to the phosphoserine residue, phenylalanine at position +3, is critical for binding Chk1. This is a surprising observation, given that the sequence conservation of the Chk1-binding motif extends beyond the phosphoserine and encompasses several other flanking amino acids (Figure 4.1). One possible explanation is that the motif may recruit other protein co-factors, which might be required for Chk1 activation, Claspin phosphorylation or some other unknown function.

Chk1 activity is improved in the presence of phosphorylated Claspin⁹³⁶⁻⁹⁵¹ peptide. One assumption on the Chk1 activation mechanism based on this result is that the Claspin peptide bind to Chk1 which leads to a conformational change making Chk1 more active. In this assumption, the Claspin peptide is supposed to remain the interaction with Chk1 to maintain the active form of Chk1. Another assumption is that the Claspin peptide elevated the level of Chk1 autophosphorylation which could lead to a conformational change contributing to higher kinase activity. More repeats and experiments are required to fully explain the effect of Claspin on Chk1 kinetic activity.

4.3 Materials and Methods

4.3.1 Generation and expression of Claspin constructs in Rosetta 2 (DE3)

IMAGE Claspin cDNA was used for the cloning of Claspin⁸⁵⁰⁻⁹⁹² and Claspin⁸⁸⁴⁻⁹⁹². Claspin⁸⁵⁰⁻⁹⁹² sequence was amplified by *Claspin850-f* and *Claspin850-r* primers (Appendix A) to create EcoRI and XhoI restriction sites. Claspin⁸⁸⁴⁻⁹⁹² sequence was amplified by *Claspin884-f* and *Claspin850-r* primers (Appendix A) to create the same restriction sites for insertion in to pMAT11 vector. The amplified sequence was verified on a 1% agarose gel and target band was cut and extracted using geneJET gel extraction kit (Thermo Scientific). Double digest using EcoRI and XhoI restriction enzymes was applied to the two Claspin PCR product and pMAT11 vector. The DNA product verification, gel extraction, ligation and transformation steps were the same as described in 2.3.1. Cells were plated on an agar plate containing 100 µg/mL ampicillin and incubated at 37°C overnight. 4 ml culture of single colony was grown and plasmid was extracted using plasmid miniprep kit (Thermo Scientific) and sequence was verified using Department of Biochemistry DNA Sequencing Facility. 100 ng plasmid was transformed to 20 µl Rosetta 2 (DE3) *E.coli* (Novagen). Transformed cells were incubated on ice for 30 min followed by a heat-shock at 42°C for 45 s. Cells were incubated on ice for 10 min and 700 µl LB medium was added to cells followed by an 1 h incubation at 37°C with shaking at 220 rpm. After recovery, cells were plated on a LB-agar plate containing 100 µg/mL ampicillin and 35 µg/mL chloramphenicol. Single colony was picked after 24 h incubation at 37 °C and was inoculated to 100 ml LB medium containing 100 µg/mL ampicillin and 35 µg/mL chloramphenicol for overnight culture at 37°C with shaking at a speed of 220 rpm. 10 ml overnight culture was inoculated to 1 L 2xYT culture containing 100 µg/mL ampicillin and 35 µg/mL chloramphenicol. Cells were incubated at 37°C with shaking at a speed of 220 rpm until OD reached 0.6 to 0.8 and were induced with 1 mM IPTG. Incubation temperature was lowered to 20 °C and cells were grown overnight.

4.3.2 Purification of Claspin constructs expressed in Rosetta 2 (DE3)

Cells were harvested by centrifugation at 4000 g for 10 mins (Beckman Coulter, JLA 8.1000). Pellet from 1 L growth culture was re-suspended in 15 ml re-suspension buffer (50 mM Hepes pH 7.5, 300 mM NaCl, 1 mM TCEP and 1 EDTA-free protease inhibitor cocktails tablet). Cell pellet re-suspension was sonicated at 25% cycle and 50% power for 3 mins. Lysate was centrifuged at 35000 g and 4 °C for 1 h. Supernatant was collected and loaded onto gravity flow Ni-NTA agarose column. The column was washed twice with 20 ml wash buffer (25 mM Hepes pH 7.5, 300 mM NaCl, 20 mM imidazole, 0.05 % Triton-X100 and 1 mM TCEP). Step wash was performed on the column with wash buffer containing 40 mM and 300 mM imidazole. Elution from the 300 mM imidazole wash was loaded onto a Superdex200 and 16/60 gel filtration column (GE Healthcare). The column was pre-equilibrated and the experiment was performed in the gel filtration buffer (25 mM Hepes pH 7.5, 300 mM NaCl and 2 mM DTT). Elution samples were analysed on a 12% acrylamide SDS-PAGE gel and fractions containing target protein were collected and concentrated. 5-10% glycerol was added to protein sample and protein aliquots were flash frozen using liquid nitrogen and stored at -80 °C.

4.3.3 Generation of Claspin^{3T/SE} construct

T916E, S945E and S982E mutagenesis was generated on pMAT11-Claspin⁸⁸⁴⁻⁹⁹² template by site-directed mutagenesis (QuickChange, Stratagene). Primers *ClaspinT916E-f* and *ClaspinT916E-r*, *ClaspinS945E-f* and *ClaspinS945E-r*, *ClaspinS982E-f* and *ClaspinS982E-r* were used to generate the mutation (Appendix A).

4.3.4 Generation of pMBAT4 vector

A sequence of MBP tag and TEV cleavage sequence was inserted into pBAT4 vector

(Peränen et al., 1996) using NcoI and EcoRI restriction sites. The MBP and the following TEV cleavage sequence from pMAT11 vector was amplified using primers *MBP-f* and *MBP-r* (Appendix A). The amplified MBP-TEV PCR product and pBAT4 vector were treated with NcoI and EcoRI restriction enzymes and were ligated to produce pMBAT4 vector containing an upstream sequence of MBP tag and TEV cleavage site. Several restriction sites remained succeeding the inserted sequence and can be used for insertions.

4.3.5 Generation of MBP-Claspin⁸⁸⁴⁻⁹⁹²-8xHis constructs

Claspin⁸⁸⁴⁻⁹⁹² construct with a C-terminal 8xHis tag was created using *Claspin884S-f* and *Claspin992X-r* primers (Appendix A) based on IMAGE Claspin cDNA sequence. The amplified sequence was inserted into the pMBAT4 vector using Sall and XhoI restriction sites.

4.3.6 Generation and expression of MBP-Claspin⁸⁸⁴⁻⁹⁹²-8xHis amber codon suppression constructs

T916Amber codon and S945Amber codon mutagenesis were introduced to pMBAT4-Claspin⁸⁸⁴⁻⁹⁹²-8xHis template using primers *ClaspinT916Am-f* and *ClaspinT916Am-r*, *ClaspinS945Am-f* and *ClaspinS945Am-r* (Appendix A) by site-directed mutagenesis (QuickChange, Stratagene). S982Amber codon mutagenesis was created by a two-step PCR. The first half of the insertion was amplified using primers *Claspin884S-f* and *ClaspinS982Am-r*. The second half of the insertion was amplified using primers *ClaspinS982Am-f* and *Claspin992X-r* (Appendix A). An overlapping region spanning S982Amber codon was created between the two PCR product which was annealed and amplified using primers *Claspin884S-f* and *Claspin992X-r*. The final PCR product was inserted into pMBAT4 vector using restriction enzymes Sall and XhoI. 100 ng recombinant plasmid was transformed to

50 µl BL21 (DE3)ΔSerB and the transformation procedure was the same as described in 4.3.1. Cells grown in 1 L 2xYT medium were induced with 1 mM IPTG and 2 mM O-Phospho-L-serine (Sigma Aldrich) and cells were incubated at 37 °C for 4 h.

4.3.7 Generation of MBP-Claspin⁸⁸⁴⁻⁹⁹²-8xHis-Avi constructs

The MBP-Claspin⁸⁸⁴⁻⁹⁹²-8xHis sequence was amplified using *Claspin884S-f* and *ClaspinAvi-r* (Appendix A) from pMBAT4-MBP-Claspin⁸⁸⁴⁻⁹⁹²-8xHis template. An C-terminal Avi tag sequence was created and the amplified PCR product was inserted to pMBAT4 vector using restriction enzymes Sall and HindIII.

4.3.8 Generation of MBP-pS945Claspin⁸⁸⁴⁻⁹⁹²-8xHis-Avi alanine scanning constructs

N936A, M937A, E938A, E939A, L940A, L941A, N942A, L943A, C944A, G946A, K947A, F948A, T949A, S950A and Q951A mutagenesis was introduced on template MBP-pS945Claspin⁸⁸⁴⁻⁹⁹²-8xHis-Avi. Primers used are listed below:

| | |
|---|---|
| N936A: <i>ClaspinN936A-f/ClaspinN936A-r</i> | C944A: <i>ClaspinC944A-f/ClaspinC944A-r</i> |
| M937A: <i>ClaspinM937A-f/ClaspinM937A-r</i> | G946A: <i>ClaspinG946A-f/ClaspinG946A-r</i> |
| E938A: <i>ClaspinE938A-f/ClaspinE938A-r</i> | K947A: <i>ClaspinK947A-f/ClaspinK947A-r</i> |
| E939A: <i>ClaspinE939A-f/ClaspinE939A-r</i> | F948A: <i>ClaspinF948A-f/ClaspinF948A-r</i> |
| L940A: <i>ClaspinL940A-f/ClaspinL940A-r</i> | T949A: <i>ClaspinT949A-f/ClaspinT949A-r</i> |
| L941A: <i>ClaspinL941A-f/ClaspinL941A-r</i> | S950A: <i>ClaspinS950A-f/ClaspinS950A-r</i> |
| N942A: <i>ClaspinN942A-f/ClaspinN942A-r</i> | Q951A: <i>ClaspinQ951A-f/ClaspinQ951A-r</i> |
| L943A: <i>ClaspinL943A-f/ClaspinL943A-r</i> | |

4.3.9 Generation of Strep-SUMO-Claspin⁸⁸⁴⁻⁹⁹²-8xHis constructs

A SUMO tag sequence followed by a TEV cleavage sequence was amplified using

primers SUMO-f and SUMO-r (Appendix A) from pRSFDuet vector (Novagen). The amplified sequence was inserted to pMBAT4 vector using restriction enzyme NcoI. The SUMO-Claspin⁸⁸⁴⁻⁹⁹² sequence was amplified using primers *Strep-f* and *Claspin992X-r* (Appendix A). An N-terminal Strep tag was created upstream of the amplified insertion and the PCR product was inserted into pMBAT4 using restriction enzymes EcoRI and XhoI.

4.3.10 Purification of Claspin constructs expressed in amber codon suppression system

Cells were harvested by centrifugation at 4000 g for 10 mins (Beckman Coulter, JLA 8.1000). Pellet from 1 L growth culture was re-suspended in 15 ml re-suspension buffer (50 mM Hepes pH 7.5, 300 mM NaCl, 1 mM TCEP, 10 mM NaF, 1 mM β -glycerolphosphate and 1 EDTA-free protease inhibitor cocktails tablet). Cell pellet re-suspension was sonicated at 25% cycle and 50% power for 3 mins. Lysate was centrifuged at 35000 g and 4 °C for 1 h. Supernatant was collected and loaded onto gravity flow Ni-NTA agarose column. The column was washed twice with 20 ml wash buffer (25 mM Hepes pH 7.5, 300 mM NaCl, 10mM NaF, 20 mM imidazole, 0.05 % Triton-X100 and 1 mM TCEP). Step wash was performed on the column with wash buffer containing 40 mM and 300 mM imidazole. Elution from the 300 mM imidazole wash was loaded onto a Superdex75 16/60 gel filtration column (GE Healthcare). The column was pre-equilibrated and the experiment was performed in the gel filtration buffer (25 mM Hepes pH 7.5, 300 mM NaCl, 10 mM NaF and 2 mM DTT). Elution samples were analysed on a 12% acrylamide SDS-PAGE gel and fractions containing target protein were collected and concentrated. 5-10% glycerol was added to protein sample and protein aliquots were flash frozen using liquid nitrogen and stored at -80 °C.

4.3.11 Pull-down assays between Claspin and Chk1 constructs

0.6 mg MBP-Claspin⁸⁸⁴⁻⁹⁹²-8xHis constructs and 0.6 mg Strep-SUMO-Claspin⁸⁸⁴⁻⁹⁹²-8xHis constructs were immobilised on 70 µl amylose resin or 80 µl StrepTactin resin respectively. Claspin constructs were incubated with the resin in a rolling motion at 4 °C for 30 min. Samples in Eppendorf tubes were spun down at 14kg at 4 °C for 2 mins. Supernatant was removed and resin was washed three times with 1 ml wash buffer (25 mM Hepes pH 7.5, 150 mM NaCl, 5 % glycerol, 0.1 % Igpal and 5 mM DTT). Resin was re-suspended with the volume of wash buffer and 20 µl of the mixture was taken as an "input" sample. 0.3 mg Chk1KD or 0.5 mg Chk1FL in 500 µl wash buffer was applied to corresponding Claspin constructs and the samples were incubated in a rolling motion at 4 °C for 1 h. Supernatant was removed and resin was washed three times with 1 ml wash buffer. Resin was re-suspended with the volume of wash buffer and 20 µl of the mixture was taken as an "beads" sample. Pull-down assays between other MBP tagged Claspin constructs (6xHis-MBP-Claspin⁸⁸⁴⁻⁹⁹², MBP-pS945Claspin⁸⁸⁴⁻⁹⁹²-8xHis alanine scanning and 6xHis-MBP-Claspin^{884-992-3T/SE}) and Chk1KD in Chapter 4 were performed in the same procedure described in this section.

4.3.12 Generation, expression and purification of CK1γ1⁴³⁻³⁵²

IMAGE Casein kinase 1γ1 cDNA was used for the cloning of CK1γ1⁴³⁻³⁵². CK1γ1⁴³⁻³⁵² sequence was amplified by *CK45-f* and *CK352-r* primers (Appendix A) to create EcoRI and HindIII restriction sites. The PCR product was inserted to pGAT11 vector (Peränen et al., 1996) using the two restriction sites. The ligation, transformation to Rosetta cells and expression procedure was the same as described in 4.3.1. Cell harvest, sonication and centrifugation procedure was the same as described in 4.3.2. Soluble fraction was applied onto gravity flow Ni-NTA agarose (Qiagen) column. The column was washed three times with 20 ml wash buffer (20 mM Tris pH 7.5, 150 mM NaCl and 20 mM imidazole). Sample was elution in 300 mM imidazole.

The elution was diluted to achieve 100 mM NaCl and was applied onto a Hitrap Q ion-exchange column (GE Healthcare). Protein was eluted along NaCl gradient wash (buffer A: 20 mM Tris pH 7.5, buffer B: 20 mM Tris pH 7.5 and 1 M NaCl). Fractions containing GST-CK⁴⁵⁻³⁵² was concentrated and loaded onto a Superdex200 and 16/60 gel filtration column (GE Healthcare). The column was pre-equilibrated and the experiment was performed in the gel filtration buffer (20 mM Tris pH 7.5 and 150 mM NaCl). Elution samples were analysed on a 12% acrylamide SDS-PAGE gel and fractions containing target protein were collected and concentrated. 5-10% glycerol was added to protein sample and protein aliquots were flash frozen using liquid nitrogen and stored at -80 °C.

4.3.13 Kinase activity and substrate specificity test of CK1 γ 1⁴³⁻³⁵² and Cdc7 ^{Δ 1-36}/Dbf4

40 μ l kinase assay reaction was set up with a final concentration of 21 μ M CK1 γ 1⁴³⁻³⁵² or 5.3 μ M Cdc7 ^{Δ 1-36}/Dbf4, 34.8 or 52.3 μ M 6xHis-MBP-Claspin/6xHis-MBP^{3T/SE}-Claspin and 100 μ M ATP. Reaction was incubated at 30 °C for 1 h. 5 μ l reaction was added to 5 μ l loading dye mix (4x loading dye, 0.5M EDTA and reducing agent was mixed at a volume ratio of 1:1:1) and the sample was boiled at 80 °C for 5 min. Sample was analysed by SDS-PAGE and exposed to storage phosphor screen (GE Healthcare). Incorporation signal was scanned on Typhoon FLA 9500 (GE Healthcare).

4.3.14 Western blotting

The bands from SDS-PAGE gel were transferred onto a nitrocellulose membrane (Thermo Scientific). The membrane was blocked with 4% milk PBST for 2 h at room temperature. The membrane was then incubated in Streptavidin-AP conjugate (1 in 2000 dilution, Sigma Aldrich) for 2 h at room temperature. Membrane was washed

with 15 ml of 2% milk PBST for 5 minutes for 3 times. The membrane was soaked in BCIP solution (Sigma Aldrich) until the bands were shown on the membrane.

4.3.15 Bio-layer interferometry studies on Claspin and Chk1 constructs using ForteBio Octet

Ligand scouting was performed to determine the ligand concentration used in binding studies. Claspin⁸⁸⁴⁻⁹⁹²-8xHis-Avi construct was used as a ligand which was attached to Dip and Read™ Streptavidin (SA) Biosensors (ForteBio). Two columns of 8-biosensors were used in each experiment with one column for reference biosensors and the other one for experiment biosensors. Experiment procedure was programmed using Octet Data Acquisition software (ForteBio). An initial wash step was performed for 60 s in the wells only containing binding buffer (25 mM Hepes pH 7.5, 150 mM NaCl, 0.1 mg/ml BSA, 0.005 % Tween-20 and 0.1 mM TCEP). The second step was a 120s-loading step where the biosensors dipped into wells with Claspin peptide at a concentration of 5-300 nM. It was followed by a 60s-wash step in binding buffer and a 60s-baseline step in fresh binding buffer. The ligand biosensors were dipped into analyte (1 μM Chk1KD) wells for a 120s-association which was followed by a 60s-dissociation step performed in the baseline well. Instead of loading ligand in the ligand wells, the reference biosensors were dipped in the second wash wells during the loading step so no Claspin peptide was attached to the reference biosensors. 20-30 nM ligand concentration contributed to a signal of 0.2-0.4 nm and was selected for ligand immobilization condition in binding assays. The procedure of the binding kinetics study was the same with the ligand scouting procedure except the ligand concentration in all loading wells was at a fixed 20-30 nM and the analyte (Chk1KD or Chk1FL) was at a concentration of 3-500 nM. Binding kinetics data was analysed using Octet Data Analysis software (ForteBio). Data processing includes double-reference subtraction, aligning Y axis to baseline, aligning to dissociation in inter-step correction and Savitzky-Golay filtering. Association and dissociation steps

were selected for analysis and data was fitted in to a 1:1 model using local and partial fitting. Averaged k_{on} and k_{off} were extracted from the 3 or 4 selected fitted binding curves and the errors of these parameters were generated from the standard deviation. The dissociation constant K_d was generated from k_{off}/k_{on} and the error was produced by the error propagation analysis: $\Delta Kd = Kd \sqrt{\left(\frac{\Delta k_{on}}{k_{on}}\right)^2 + \left(\frac{\Delta k_{off}}{k_{off}}\right)^2}$

4.3.16 Circular dichroism analysis for pS945Claspin⁸⁸⁴⁻⁹⁹²-8xHis-Avi constructs

pS945Claspin⁸⁸⁴⁻⁹⁹²-8xHis-Avi and pS945Claspin^{884-992-F948A}-8xHis-Avi was buffer exchanged into experiment buffer (10 mM phosphate pH 7.5 and 150 mM NaF) using PD10 columns (GE Healthcare). The CD spectrum from 190 nm to 260 nm at 0.5 nm increment (Aviv 400 spectrometer) for 0.5 mg/ml Claspin constructs was measured in a 1 mm path-length cuvette at 25°C. Buffer subtraction and curve smoothing were applied during data analysis.

4.3.17 Fluorescence polarization assay for Claspin peptide and Chk1 constructs

Series dilutions (100 nM to 5 nM) of fluorescence-labelled Claspin peptide (5&6Flu-NMEELLNLCSGKFTSQ, Cambridge Peptides, phosphorylated serine was underlined) were made in reaction buffer (25 mM Hepes pH 7.5, 150 mM NaCl, 0.005 % Tween-20 and 5 mM DTT) and added to a 96-well assay plate (Corning) to measure the lowest concentration of the Claspin peptide which produced liable anisotropy measurement from fluorescence background. 10 nM was selected as experimental concentration for fluorescence polarization assay. 30 nM free fluorescein was used as a reference for 35 mP. Series dilutions of receptor proteins (2 nM to 5 μ M for Chk1KD and 20 nM to 3 μ M for Chk1FL) were made and mixed with 10 nM Claspin peptide. Anisotropy of each well was measured on PHERAStar

(BMG Labtech). Each experiment was performed in triplicate and data was plotted and fitted in Pro Fit software (<http://quansoft.com>) using the binding model based on the equation:

$$r = r_0 + \frac{(r_{max}-r_0)C^n}{K_d+C^n}$$

r : anisotropy; r_0 : anisotropy of free Claspin peptide; r_{max} : maximal anisotropy reached in the system; K_d : dissociate constant; C : Chk1KD or Chk1FL concentration in micromolar; n : number of binding sites (set to 1 in this experiment).

4.3.18 Kinase assays of Chk1 constructs in the presence of pClaspin peptide

50 μ l reaction containing 120 μ M Cdc25C peptide, 1 mM ATP, 12, 60, 120, 240, 600 or 1200 μ M phosphorylated Claspin peptide (NMEELLNLCSGKFTSQ, phosphorylated serine is underlined) and 0.05 μ M Chk1KD or 0.5 μ M Chk1FL was performed in reaction buffer. Assay procedure was described in 3.3.8.

4.3.19 Crystallization trials of Chk1 and Claspin peptide

A sitting drop crystal tray for Chk1KD was set up with precipitant and buffer scales designed according to a published condition (Chen et al., 2000). Crystals were produced in two conditions (7% or 11% PEG8000, 0.1 M Ammonium sulphate, 0.1 M Sodium cacodylate and 2% glycerol). 0.2 μ l fluorescein labelled phosphorylated Claspin peptide at a concentration of 0.7 to 4.8 mM were soaked into Chk1KD crystals. Chk1KD crystals did not crack after 24 h. The crystals were briefly soaked in reservoir buffer containing 25 % glycerol and were mounted into cryo-loops (Hampton Research). X-ray diffraction data was collected for one crystal and the resolution reached 1.8 \AA (Diamond light source, I03). An electron density map was obtained by molecular replacement in Phenix software using Chk1KD (PDB accession code 1IA8) as a search model. The Claspin peptide was not observed in the

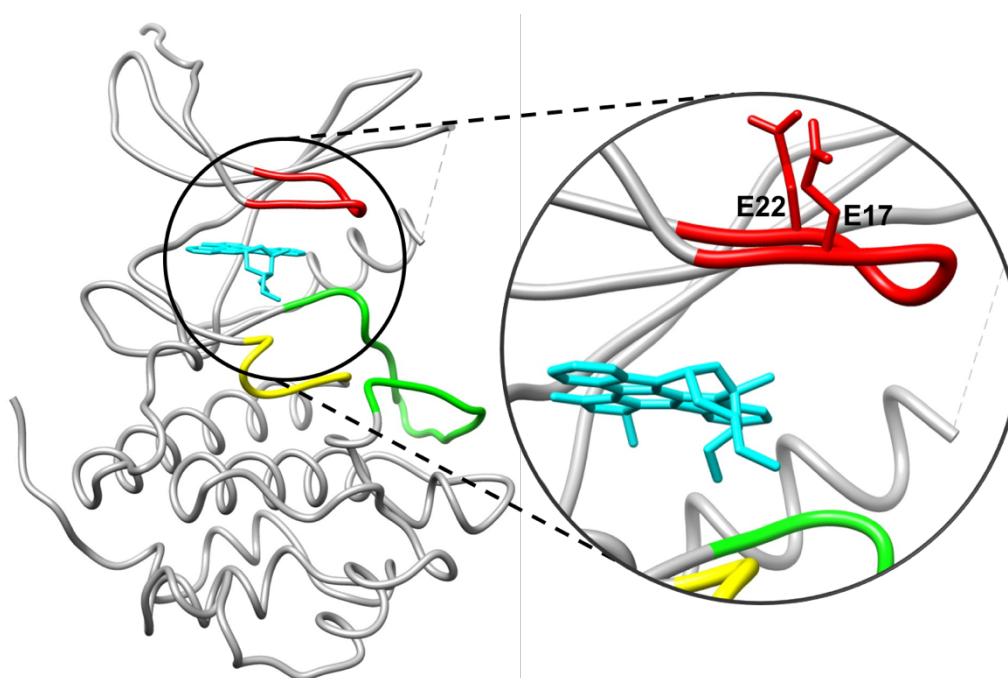
density map.

Co-crystallization trials for 200-240 μ M Chk1KD and un-labelled phosphorylated Claspin peptide were performed at a molar ratio of 1:1.5 and 1:3 on screening plates: JCSG+, PACT, Morpheus, Classics, PEGSI, PEGSII, Protein Complex (Qiagen), Wizard I&II. Clusters of needle-shaped crystals were produced in reservoir condition of 0.1 M PCPT pH 8 or pH 9 and 25 % w/v PEG 1500. Optimization was performed and plate-shaped crystals were produced in conditions of 0.1 M PCPT pH 7.5-9, 25-30 % PEG 1500 and 0.2 M LiNO₃. Crystals were briefly soaked in buffer containing corresponding reservoir buffer and 30 % glycerol and were mounted in cryo-loops. X-ray diffraction data was collected and the resolution reached 1.8 Å (Diamond light source, I04). An electron density map was obtained by molecular replacement in Phenix software using Chk1KD (PDB accession code 1IA8) as a search model. The Claspin peptide was not observed in the density map.

180 μ M Chk1KD^{P268S} in complex with phosphorylated Claspin peptide at molar ratios of 1:1.5 and 1:3 was applied on screening plates PEGSI, PEGSII, PACT and Morpheus using the protocol described in 2.3.9. No hit was produced in the conditions tested.

CHAPTER 5 DISCUSSION AND FUTURE DIRECTIONS

The work in this thesis showed that Chk1KD was about two orders of magnitude more efficient in ATP turnover than Chk1FL and therefore ATP turnover is speculated to be the rate-limiting step in Chk1 kinase assay. A tight binding between Chk1KD and Chk1RD was observed though no structural information on this intramolecular interaction was available. Critical residues responsible to Chk1RD binding were firstly identified in this thesis based on HDX and kinase assay studies. The two glutamate residues on the N-terminal glycine-rich loop on Chk1KD are proposed to bind to Chk1RD through electrostatic interaction. A glycine-rich loop (GxGxxG) is a conserved feature on a kinase catalytic domain and it is responsible to ATP positioning (Figure 5.1). Combining to the evidence collected in this thesis, a preliminary auto-inhibitory model can be depicted: Chk1RD interacts with the glycine-loop on Chk1KD through electrostatic interaction and inhibits kinase activity through interrupting ATP binding. Additional structural information will shed light on completion of this Chk1 activity regulation model. Structural analysis on Chk1FL can be achieved through study in complex with other binding partners which have a role in stabilising the flexible linker on Chk1FL.



(Caption on next page)

Figure 5.1 Chk1KD structure in complex with UCN-01 (PDB#1NVQ) highlighting the positioning of the glycine-rich loop and the ATP-binding pocket

The glycine-rich loop (in red) is on the N-terminal lobe which stabilises ATP binding. ATP-binding pocket is occupied by UCN-01, a Chk1 inhibitor, which is shown in cyan. The putative Chk1RD-interacting glutamate residues (E17 and E22) locates in the glycine-rich loop and present on the surface of Chk1KD. The catalytic loop (R129-N135) and the activation loop (D148-T170) are shown in yellow and green respectively. The figure was generated in Chimera (Pettersen et al., 2004).

The aim of *in vitro* studies is always to understand an *in vivo* mechanism. Upon checkpoint activation, *in vivo* Chk1 activation is performed by ATR, although the molecular mechanism is still elusive. Kinetic studies on ATR phosphorylated Chk1 will shed light on interpretation of *in vivo* Chk1 activation mechanism by comparing it with Chk1KD and Chk1FL, the two extreme forms of Chk1 in terms of activity. Kinetic parameters including ATP and substrate binding affinity will help understand the Chk1 catalysis mechanism. Moreover, a dynamic catalysis mechanism can be depicted which will shed light on selective drug development.

The work in this thesis revealed critical residues on Chk1-binding in a sequence of T/S*xxF (* indicates a phosphorylation site, x indicates any residue). Claspin contains three of these tandem motifs and each of them contributes to the same level of binding to Chk1. The number of the conserved motifs varies among species which generates a question on why human Claspin adopts three motifs. When all the motifs are phosphorylated, structural information on Claspin in complex with Chk1 can be analysed by cryo-EM and the result should provide information on whether Claspin forms a platform to recruit one Chk1 molecule on each of the tandem Chk1-binding motif. Whether binding to Claspin leads to conformational change and to what extent can be learnt from a high-resolution structure. Given that no kinase was found to be responsible to Claspin phosphorylation on its Chk1-binding motifs *in vitro*, it is speculated that the Claspin phosphorylation process stimulated by checkpoint activation is a consequence of a series of post-translational events *in vivo*. This should

be taken into consideration when investigating the upstream kinase of Claspin's Chk1-binding motifs.

This thesis also provides insight into Claspin's function on Chk1 activation. An increase of Chk1 activity was observed in the presence of a phosphorylated Claspin peptide spanning the region of one Chk1-binding motif, although the Chk1 upstream kinase ATR was in absence. It provides evidence for a Chk1 activation model that binding to Claspin leads to an activating conformational change on Chk1 which provides structural basis for ATR phosphorylation. The active status of Chk1 is further stabilised after phosphorylation at 317 and 345. Further analyses include Chk1 kinetic studies in the presence of Claspin peptide and structural determination of the Chk1-Claspin peptide complex should be performed to explain the increased Chk1 activity and to reveal the potential conformational change. The result will shed light on a dynamic Chk1 activation model from an atomic-level.

Cancer cell generates excessive amount of replication stress during proliferation and it relies on DDR, especially ATR/Chk1 pathway, to survive. Chk1 is thus rendered as an important target of cancer therapy. A number of Chk1 inhibitors have been developed and some of them have entered early stage of clinical trials. This conventional strategy, however, generates excessive toxicity which is detrimental to cancer cells as well normal cells. A novel therapy targeting a constitutively active Chk1 may avoid this side effect. Chk1 activator can be generated based on the Chk1 activation model and it will block cancer cell proliferation by constitutively inhibiting cell cycle progression. This novel therapy does not require toxic reagents like chemotherapy and its' application will be a milder choice for cancer therapy comparing to Chk1 inhibitors.

REFERENCE

- Abraham, R.T. (2001). Cell cycle checkpoint signaling through the ATM and ATR kinases. *Genes & Development* *15*, 2177, 2196.
- Adam, K.v., Cartel, M.I., Lambert, M., David, L., Yuan, L., Besson, A., Mayeux, P., Manenti, S., and Didier, C. (2018). A PIM-CHK1 signaling pathway regulates PLK1 phosphorylation and function during mitosis. *The Company of Biologists* *131*, 1,12.
- Ammazzalorso, F., Pirzio, L.M., Bignami, M., Franchitto, A., and Pichierri, P. (2010). ATR and ATM differently regulate WRN to prevent DSBs at stalled replication forks and promote replication fork recovery. *The EMBO Journal* *29*, 3156, 3169.
- Aze, A., and Maiorano, D. (2018). Recent advances in understanding DNA replication: cell type-specific adaptation of the DNA replication program. *F1000Research* *7*, 1351.
- Baker, N.A., Sept, D., Joseph, S., Holst, M.J., and McCammon, J.A. (2001). Electrostatics of nanosystems: Application to microtubules and the ribosome. *PNAS* *98*, 10037, 10041.
- Bakkenist, C.J., and Kastan, M.B. (2003). DNA damage activates ATM through intermolecular autophosphorylation and dimer dissociation. *Nature* *421*, 499, 506.
- Ball, H.L., Ehrhardt, M.R., Mordes, D.A., Glick, G.G., Chazin, W.J., and Cortez, D. (2007). Function of a conserved checkpoint recruitment domain in ATRIP proteins. *Molecular and Cellular Biology* *27*, 3367, 3377.
- Ballabeni, A., Melixetian, M., Zamponi, R., Masiero, L., Marinoni, F., and Helin, K. (2004). Human Geminin promotes pre-RC formation and DNA replication by stabilizing CDT1 in mitosis. *The EMBO Journal* *23*, 3122, 3132.
- Bando, M., Katou, Y., Komata, M., Tanaka, H., Itoh, T., Sutani, T., and Shirahige, K. (2009). Csm3, Tof1, and Mrc1 form a heterotrimeric mediator complex that associates with DNA replication forks. *The Journal of Biological Chemistry* *284*, 34355, 34365.
- Bannister, A.J., Gottlieb, T.M., Kouzarides, T., and Jackson, S.P. (1993). c-Jun is phosphorylated by the DNA-dependent protein kinase in vitro; definition of the minimal kinase recognition motif. *Nucleic Acids Research* *21*, 1289, 1295.
- Bassermann, F., Frescas, D., Guardavaccaro, D., Busino, L., Peschiaroli, A., and Pagano, M. (2008). The Cdc14B-Cdh1-Plk1 axis controls the G2 DNA damage response checkpoint. *Cell* *134*, 256, 267.
- Bastin-Shanower, S.A., and Brill, S.J. (2001). Functional analysis of the four DNA binding domains of replication protein A: the role of RPA2 in ssDNA binding. *Journal of Biological Chemistry* *276*, 36446, 36453.
- Bell, S.P., and Dutta, A. (2002). DNA replication in eukaryotic cells. *Annual Review of Biochemistry* *71*, 333, 374.
- Bennett, L.N., and Clarke, P.R. (2006). Regulation of Claspin degradation by the ubiquitin-proteasome pathway during the cell cycle and in response to ATR-dependent checkpoint activation. *FEBS Letters* *580*, 4176, 4181.
- Blackford, A.N., and Jackson, S.P. (2017). ATM, ATR, and DNA-PK: The trinity at the heart of the DNA damage response. *Molecular Cell* *66*, 801, 817.
- Bont, R.D., and Larebeke, N.v. (2004). Endogenous DNA damage in humans: a review of quantitative data. *Mutagenesis* *19*, 169, 185.
- Brown, E.J., and Baltimore, D. (2000). ATR disruption leads to chromosomal fragmentation and early embryonic lethality. *Genes & Development* *14*, 397, 402.

Buisson, R., Boisvert, J.L., Benes, C.H., and Zou, L. (2015). Distinct but concerted roles of ATR, DNA-PK, and Chk1 in countering replication stress during S phase. *Molecular Cell* *59*, 1011, 1024.

Callegari, A.J., and Kelly, T.J. (2007). Shedding light on the DNA damage checkpoint. *Cell Cycle* *6*, 660, 666.

Cappell, S.D., Chung, M., Jaimovich, A., Spencer, S.L., and Meyer, T. (2016). Irreversible APCDdh1 inactivation underlies the point of no return for cell-cycle entry. *Cell* *166*, 167, 180.

Chagin, V.O., Casas-Delucchi, C.S., Reinhart, M., Schermelleh, L., Markaki, Y., Maiser, A., Bolius, J.J., Bensimon, A., Fillies, M., Domaing, P., *et al.* (2016). 4D Visualization of replication foci in mammalian cells corresponding to individual replicons. *Nature Communications* *7*, 11231.

Chaudhury, I., and Koepp, D.M. (2016). Recovery from the DNA replication checkpoint. *Genes* *7*, 1, 11.

Chen, P., Luo, C., Deng, Y., Ryan, K., Register, J., Margosiak, S., Tempczyk-Russell, A., Nguyen, B., Myers, P., Lundgren, K., *et al.* (2000). The 1.7 Å crystal structure of human cell cycle checkpoint kinase Chk1: Implications for Chk1 regulation. *Cell* *100*, 681, 692.

Cheng, Y.-C., Lin, T.-Y., and Shieh, S.-Y. (2013). Candidate tumor suppressor BTG3 maintains genomic stability by promoting Lys63-linked ubiquitination and activation of the checkpoint kinase CHK1. *PNAS* *110*, 5993, 5998.

Cheng, Y.-C., and Shieh, S.-Y. (2018). Deubiquitinating enzyme USP3 controls CHK1 chromatin association and activation. *PNAS* *115*, 5546, 5551.

Chini, C., Wood, J., and Chen, J. (2006). Chk1 is required to maintain Claspin stability. *Oncogene* *25*, 4165, 4171.

Choi, M., Kipps, T., and Kurzrock, R. (2016). ATM mutations in cancer: Therapeutic implications. *Molecular Cancer Therapeutics* *15*, 1781, 1791.

Ciccia, A., and Elledge, S.J. (2010). The DNA damage response: Making it safe to play with knives. *Molecular Cell* *40*, 179, 204.

Cimprich, K.A., and Cortez, D. (2008). ATR: an essential regulator of genome integrity. *Nature Reviews Molecular Cell Biology* *9*, 616, 627.

Cortez, D. (2015). Preventing replication fork collapse to maintain genome integrity. *DNA Repair* *32*, 149, 157.

Couch, F.B., Bansbach, C.E., Driscoll, R., Luzwick, J.W., Glick, G.G., Betous, R., Carroll, C.M., Jung, S.Y., Qin, J., Cimprich, K.A., *et al.* (2013). ATR phosphorylates SMARCAL1 to prevent replication fork collapse. *Genes and Development* *27*, 1610, 1623.

Coverley, D., Pelizon, C., Trewick, S., and Laskey, R.A. (2000). Chromatin-bound Cdc6 persists in S and G2 phases in human cells, while soluble Cdc6 is destroyed in a cyclin A-cdk2 dependent process. *Journal of Cell Science* *113*, 1929, 1938.

Dandoulaki, M., Petsalaki, E., Sumpton, D., Zanivan, S., and Zachos, G. (2018). Src activation by Chk1 promotes actin patch formation and prevents chromatin bridge breakage in cytokinesis. *Journal of Cell Biology* *217*, 3071, 3089.

Davies, S.L., North, P.S., Dart, A., Lakin, N.D., and Hickson, I.D. (2004). Phosphorylation of the Bloom's syndrome helicase and its role in recovery from S-phase arrest. *Molecular and Cellular Biology* *24*, 1279, 1291.

Delacroix, S., Wagner, J.M., Kobayashi, M., Yamamoto, K.-i., and Karnitz, L.M. (2007). The Rad9–Hus1–Rad1 (9–1–1) clamp activates checkpoint signaling via TopBP1. *Genes and Development* *21*, 1472, 1477.

Dewar, J.M., Budzowska, M., and Walter, J.C. (2015). The mechanism of DNA replication termination in

vertebrates. *Nature* 525, 345, 350.

Duch, A., Canal, B., Barroso, S.I., García-Rubio, M.a., Seisenbacher, G., Aguilera, A.s., Nadal, E.I.d., and Posas, F. (2018). Multiple signaling kinases target Mrc1 to prevent genomic instability triggered by transcription-replication conflicts. *Nature Communications* 9, 379.

Duzdevich, D., Warner, M.D., Ticau, S., Ivica, N.A., Bell, S.P., and Greene, E.C. (2015). The dynamics of eukaryotic replication initiation: Origin specificity, licensing, and riring at the single-molecule level. *Molecular Cell* 58, 483, 494.

Emptage, R.P., Schoenberger, M.J., Ferguson, K.M., and Marmorstein, R. (2017). Intramolecular autoinhibition of checkpoint kinase 1 is mediated by conserved basic motifs of the C-terminal kinase-associated 1 domain. *Journal of Biological Chemistry* 292, 19024,19033.

Enomoto, M., Goto, H., Tomono, Y., Kasahara, K., Tsujimura, K., Kiyono, T., and Inagaki, M. (2009). Novel positive feedback loop between Cdk1 and Chk1 in the nucleus during G2/M transition. *Journal of Biological Chemistry* 284, 34223, 34230.

Errico, A., and Costanzo, V. (2012). Mechanisms of replication fork protection: a safeguard for genome stability. *Critical Reviews in Biochemistry and Molecular Biology* 47, 222, 235.

Falck, J., Coates, J., and Jackson, S.P. (2005). Conserved modes of recruitment of ATM, ATR and DNA-PKcs to sites of DNA damage. *Nature* 434, 605, 611.

Faustrop, H., Bekker-Jensen, S., Bartek, J., Lukas, J., and Mailand, N. (2009). USP7 counteracts SCF TrCP- but not APCCdh1-mediated proteolysis of Claspin. *The Journal of Cell Biology* 184, 13, 19.

Ferreira, M.G., Santocanele, C., Drury, L.S., and Diffley, J.F.X. (2000). Dbf4p, an essential S phase-promoting factor, is targeted for degradation by the anaphase-promoting complex. *Molecular and Cellular Biology* 20, 242, 248.

Flynn, R.L., and Zou, L. (2011). ATR: a master conductor of cellular responses to DNA replication stress. *Trends in Biochemical Sciences* 36, 133, 140.

Fragkos, M., Ganier, O., Coulombe, P., and Méchali, M. (2015). DNA replication origin activation in space and time. *Nature Reviews Molecular Cell Biology* 16, 360, 376.

Gambus, A., Deursen, F.v., Polychronopoulos, D., Foltman, M., Jones, R.C., Edmondson, R.D., Calzada, A., and Labib, K. (2009). A key role for Ctf4 in coupling the MCM2-7 helicase to DNA polymerase α within the eukaryotic replisome. *The EMBO Journal* 28, 2992, 3004.

Gao, D., Inuzuka, H., Korenjak, M., Tseng, A., Wu, T., Wan, L., Kirschner, M., Dyson, N., and Wei, W. (2009). Cdh1 regulates cell cycle through modulating the Claspin/Chk1 and the Rb/E2F1 pathways. *Molecular Biology of the Cell* 20, 3305, 3316.

Garcia, V., Furuya, K., and Carr, A.M. (2005). Identification and functional analysis of TopBP1 and its homologs. *DNA Repair* 4, 1227, 1239.

Gelmon, K.A., Tischkowitz, M., Mackay, H., Swenerton, K., Robidoux, A., Tonkin, K., Hirte, H., Huntsman, D., Clemons, M., Gilks, B., *et al.* (2011). Olaparib in patients with recurrent high-grade serous or poorly differentiated ovarian carcinoma or triple-negative breast cancer: a phase 2, multicentre, open-label, non-randomised study. *Lancet Oncology* 12, 852, 861.

Gopalakrishnan, V., Simancek, P., Houchens, C., Snaith, H.A., Frattini, M.G., Sazer, S., and Kelly, T.J. (2001). Redundant control of rereplication in fission yeast. *PNAS* 98, 13114, 13119.

Graham, T.G.W., Walter, J.C., and Loparo, J.J. (2016). Two-stage synapsis of DNA ends during non-homologous end joining. *Molecular Cell* 61, 850, 858.

Guo, C., Kumagai, A., Schlacher, K., Shevchenko, A., Shevchenko, A., and Dunphy, W.G. (2015). Interaction of Chk1 with Treslin negatively regulates the initiation of chromosomal DNA replication.

Molecular Cell 57, 492, 505.

Hao, J., Renty, C.d., Li, Y., Xiao, H., Kemp, M.G., Han, Z., DePamphilis, M.L., and Zhu, W. (2015). And-1 coordinates with Claspin for efficient Chk1 activation in response to replication stress. *The EMBO Journal* 34, 2096, 2110.

Harbour, J.W., Luo, R.X., Santi, A.D., Postigo, A.A., and Dean, D.C. (1999). Cdk phosphorylation triggers sequential intramolecular interactions that progressively block Rb functions as cells move through G1. *Cell* 98, 859, 869.

Hastie, C.J., HcLauchlan, H.J., and Cohen, P. (2006). Assay of protein kinases using radiolabeled ATP: a protocol. *Nature Protocols* 1, 968, 971.

Heffernan, T.P., Ünsal-Kaçmaz, K., Heinloth, A.N., Simpson, D.A., Paules, R.S., Sancar, A., Cordeiro-Stone, M., and Kaufmann, W.K. (2007). Cdc7/Dbf4 and the human S checkpoint response to UVC. *Journal of Biological Chemistry* 282, 9458, 9468.

Hills, S.A., and Diffley, J.F.X. (2014). DNA replication and oncogene-induced review replicative stress. *Current Biology* 24, R435, R444.

Hochegger, H., Takeda, S., and Hunt, T. (2008). Cyclin-dependent kinases and cell-cycle transitions: does one fit all? *Nature Reviews Molecular Cell Biology* 9, 910, 916.

Hunter, T. (1995). Protein kinases and phosphatases: Review the Yin and Yang of protein phosphorylation and signaling. *Cell* 80, 225, 236.

Hutchins, J.R.A., Hughes, M., and Clarke, P.R. (2000). Substrate specificity determinants of the checkpoint protein kinase Chk1. *FEBS Letters* 466, 91, 95.

Iwanaga, R., Komori, H., Ishida, S., Okamura, N., Nakayama, K., Nakayama, K., and Ohtani, K. (2006). Identification of novel E2F1 target genes regulated in cell cycle-dependent and independent manners. *Oncogene* 25, 1786, 1798.

Jazayeri, A., Falck, J., Lukas, C., Bartek, J., Smith, G.C.M., Lukas, J., and Jackson, S.P. (2005). ATM- and cell cycle-dependent regulation of ATR in response to DNA double-strand breaks. *Nature Cell Biology* 8, 37, 45.

Jeong, S.-Y., Kumagai, A., Lee, J., and Dunphy, W.G. (2003). Phosphorylated Claspin interacts with a phosphate-binding site in the kinase domain of Chk1 during ATR-mediated activation. *Journal of Biological Chemistry* 278, 46782, 46788.

Jette, N., and Lees-Miller, S.P. (2015). The DNA-dependent protein kinase: A multifunctional protein kinase with roles in DNA double strand break repair and mitosis. *Progress in Biophysics and Molecular Biology* 117, 194, 205.

Jiang, K., Pereira, E., Maxfield, M., Russell, B., Goudelock, D.M., and Sanchez, Y. (2003). Regulation of Chk1 includes chromatin association and 14-3-3 binding following phosphorylation on Ser345. *Journal of Biological Chemistry* 278, 25207, 25217.

Jin, J., Shirogane, T., Xu, L., Nalepa, G., Qin, J., Elledge, S.J., and Harper, J.W. (2003). SCF^β-TRCP links Chk1 signaling to degradation of the Cdc25A protein phosphatase. *Genes and Development* 17, 3062, 3074.

Jossen, R., and Bermejo, R. (2013). The DNA damage checkpoint response to replication stress: A game of forks. *Frontiers in Genetics* 4, 1, 14.

Kang, S., Kang, M.-S., Ryua, E., and Myung, K. (2017). Eukaryotic DNA replication: Orchestrated action of multi-subunit protein complexes. *Mutat Res Fund Mol Mech Mutagen* 809, 58, 69.

Kasahara, K., Goto, H., Enomoto, M., Tomono, Y., Kiyono, T., and Inagaki, M. (2010). 14-3-3 γ mediates Cdc25A proteolysis to block premature mitotic entry after DNA damage. *The EMBO Journal* 29, 2802,

2812.

Kim, J.M., Kakusho, N., Yamada, M., Kanoh, Y., Takemoto, N., and Masai, H. (2007). Cdc7 kinase mediates Claspin phosphorylation in DNA replication checkpoint. *Oncogene* 27, 3475, 3482.

Kim, S., Dallmann, H.G., McHenry, C.S., and Marians, K.J. (1996). Coupling of a replicative polymerase and helicase: At-DnaB interaction mediates rapid replication fork movement. *Cell* 84, 643, 650.

Kim, S.-T., Lim, D.-S., Canman, C.E., and Kastan, M.B. (1999). Substrate specificities and identification of putative substrates of ATM kinase family members. *The Journal of Biological Chemistry* 274, 37538, 37543.

Knighton, D., Zheng, J., Eyck, L.T., Ashford, V., Xuong, N., Taylor, S., and Sowadski, J. (1991). Crystal structure of the catalytic subunit of cyclic adenosine monophosphate-dependent protein kinase. *Science* 253, 407, 414.

Konermann, L., Pan, J., and Liu, Y.-H. (2011). Hydrogen exchange mass spectrometry for studying protein structure and dynamics. *The Royal Society of Chemistry* 40, 1224, 1234.

Koundrioukoff, S., Carignon, S., Techer, H., Letessier, A., Brison, O., and Debatisse, M. (2013). Stepwise activation of the ATR signaling pathway upon increasing replication stress impacts fragile site integrity. *PLOS Genetics* 9, e1003643.

Kumagai, A., and Dunphy, W.G. (2000). Claspin, a novel protein required for the activation of Chk1 during a DNA replication checkpoint response in *Xenopus* egg extracts. *Molecular Cell* 6, 839, 849.

Kumagai, A., and Dunphy, W.G. (2003). Repeated phosphopeptide motifs in Claspin mediate the regulated binding of Chk1. *Nature Cell Biology* 5, 161, 165.

Kumagai, A., Shevchenko, A., Shevchenko, A., and Dunphy, W.G. (2011). Direct regulation of Treslin by cyclin-dependent kinase is essential for the onset of DNA replication. *The Journal of Cell Biology* 193, 995, 1007.

Labib, K. (2010). How do Cdc7 and cyclin-dependent kinases trigger the initiation of chromosome replication in eukaryotic cells? *Genes & Development* 24, 1208, 1219.

Larkin, M., Blackshields, G., Brown, N., Chenna, R., McGettigan, P., McWilliam, H., Valentin, F., Wallace, I., Wilm, A., Lopez, R., *et al.* (2007). Clustal W and Clustal X version 2.0. *Bioinformatics* 23, 2947, 2948.

Lee, J., Kumagai, A., and Dunphy, W.G. (2001). Positive regulation of Wee1 by Chk1 and 14-3-3 proteins. *Molecular Biology of the Cell* 12, 551, 563.

Lee, J., Kumagai, A., and Dunphy, W.G. (2003). Claspin, a Chk1-regulatory protein, monitors DNA replication on chromatin independently of RPA, ATR, and Rad17. *Molecular Cell* 11, 329, 340.

Lindberg, R.A., Quinn, A.M., and Hunter, T. (1992). Dual-specificity protein kinases: will any hydroxyl do? *Trends in Biochemical Sciences* 17, 114, 119.

Liu, S., Shiotani, B., Lahiri, M., Marechal, A., Tse, A., Leung, C.C.Y., Glover, J.N.M., Yang, X.H., and Zou, L. (2011). ATR autophosphorylation as a molecular switch for checkpoint activation. *Molecular Cell* 43, 192, 202.

Liu, S., Song, N., and Zou, L. (2012). The conserved C terminus of Claspin interacts with Rad9 and promotes rapid activation of Chk1. *Cell Cycle* 11, 2711, 2716.

Lossain, G., Larroque, M., Ribeyre, C., Bec, N., Larroque, C., Decaillet, C., Gari, K., and Constantinou, A. (2013). FANCD2 binds MCM proteins and controls replisome function upon activation of S phase checkpoint signaling. *Molecular Cell* 51, 678, 690.

Macheret, M., and Halazonetis, T.D. (2015). DNA replication stress as a hallmark of cancer. *Annu Rev Pathol Mech Dis* 10, 425, 448.

Macurek, L., Lindqvist, A., Voets, O., Kool, J., Vos, H., and Medema, R. (2010). Wip1 phosphatase is

associated with chromatin and dephosphorylates γ H2AX to promote checkpoint inhibition. *Oncogene* 29, 2281, 2291.

Madhusudan, Akamine, P., Xuong, N.-H., and Taylor, S.S. (2002). Crystal structure of a transition state mimic of the catalytic subunit of cAMP-dependent protein kinase. *Nature Structural Biology* 9, 273, 277.

Madhusudan, P.A., Wu, J., Xuong, N.-H., Eyck, L.F.T., and Taylor, S.S. (2003). Dynamic features of cAMP-dependent protein kinase revealed by apoenzyme crystal structure. *Journal of Molecular Biology* 327, 159, 171.

Malumbres, M. (2014). Cyclin-dependent kinases. *Genome Biology* 15, 122.

Malumbres, M., and Barbacid, M. (2005). Mammalian cyclin-dependent kinases. *Trends in Biochemical Sciences* 30, 630, 641.

Manchado, E., Eguren, M., and Malumbres, M. (2010). The anaphase-promoting complex/cyclosome (APC/C): cell-cycle-dependent and -independent functions. *Biochemical Society Transactions* 38, 65, 71.

Manning, G., Whyte, D.B., Martinez, R., Hunter, T., and Sudarsanam, S. (2002). The protein kinase complement of the human genome. *Science* 298, 1912, 1934.

Marechal, A., and Zou, L. (2013). DNA damage sensing by the ATM and ATR kinases. *Cold Spring Harbour Perspectives in Biology* 5, a012716.

Margottin-Goguet, F., Hsu, J.Y., Loktev, A., Hsieh, H.-M., Reimann, J.D.R., and Jackson, P.K. (2003). Prophase destruction of Emi1 by the SCF TrCP/Slimb ubiquitin ligase activates the anaphase promoting complex to allow progression beyond prometaphase. *Developmental Cell* 4, 813, 826.

Matsumoto, S., Kanoh, Y., Shimmoto, M., Hayano, M., Ueda, K., Fukatsu, R., Kakusho, N., and Masai, H. (2017). Checkpoint-independent regulation of origin firing by Mrc1 through interaction with Hsk1 kinase. *Molecular and Cellular Biology* 37, e00355-00316.

Matsuno, K., Kumano, M., Kubota, Y., Hashimoto, Y., and Takisawa, H. (2006). The N-terminal noncatalytic region of *Xenopus* RecQ4 is required for chromatin binding of DNA polymerase in the initiation of DNA replication. *Molecular and Cellular Biology* 26, 4843, 4852.

Matsuoka, S., Ballif, B.A., Smogorzewska, A., McDonald, E.R., Hurov, K.E., Luo, J., Bakalarski, C.E., Zhao, Z., Solimini, N., Lerenthal, Y., *et al.* (2007). ATM and ATR substrate analysis reveals extensive protein networks responsive to DNA damage. *Science* 316, 1160, 1166.

McIntosh, D., and Blow, J.J. (2012). Dormant origins, the licensing checkpoint, and the response to replicative stresses. *Cold Spring Harb Perspect Biol* 4, a012955.

Meng, Z., Capalbo, L., Glover, D.M., and Dunphy, W.G. (2011). Role for casein kinase 1 in the phosphorylation of Claspin on critical residues necessary for the activation of Chk1. *Molecular Biology of the Cell* 22, 2797, 2982.

Minchom, A., Aversa, C., and Lopez, J. (2018). Dancing with the DNA damage response: next-generation anti-cancer therapeutic strategies. *Therapeutic Advances in Medical Oncology* 10, 1, 18.

Moiseeva, T.N., and Bakkenist, C.J. (2018). Regulation of the initiation of DNA replication in human cells. *DNA Repair* 72, 99, 106.

Moreno, S.P., Bailey, R., Campion, N., Herron, S., and Gambus, A. (2014). Polyubiquitylation drives replisome disassembly at the termination of DNA replication. *Science* 346, 477, 481.

Moser, J., Miller, I., Carter, D., and Spencer, S.L. (2018). Control of the restriction point by Rb and p21. *PNAS* 115, E8219, E8227.

Mutreja, K., Krietsch, J., Hess, J., Ursich, S., Berti, M., Roessler, F.K., Zellweger, R., Patra, M., Gasser, G., and Lopes, M. (2018). ATR-mediated global fork slowing and reversal assist fork traverse and prevent chromosomal breakage at DNA interstrand cross-links. *Cell Reports* 24, 2629, 2642.

Nguyen, V.Q., Co, C., and Li, J.J. (2001). Cyclin-dependent kinases prevent DNA re-replication through multiple mechanisms. *Nature* 411, 1068, 1073.

Ni, Z.-J., Barsanti, P., Brammeier, N., Diebes, A., Poon, D.J., Ng, S., Pecchi, S., Pfister, K., Renhow, P.A., Ramurthy, S., *et al.* (2006). 4-(Aminoalkylamino)-3-benzimidazole-quinolinones as potent CHK-1 inhibitors. *Bioorganic & Medicinal Chemistry Letters* 16, 3121, 3124.

O'Carrigan, B., Luken, M.J.d.M., Papadatos-Pastos, D., Brown, J., Tunariu, N., Lopez, R.P., Ganegoda, M., Riisnaes, R., Figueiredo, I., Carreira, S., *et al.* (2016). Phase I trial of a first-in-class ATR inhibitor VX-970 as monotherapy (mono) or in combination (combo) with carboplatin (CP) incorporating pharmacodynamics (PD) studies. *Journal of Clinical Oncology* 34, 2504.

Okita, N., Minato, S., Ohmi, E., Tanuma, S.-i., and Higami, Y. (2012). DNA damage-induced CHK1 autophosphorylation at Ser296 is regulated by an intramolecular mechanism. *FEBS Letters* 586, 3974, 3979.

Oza, V., Ashwell, S., Almeida, L., Brassil, P., Breed, J., Deng, C., Gero, T., Grondine, M., Horn, C., Ioannidis, S., *et al.* (2012). Discovery of checkpoint kinase inhibitor (S)-5-(3-fluorophenyl)-N-(piperidin-3-yl)-3-ureidothiophene-2-carboxamide (AZD7762) by structure-based design and optimization of thiophenecarboxamide ureas. *Journal of Medicinal Chemistry* 55, 5130, 5142.

Parker, M.W., Botchan, M.R., and Berger, J.M. (2017). Mechanisms and regulation of DNA replication initiation in eukaryotes. *Crit Rev Biochem Mol Biol* 52, 107, 144.

Peränen, J., Rikkonen, M., Hyvönen, M., and Kääriäinen, L. (1996). T7 vectors with a modified T7lac promoter for expression of proteins in *Escherichia coli*. *Analytical Biochemistry* 236, 371, 373.

Peschiaroli, A., Dorrello, N.V., Guardavaccaro, D., Venere, M., Halazonetis, T., Sherman, N.E., and Pagano, M. (2006). SCFbTrCP-mediated degradation of Claspin regulates recovery from the DNA replication checkpoint response. *Molecular Cell* 23, 319, 329.

Petermann, E., Helleday, T., and Caldecott, K.W. (2008). Claspin promotes normal replication fork rates in human cells. *Molecular Biology of the Cell* 19, 2373, 2378.

Peters, J.-M. (2002). The anaphase-promoting complex: Review proteolysis in mitosis and beyond. *Molecular cell* 9, 932, 943.

Pettersen, E.F., Goddard, T.D., Huang, C.C., Couch, G.S., Greenblatt, D.M., Meng, E.C., and Ferrin, T.E. (2004). UCSF Chimera- a visualization system for exploratory research and analysis. *Journal of Computational Chemistry* 25, 1605, 1612.

Pintard, L., and Archambault, V. (2018). A unified view of spatio-temporal control of mitotic entry: Polo kinase as the key. *Open Biology* 8, 180114.

Plummer, E.R., Dean, E.J., Evans, T.R.J., Greystoke, A., Herbschleb, K., Ranson, M., Brown, J., Zhang, Y., Karan, S., Pollard, J., *et al.* (2016). Phase I trial of first-in-class ATR inhibitor VX-970 in combination with gemcitabine (Gem) in advanced solid tumors (NCT02157792). *Journal of clinical oncology* 34, 2531.

Qiu, Z., Oleinick, N.L., and Zhang, J. (2017). ATR/CHK1 inhibitors and cancer therapy. *Radiotherapy and Oncology* 126, 450, 464.

Quan, Y., Xia, Y., Liu, L., Cui, J., Li, Z., Cao, Q., Chen, X.S., Campbell, J.L., and Lou, H. (2015). Cell-cycle-regulated interaction between Mcm10 and double hexameric Mcm2-7 is required for helicase splitting and activation during S phase. *Cell Reports* 13, 2576, 2586.

Rabik, C.A., and Dolan, M.E. (2007). Molecular mechanisms of resistance and toxicity associated with platinating agents. *Cancer Treat Rev* 33, 9, 23.

Ren, S., and Rollins, B.J. (2004). Cyclin C/Cdk3 promotes Rb-dependent G0 exit. *Cell* 117, 239, 251.

Rogerson, D.T., Sachdeva, A., Wang, K., Haq, T., Kazlauskaitė, A., Hancock, S.M., Huguenin-Dezot, N., Muqit, M.M.K., Fry, A.M., Bayliss, R., *et al.* (2016). Efficient genetic encoding of phosphoserine and its non-hydrolyzable analog. *Nat Chem Biol* 11, 496, 503.

Sanchez, Y., Wong, C., Thoma, R.S., Richman, R., Wu, Z., Piwnica-Worms, H., and Elledge, S.J. (1997). Conservation of the Chk1 checkpoint pathway in mammals: Linkage of DNA damage to Cdk regulation through Cdc25. *Science* 277, 1497, 1501.

Sanchez-Pulido, L., Diffley, J.F.X., and Ponting, C.P. (2010). Homology explains the functional similarities of Treslin/Ticrr and Sld3. *Current Biology* 20, R509, R510.

Sar, F., Lindsey-Boltz, L.A., Subramanian, D., Croteau, D.L., Hutsell, S.Q., Griffith, J.D., and Sancar, A. (2004). Human Claspin is a ring-shaped DNA-binding protein with high affinity to branched DNA structures. *The Journal of Biological Chemistry* 279, 39289, 39295.

Sasi, N.K., Coquel, F., Lin, Y.-L., MacKeigan, J.P., Pasero, P., and Weinreich, M. (2017). DDK has a primary role in processing stalled replication forks to initiate downstream checkpoint signaling. *BioRxiv* 20, 985, 995.

Sato, K., Sundaramoorthy, E., Rajendra, E., Hattori, H., Jeyasekharan, A.D., Ayoub, N., Schiess, R., Aebersold, R., Nishikawa, H., Sedukhina, A.S., *et al.* (2012). A DNA-damage selective role for BRCA1 E3 ligase in Claspin ubiquitylation, CHK1 activation, and DNA repair. *Current Biology* 22, 1659, 1666.

Schmitt, E., Boutros, R., Froment, C., Monsarrat, B., Ducommun, B., and Dozier, C. (2006). CHK1 phosphorylates CDC25B during the cell cycle in the absence of DNA damage. *Journal of Cell Science* 119, 4269, 4275.

Scorah, J., and McGowan, C.H. (2009). Claspin and Chk1 regulate replication fork stability by different mechanisms. *Cell Cycle* 8, 1036, 1043.

Sengupta, S., Deursen, F.v., Piccoli, G.d., and Labib, K. (2013). Dpb2 integrates the leading-strand DNA polymerase into the eukaryotic replisome. *Current Biology* 23, 543, 552.

Serçin, O.z., and Kemp, M.G. (2011). Characterization of functional domains in human Claspin. *Cell Cycle* 10, 1599, 1606.

Shapiro, G., Wesolowski, R., Middleton, M., Devoe, C., Constantinidou, A., Papadatos-Pastos, D., Fricano, M., Zhang, Y., Karan, S., Pollard, J., *et al.* (2016). Phase 1 trial of first-in-class ATR inhibitor VX-970 in combination with cisplatin (Cis) in patients (pts) with advanced solid tumors (NCT02157792). *Cancer Research* 76.

Shechter, D., Costanzo, V., and Gautier, J. (2004). ATR and ATM regulate the timing of DNA replication origin firing. *Nature Cell Biology* 6, 648, 655.

Sibanda, B.L., Chirgadze, D.Y., Ascher, D.B., and Blundell, T.L. (2017). DNA-PKcs structure suggests an allosteric mechanism modulating DNA double-strand break repair. *Science* 355, 520, 524.

Smith, C.M., Radzio-Andzelm, E., Madhusudan, Akamine, P., and Taylor, S.S. (1999). The catalytic subunit of cAMP-dependent protein kinase: prototype for an extended network of communication. *Progress in Biophysics & Molecular Biology* 71, 313, 341.

Smits, V.A.J., Cabrera, E., Freire, R., and Gillespie, D.A. (2018). Claspin – checkpoint adaptor and DNA replication factor. *The FEBS Journal* 286, 441, 455.

Smits, V.A.J., Reaper, P.M., and Jackson, S.P. (2006). Rapid PIKK-dependent release of Chk1 from chromatin promotes the DNA-damage checkpoint response. *Current Biology* 16, 150, 159.

Solomon, M.J., Harper, J.W., and Shuttleworth, J. (1993). CAK, the p34cdc2 activating kinase, contains a protein identical or closely related to p40MO15. *Trends in Genetics* 9, 342.

Stiff, T., Walker, S.A., Cerosaletti, K., Goodarzi, A.A., Petermann, E., Concannon, P., O'Driscoll, M., and Jeggo, P.A. (2006). ATR-dependent phosphorylation and activation of ATM in response to UV treatment or replication fork stalling. *The EMBO Journal* 25, 5775, 5782.

Stokes, M.P., Rush, J., MacNeill, J., Ren, J.M., Sprott, K., Nardone, J., Yang, V., Beausoleil, S.A., Gygi, S.P., Livingstone, M., *et al.* (2007). Profiling of UV-induced ATM/ATR signaling pathways. *PNAS* 104, 19855, 19860.

Sur, S., and Agrawal, D.K. (2016). Phosphatases and kinases regulating CDC25 activity in the cell cycle: Clinical implications of CDC25 overexpression and potential treatment strategies. *Mol Cell Biochem* 416, 33, 46.

Surova, O., and Zhivotovsky, B. (2013). Various modes of cell death induced by DNA damage. *Oncogene* 32, 3789, 3797.

Swilius, M.T., and Waxham, M.N. (2008). Ca²⁺/Calmodulin-dependent protein kinases. *Cell Mol Life Sci* 65, 2637, 2657.

Syljuåsen, R.G., Sørensen, C.S., Hansen, L.T., Fugger, K., Lundin, C., Johansson, F., Helleday, T., Sehested, M., Lukas, J., and Bartek, J. (2005). Inhibition of human Chk1 causes increased initiation of DNA replication, phosphorylation of ATR targets, and DNA breakage. *Molecular and Cellular Biology* 25, 3553, 3562.

Talor, S.S., Knighton, D.R., Zheng, J., Eyck, L.F.T., and Sowadski, J.M. (1992). Structural framework for the protein kinase family. *Annu Rev Cell Biol* 8, 429, 462.

Taylor, S.S., and Kornev, A.P. (2011). Protein kinases: Evolution of dynamic regulatory proteins. *Trends Biochem Sci* 36, 65, 77.

Taylor, S.S., Radzio-Andzelm, E., and Hunter, T. (1995). How do protein kinases discriminate between serine/threonine and tyrosine? Structural insights from the insulin receptor protein-tyrosine kinase. *FASEB J* 9, 1255, 1266.

Taylor, S.S., Yang, J., Wu, J., Haste, N.M., Radzio-Andzelm, E., and Anand, G. (2004). PKA: a portrait of protein kinase dynamics. *Biochimica et Biophysica Acta (BBA) - Proteins and Proteomics* 1697, 259, 269.

Ticau, S., Friedman, L.J., Champasa, K., Jr, I.R.C.a., Gelles, J., and Bell, S.P. (2017). Mechanism and timing of Mcm2–7 ring closure during DNA replication origin licensing. *Nat Struct Mol Biol* 24, 309, 315.

Toledo, L.I., Altmeyer, M., Rask, M.-B., Lukas, C., Larsen, D.H., Povlsen, L.K., Bekker-Jensen, S., Mailand, N., Bartek, J., and Lukas, J. (2013). ATR prohibits replication catastrophe by preventing global exhaustion of RPA. *Cell* 155, 1088, 1103.

Torgovnick, A., and Schumacher, B. (2015). DNA repair mechanisms in cancer development and therapy. *Frontiers in Genetics* 6, 157.

Toyoshima-Morimoto, F., Taniguchi, E., and Nishida, E. (2002). Plk1 promotes nuclear translocation of human Cdc25C during prophase. *EMBO Reports* 3, 341, 348.

Tu, Y., Liu, H., Zhu, X., Shen, H., Ma, X., Wang, F., Huang, M., Gong, J., Li, X., Wang, Y., *et al.* (2017). Ataxin-3 promotes genome integrity by stabilizing Chk1. *Nucleic Acids Research* 45, 4532, 4549.

Turner, N., Tutt, A., and Ashworth, A. (2005). Targeting the DNA repair defect of BRCA tumours. *Current Opinion in Pharmacology* 5, 388, 393.

Tutt, A., Robson, M., Garber, J.E., Domchek, S.M., Audeh, M.W., Weitzel, J.N., Friedlander, M., Arun, B.,

Loman, N., Schmutzler, R.K., *et al.* (2010). Oral poly(ADP-ribose) polymerase inhibitor olaparib in patients with BRCA1 or BRCA2 mutations and advanced breast cancer: a proof-of-concept trial. *Lancet* 376, 235, 244.

Vendetti, F.P., Lau, A., Schamus, S., Conrads, T.P., O'Connor, M.J., and Bakkenist, C.J. (2015). The orally active and bioavailable ATR kinase inhibitor AZD6738 potentiates the anti-tumor effects of cisplatin to resolve ATM-deficient non-small cell lung cancer in vivo. *Oncotarget* 6, 44289, 44305.

Vodermaier, H.C. (2004). APC/C and SCF: Controlling each other and the cell cycle. *Current Biology* 14, 787, 796.

Vugt, M.A.T.M.v., Bras, A., and Medema, R.H. (2004). Polo-like kinase-1 controls recovery from a G2 DNA damage-induced arrest in mammalian cells. *Molecular Cell* 15, 799, 811.

Walsh, D.A., Perkins, J.P., and Krebs, E.G. (1968). An adenosine 3',5'-monophosphate-dependant protein kinase from rabbit skeletal muscle. *The Journal of Biological Chemistry* 243, 3763, 3765.

Wang, J., Han, X., Feng, X., Wang, Z., and Zhang, Y. (2012a). Coupling cellular localization and function of checkpoint kinase 1 (Chk1) in checkpoints and cell viability. *Journal of Biological Chemistry* 287, 25501, 25509.

Wang, J., Han, X., and Zhang, Y. (2012b). Auto-regulatory mechanisms of phosphorylation of checkpoint kinase 1 (Chk1). *Cancer Research* 72, 3786, 3794.

Watanabe, N., Arai, H., Iwasaki, J.-i., Shiina, M., Ogata, K., Hunter, T., and Osada, H. (2005). Cyclin-dependent kinase (CDK) phosphorylation destabilizes somatic Wee1 via multiple pathways. *PNAS* 102, 11663, 11668.

Waterhouse, A.M., Procter, J.B., Martin, D.M.A., Clamp, M.I., and Barton, G.J. (2009). Jalview Version 2—a multiple sequence alignment editor and analysis workbench. *Bioinformatics* 25, 1189, 1191.

Wilsker, D., Petermann, E., Helleday, T., and Bunz, F. (2008). Essential function of Chk1 can be uncoupled from DNA damage checkpoint and replication control. *PNAS* 105, 20752, 20757.

Witosch, J., Wolf, E., and Mizuno, N. (2014). Architecture and ssDNA interaction of the Timeless-Tipin-RPA complex. *Nucleic Acids Research* 42, 12912, 12927.

Yajima, H., Lee, K.-J., Zhang, S., Kobayashi, J., and Chen, B.P.C. (2009). DNA double strand break formation upon UV-induced replication stress activates ATM and DNA-PKcs kinases. *Journal of Molecular Biology* 385, 800, 810.

Yang, C.-C., Suzuki, M., Yamakawa, S., Uno, S., Ishii, A., Yamazaki, S., Fukatsu, R., Fujisawa, R., Sakimura, K., Tsurimoto, T., *et al.* (2016). Claspin recruits Cdc7 kinase for initiation of DNA replication in human cells. *Nature Communications* 7, 12135.

Yekezare, M., Gomez-Gonzalez, B., and Diffley, J.F.X. (2013). Controlling DNA replication origins in response to DNA damage – inhibit globally, activate locally. *Journal of Cell Science* 126, 1297, 1306.

Zegerman, P., and Diffley, J.F.X. (2011). Checkpoint dependent inhibition of DNA replication initiation by Sld3 and Dbf4 phosphorylation. *Nature* 467, 474, 478.

Zeman, M.K., and Cimprich, K.A. (2014). Causes and consequences of replication stress. *Nat Cell Biol* 16, 2, 9.

Zhang, H., Head, P.E., Daddacha, W., Park, S.-H., Li, X., Pan, Y., Madden, M.Z., Duong, D.M., Xie, M., Yu, B., *et al.* (2016). ATRIP deacetylation by SIRT2 drives ATR checkpoint activation by promoting binding to RPA-ssDNA. *Cell Reports* 14, 1435, 1447.

Zhang, Y.-W., Otterness, D.M., Chiang, G.G., Xie, W., Liu, Y.-C., Mercurio, F., and Abraham, R.T. (2005). Genotoxic stress targets human Chk1 for degradation by the ubiquitin-proteasome pathway. *Molecular Cell* 19, 607, 618.

Zhao, B., Bower, M.J., McDevitt, P.J., Zhao, H., Davis, S.T., Johanson, K.O., Green, S.M., Concha, N.O., and Zhou, B.-B.S. (2002). Structural basis for Chk1 inhibition by UCN-01. *The Journal of Biological Chemistry* 277, 46609, 46615.

Zhou, Z.-W., Liu, C., Li, T.-L., Bruhn, C., Krueger, A., Min, W., Wang, Z.-Q., and Carr, A.M. (2013). An essential function for the ATR-activation-domain (AAD) of TopBP1 in mouse development and cellular senescence. *PLOS Genetics* 9, e1003702.

Zhu, M., Zhao, H., Liao, J., and Xu, X. (2014). HERC2/USP20 coordinates CHK1 activation by modulating CLASPIN stability. *Nucleic Acids Research* 42, 13074, 13081.

APPENDIX A

| Primer | Sequence |
|------------------------|---|
| <i>Chk1KD-f</i> | agtctagcggccgcagtgccctttgtggaagac |
| <i>pUC/M13-f</i> | cccagtcacgacgttgtaaaacg |
| <i>EcChk1Ntag-f</i> | agctgagcggccgcgccaccatgcatcaccatcaccatcaccatcacgaaaaccttacttccaag gcatgccgaaatacgaattgcaag |
| <i>EcChk1Ctag-f</i> | agctgagcggccgcgccaccatgccgaaatacgaattgcaag |
| <i>Chk1FL2-f</i> | agctgagcggccgcgccaccatgcatcaccatcaccatcaccatcacgaaaaccttacttccaag gcatggcagtgccctttgt |
| <i>Chk1D130A-f</i> | ggaataactcacagggccattaaccagaaaatcttc |
| <i>Chk1TEV1-f</i> | gtcgacgcggccgcagtgcatcaccatcaccatcaccatcacatggcagtgccctttgtgg |
| <i>Chk1TEV2-f</i> | cagagtctcccagtgagagaatcttacttcaattttctaagcacattc |
| <i>Cdc25C-f</i> | tatagtccatggaagatcaggaagccaaagtg |
| <i>Cdc25CS216A-f</i> | ggcctgtaccgctctccagcagtgccgaaaaatctcaacc |
| <i>Chk1S317E-f</i> | tgtgaagtactccagtgaaacagccagaaccccgcacaggt |
| <i>Chk1S345E-f</i> | tggtaacagggatcagctttgaacagcccacatgtcctgat |
| <i>Chk1Δturn-f</i> | ggagaagttcaactgctacaggggatccgtcgcagtgaaattgtagatag |
| <i>Chk1E17T-f</i> | gggacttggtgcaaaccctgggaacaggtgcctatggagaagttc |
| <i>Chk1E22T-f</i> | caggtgcctatggaacagttcaacttctg |
| <i>Chk1E32T/E33S-f</i> | gtgaatagagtaactcaacagcagtcgcagtgaaag |
| <i>Claspin850-f</i> | catgtagaattcaagacacttttcttaggagcagg |
| <i>Claspin884-f</i> | gtcagagaattcaggaatcagtagcaagctttgaaag |
| <i>ClaspinT916E-f</i> | gagctgttgattgtgtgagggaaagttcacatctcag |
| <i>ClaspinT945E-f</i> | ggaacttctgaacctttgtgaaggaaaattcacttctcag |
| <i>ClaspinT982E-f</i> | cacttgctctttgcgaaggctctttcccacagac |
| <i>MBP-f</i> | acgtgaccatggataaaatcgaagaaggtaaac |
| <i>Claspin884S-f</i> | aactaggtcgacaggaatcagtagcagctttgaaag |
| <i>ClaspinT916Am-f</i> | atgagctgttgattgtgttagggaaagttcacatctca |
| <i>ClaspinT945Am-f</i> | aggaaacttctgaacctttgttagggaaaattcacttctca |
| <i>ClaspinT982Am-f</i> | cacttgctctttgctagggctctttcccacagac |
| <i>ClaspinN936A-f</i> | gaagagtgacaagaagagggcagtgaggaaacttctgaac |
| <i>ClaspinM937A-f</i> | gtgacaagaagagaacgcggaggaacttctgaac |
| <i>ClaspinE938A-f</i> | caagaagagaacatggcggaaacttctgaacctttg |
| <i>ClaspinE939A-f</i> | gaaagagaacatggagcgccttctgaacctttgttag |
| <i>ClaspinL940A-f</i> | gagaacatggaggaagcgtgaacctttgttagg |
| <i>ClaspinL941A-f</i> | gaacatggaggaacttgcgaacctttgttaggg |
| <i>ClaspinN942A-f</i> | gaacatggaggaacttctggcgcctttgttagggaaaattc |
| <i>ClaspinL943A-f</i> | ggaggaacttctgaacgcgtgttagggaaaattcac |
| <i>ClaspinC944A-f</i> | ggaacttctgaaccttgcgtagggaaaattcacttc |
| <i>ClaspinG946A-f</i> | ctgaacctttgttaggcgaaattcacttctcagg |
| <i>ClaspinK947A-f</i> | ctgaacctttgttagggagcgttcaacttctcaggatgc |
| <i>ClaspinF948A-f</i> | cctttgttagggaaaagcacttctcaggatgcctc |

| | |
|------------------------|--|
| <i>ClaspinT949A-f</i> | ctttgttagggaaaattcgcgtctcaggatgcctccac |
| <i>ClaspinS950A-f</i> | gttagggaaaattcactgcgcaggatgcctccactc |
| <i>ClaspinQ951A-f</i> | gaaaattcacttctgcggatgcctccactc |
| <i>Strep-f</i> | atgctcgaattctctgcttgagccaccctcagtttgagaagatggatagtgctagcgaagtc |
| <i>CK45-f</i> | tcgactgaattcatgagggttgcaagaagatagg |
| <i>Chk1KD-r</i> | gctagtaagcttttagtgatggtgatggtgatggtgatggccagagccttggaaagtagaggtttctcc actgggagactctgacac |
| <i>Chk1FL-r</i> | gctagtaagcttttagtgatggtgatggtgatggtgatggccagagccttggaaagtagaggtttctgt ggcaggaagccaaacc |
| <i>pUC/M13-r</i> | agcggataacaatttcacacagg |
| <i>EcChk1Ntag-r</i> | tcgtacaagctttcatatttcgttagagaatag |
| <i>EcChk1Ctag-r</i> | gctagtaagcttttagtgatggtgatggtgatggtgatggccagagccttggaaagtagaggtttctatt tcgttagagaatag |
| <i>Chk1FL2-r</i> | tcgtacaagctttcatgtggcaggaagccaaa |
| <i>Chk1D130A-r</i> | gaagattttctggttaatggccctgtgagtattcc |
| <i>Chk1TEV1-r</i> | gtcataaagctttcactcatgccactcgatcttttgcctcaaataatgcattgagtcactcgtgtttgt ggcaggaagccaaacc |
| <i>Chk1TEV2-r</i> | gaatgtgcttagaaaattgaaagtagagattctctccactgggagactctg |
| <i>Cdc25C-r</i> | ttacagaagcttttacagaccttccggag |
| <i>Cdc25CS216A-r</i> | ggttgagattttctggcatcgtggagagcgggtacaggcc |
| <i>Chk1S317E-r</i> | acctgtgcggggttctggctgttactggagtacttaca |
| <i>Chk1S345E-r</i> | atcaggacatgtgggctgttcaaagctgatccctgtacca |
| <i>Chk1Δturn-r</i> | catatctacaattcactcgcacggatccgctgtagcaagttgaacttctcc |
| <i>Chk1E17T-r</i> | gaactctccatagggcacctgtcccagggtttgcaccaagtccc |
| <i>Chk1E22T-r</i> | cagcaagttgaactgttccataggcacctg |
| <i>Chk1E32T/E32S-r</i> | cttactcgcactgctgttgaagtactctattcac |
| <i>Claspin850-r</i> | gatcgactcgagttattcctctctctgtctgtggg |
| <i>ClaspinAvi-r</i> | tcgactaagctttattcatgcccattttctgcgcttcgaaaatgcatcagtcactagtggtgtga tggtgatggtgatggtgatggcc |
| <i>ClaspinT916E-r</i> | ctgagatgtgaactttccctcacacaaatccaacagctc |
| <i>ClaspinT945E-r</i> | ctgagaagtgaattttcctcacaaaaggttcagaagtcc |
| <i>ClaspinT982E-r</i> | gtctgtgggaaaagagccttcgcaaagagcaagtg |
| <i>MBP-r</i> | gcagctgaattcggaacctggaagtacag |
| <i>Claspin992X-r</i> | atgctaaagcttttagtgatggtgatggtgatggtgatggccagattcctctctctgtctg |
| <i>ClaspinT916Am-r</i> | tgagatgtgaactttccctaacacaaatccaacagctcat |
| <i>ClaspinT945Am-r</i> | aggaaacttctgaacctttgttagggaaaattcacttctca |
| <i>ClaspinT982Am-r</i> | gtctgtgggaaaagagccttagcaaagagcaagtg |
| <i>ClaspinN936A-r</i> | gttcagaagttcctccatcgcctctttctgtcactcttc |
| <i>ClaspinM937A-r</i> | gttcagaagttcctccgcttctctttctgtcac |
| <i>ClaspinE938A-r</i> | caaaggttcagaagttccgcatgttctctttctg |
| <i>ClaspinE939A-r</i> | ctaacaaggttcagaagcgcctccatgttctcttcc |
| <i>ClaspinL940A-r</i> | cctaacaaggttcagcgttctccatgttctc |
| <i>ClaspinL941A-r</i> | ccctaacaaggttcgaagttcctccatgttc |

| | |
|-----------------------|---------------------------------------|
| <i>ClaspinN942A-r</i> | gaatttcctaacaagcgccagaagttcctccatgttc |
| <i>ClaspinL943A-r</i> | gtgaatttcctaacacggtcagaagttcctcc |
| <i>ClaspinC944A-r</i> | gaagtgaatttcctacgcaaggtcagaagtcc |
| <i>ClaspinG946A-r</i> | cctgagaagtgaatttcgctaacaaggttcag |
| <i>ClaspinK947A-r</i> | gcatcctgagaagtgaacgctcctaacaaggttcag |
| <i>ClaspinF948A-r</i> | gaggcatcctgagaagtcgcttttcctaacaagg |
| <i>ClaspinT949A-r</i> | gtggaggcatcctgagacgcaatttcctaacaag |
| <i>ClaspinS950A-r</i> | gagtggaggcatcctgcgcagtgaatttcctaac |
| <i>ClaspinQ951A-r</i> | gagtggaggcatccgcagaagtgaatttc |
| <i>CK352-r</i> | tgtcagaagcttcattctcgagtattgcag |